Optimization of Craniosynostosis Surgery: Virtual Planning, Intraoperative 3D Photography and Surgical Navigation

by

David García Mato

A dissertation submitted in partial fulfillment of the requirements for the degree of Doctor of Philosophy in

Biomedical Science and Technology

Universidad Carlos III de Madrid

Advisor:

Javier Pascau González-Garzón

Tutor:

Javier Pascau González-Garzón

January 2021

Para ti Abu

I dreamed a dream of the bonny
In a vision in the back of my eye
And when the walls came down
It was the only thing that kept me alive

Go on and build the bonny
Build the bonfire big and high
A fire so big that the flames light up the sky

Believe and build your bonny
Gonna never know unless you try
One life is a short time
And no one knows where you go when you die

For the people that you loved and lost
That you never got to tell goodbye
Stand tall while the walls fall down
With a smile and a tear in your eye

The Bonny – Gerry Cinnamon

AGRADECIMIENTOS

Me gustaría agradecer a mi tutor, **Javi**, por confiar en mí y darme la oportunidad de crecer como ingeniero, como investigador, y como persona. Muchas gracias por estar siempre ahí dispuesto a ayudar, por tu empatía, por tu conocimiento, y por tu forma de ser. Ha sido un placer tenerte como tutor durante todos estos años.

También agradecer a mis compañeros inseparables. A **Moni**, por aparecer en mi vida y ser la mejor compañera de viaje. Por su mirada, su sonrisa, su empatía, por ponerle música y color a mi vida, y por mucho más. A **Rafa**, por su energía, su humor, su honestidad, su generosidad, su capacidad de escuchar, sus tonterías en los momentos buenos, sus ánimos en los momentos difíciles, sus críticas constructivas, y su personalidad. Ha sido un placer trabajar junto a vosotros estos últimos 4 años, y sois claramente los culpables de haber hecho del doctorado la mejor etapa de mi vida. Sin vosotros todo esto habría sido muy distinto. Gracias por nuestros experimentos, nuestras cirugías, nuestros inventos, nuestros viajes (Heidelberg, Toronto, Barcelona, Bilbao, Nuremberg, Berlín, Favignana, Granada, Washington, Londres, …), nuestros conciertos, nuestros festivales (Mad Cools, DCodes, …), nuestra banda indie (The Pascaus), nuestras pruebas de impresión 3D, y por todos los momentos vividos. Por muchos más años a vuestro lado.

A todo el equipo de Cirugía Oral y Maxilofacial del Hospital General Universitario Gregorio Marañón. En especial, me gustaría dar las gracias al **Dr. Santiago Ochandiano** por sus ganas infinitas de seguir investigando y mejorando, por su confianza, por su paciencia, por sus ánimos, por su capacidad de liderazgo, y por formar parte de esto. Sin ti, nada de esto habría sido posible. También agradecer al resto del equipo: **Manuel**, **Gema**, **Pablo**, **Elena**, **Samuel**, **Carlos**, y **José Ignacio**. Por estar siempre dispuestos a ayudar y por su profesionalidad.

A todo el equipo de Neurocirugía del Hospital General Universitario Gregorio Marañón. En especial, al **Dr. Roberto García Leal**, por su profesionalidad, perfeccionismo, ánimos, y ayuda en todo momento. También agradecer la labor de **Juanvi** y **Óscar**, por su ayuda durante las cirugías, sus comentarios, y sus consejos.

A toda mi familia. A **mis padres**, porque gran parte de lo que soy se lo debo a ellos. Gracias por ayudarme a encontrar mi camino, por apoyarme siempre en todas mis decisiones y quererme tal y como soy. A mi hermana **Paula (Puru)**, por comprenderme, por aguantarme, por saber siempre cómo sacarme una sonrisa, por ser tan fuerte, por ser tan valiente, por dar todo por la familia, y por su apoyo constante. Estoy muy orgulloso de ti. A **mis abuelas**, por su fortaleza, por su

generosidad, por saber escuchar, por sus historias, y por su valentía. A **mi Abu**, por cuidar de mí, por su cariño, por inspirarme, por su personalidad única, por ser mi ejemplo a seguir en la vida, por enseñarme el significado del amor verdadero, y porque merecías estar aquí para presenciar esto. Esta tesis va por ti.

Al resto de mis compañeros del equipo navegación a lo largo de estos años. A **Eu**, por enseñarme mucho de la ciencia y de la vida, y por ser mi referencia en mis primeros años de investigación. A **Rocío**, por su personalidad, su lado salvaje, las risas, los momentos únicos, y por nuestros días de bouldering y rutas. A **Bego**, por su sonrisa y apoyo constante. A **Laura Sanz**, por su forma de ser y toda la ayuda recibida. A **Vero**, por sus ganas infinitas de ayudar. A **Mikael**, por introducirme en 3D Slicer y en la escalada. A **Maite** y **Lucía**, por hacerme sentir orgullo como docente. A **Manu (sosio)**, **Alicia**, **Anxela**, y **Estela** por ser unos grandes compañeros de equipo.

A todos mis compañeros del Departamento de Bioingeniería e Ingeniería Aeroespacial y del Laboratorio de Imagen Médica (LIM) con los que he tenido la oportunidad de coincidir durante estos años. En especial, a **Álvaro**, **Mario (unbreakable)**, **Cristóbal**, **Claudia**, **Alba**, **Lanillos**, **Inés**, **Iván**, **Asier**, **Ana**, **Estibaliz**, **Laura**, **Nerea**, **Rigo**, **Pedro**, **Juanjo**, **Arrate**, **Jorge**, **Mónica**, **Manolo**, **Ramón**, **David**, **Marta**, **Aurora**, **Lorena**, **Bea**, **Esther**, **María de la Jara**, **María Muñoz**, **Patricio**, **Blanca**, **Dani**, **Nico**, **Trajana**, **Paula**, **Elena**, **Marisa**, **Juan**, **Joaquín**, **Alessandro**, **Nik**, **Leo**, **Josu**, **Carlos**, **Claire**, **Clara**, **Patricia**, **Marina**. Ha sido un placer trabajar con todos y cada uno de vosotros durante estos años.

A los amigos que siempre están ahí. A **Raquel**, por su fortaleza, su forma de ser, y por estar ahí tanto en lo bueno como en lo malo. A **Ernesto**, por su personalidad, sabiduría, y sus consejos durante más de 20 años juntos. A **Kevin (Bujo)**, **Karla**, y **Sarah**, mi segunda familia en Mexico. A **Vickinson**, por entenderme y por no fallarme nunca. A los **Beers Cheers** (**Patri**, **Bruno**, **Calvo**, **Nuri**, **Luis**, **Chari**), por nuestras noches infinitas de juegos de mesa y confidencias. A **Aida** (**Mrs. Red**), por su generosidad y su forma de ver la vida. A los **Peaky Valders** (**Molina**, **Andrés**, **Tomás**, **Víctor**, **Cristian**), la línea dura de Valderas, porque siempre nos quedará "El Miguel".

A todos mis amigos del **Club de Montaña Cara Sur UC3M** y a los tochos de **The Climb**. Por todas las montañas conquistadas, las vías escaladas, los porteos, y las rutas inolvidables. A mis compañeros del equipo **Athletic Besiktas** (baloncesto y voleibol) de la liga interna de la universidad. Ha sido un placer ser capitán y jugador de este equipo.

ACKNOWLEDGEMENTS

I would like to thank and express my appreciation to all my colleagues at the Sheikh Zayed Institute for Pediatric Surgical Innovation at Children's National Hospital in Washington, DC, United States. Especially to **Dr. Marius George Linguraru** and **Dr. Antonio Reyes Porras**. Their knowledge, patience, and willingness to host me in their laboratory has added immense value to my academic experience. Also, I would like to thank the rest of my colleagues at Children's National: **Liyun**, **Titus**, **Tyler**, **Daniel**, **Eleni**, **Reza**, **Awais**, and **Paige**.

Also, I would like to thank **Dr. Gabor Fichtinger**, for his expertise, personality, and willingness to take me under his wing as a visiting research student in the Laboratory of Percutaneous Surgery (PerkLab) at Queen's University in Kingston, ON, Canada. I would like to acknowledge all the PerkLab family: **Csaba**, **Tamas**, **Andras**, **Mark**, **Matthew**, **Zsuzsanna**, **Vinyas**, **Zac**, **Hillary**, **Anna**, **Rachael**, **Grace**, **Thomas**, **Kyle**, and **Sal**. I thank you all for making my time at Kingston so special. I could not have hoped for a better time working in the Perk Lab. Also, I would like to thank all my friends from the **Queen's Outdoors Club** for the amazing hikes, cross-country skiing, climbing, camping spots, and other incredible outdoor adventures. Keep it wild guys!

Journal Articles:

[1] **D. García-Mato**, M. García-Sevilla, A.R. Porras, S. Ochandiano, J.V. Darriba-Allés, R. García-Leal, J.I. Salmerón, M.G. Linguraru, J. Pascau. Three-Dimensional Photography for Intraoperative Morphometric Analysis in Metopic Craniosynostosis Surgery. *Int J CARS* (2021) *https://doi.org/10.1007/s11548-020-02301-0* [Impact factor: 2.473; Q2]

Author contributions: David García Mato was responsible for data acquisition, data analysis, and writing the paper. All authors were responsible for conceptualizing the framework, writing, editing, and reviewing the paper.

Contribution completely included in chapter 4. Figures from this paper have been reprinted with permission from the copyright holder, Springer Nature.

[2] **D. García-Mato**, S. Ochandiano, M. García-Sevilla, C. Navarro-Cuéllar, J. V. Darriba-Allés, R. García-Leal, J. A. Calvo-Haro, R. Pérez-Mañanes, J. I. Salmerón, J. Pascau. Craniosynostosis surgery: workflow based on virtual surgical planning, intraoperative navigation and 3D printed patient-specific guides and templates. *Scientific Reports*, vol. 9, 17691, 2019. *https://doi.org/10.1038/s41598-019-54148-4* [Impact factor: 3.998; Q1]

Author contributions: David García Mato was responsible for software development, data acquisition, data analysis, and writing the paper. All authors were responsible for conceptualizing the framework, writing, editing, and reviewing the paper.

Contribution completely included in chapter 5.

[3] **D. García-Mato**, R. Moreta-Martinez, M. García-Sevilla, S. Ochandiano, R. García-Leal, R. Pérez-Mañanes, J. A. Calvo-Haro, J.I. Salmerón, J. Pascau. Augmented reality visualization for craniosynostosis surgery. *Comput. Methods Biomech. Biomed. Eng. Imaging Vis.*, vol. 0, no. 0, pp. 1–8, 2020. *https://doi.org/10.1080/21681163.2020.1834876* [Impact factor: 1.502; Q3]

Author contributions: David García Mato was responsible for data acquisition, data analysis, and writing the paper. All authors were responsible for conceptualizing the framework, writing, editing, and reviewing the paper.

Contribution completely included in chapter 6. Figures from this paper have been reprinted with permission from the copyright holder, Taylor & Francis.

[4] **D. García-Mato**, A. R. Porras, S. Ochandiano, G. F. Rogers, J. Pascau, M. G. Linguraru. Automatic Planning of Fronto-Orbital Advancement for the Surgical Correction of Metopic Craniosynostosis. *Plast. Reconstr. Surg.* (2021) [Impact factor: 4.235; Q1] (submitted)

Author contributions: David García Mato was responsible for software development, data analysis, and writing the paper. All authors were responsible for conceptualizing the framework, writing, editing, and reviewing the paper.

Contribution completely included in chapter 3.

[5] S. Ochandiano, **D. García-Mato**, C. Navarro Cuellar, J. V. Darriba-Allés, R. García-Leal, A. R. Porras, M. G. Linguraru, J. Pascau, J. I. Salmerón. Patient-specific virtual planning and image-guided surgical correction in craniosynostosis: a case report from a multi-institutional collaboration. *Journal of Cranio-Maxillo-Facial Surgery* [Impact factor: 1.766; Q3] (submitted)

Author contributions: David García Mato was responsible for software development, data acquisition, and data analysis. All authors were responsible for conceptualizing the framework, writing, editing, and reviewing the paper.

Contribution partially included in chapters 3, 4, 5, and 6.

Book chapters:

[1] **D. García-Mato**, J. Pascau, S. Ochandiano. New Technologies to Improve Surgical Outcome during Open Cranial Vault Remodeling. *In: Craniosynostosis - New Perspectives of Prevention and Treatment*. IntechOpen, 2020. https://doi.org/10.5772/intechopen.94536

Author contributions: David García Mato was responsible for writing the chapter. All authors were responsible for conceptualizing the framework, writing, editing, and reviewing the chapter.

Contribution partially included in chapters 1 and 7.

Conference proceedings:

[1] **D. García-Mato**, M. García-Sevilla, S. Ochandiano, R. Moreta-Martinez, J. V. Darriba-Allés, R. García-Leal, J. I. Salmerón, J. Pascau. Intraoperative Outcome Evaluation in Craniosynostosis Reconstruction Surgery using 3D Photography. *In: CARS 2020 - Computer Assisted Radiology and Surgery Proceedings of the 34th International Congress and Exhibition, Munich, Germany, June 23–27, 2020. Int J CARS 15, 1–214* (2020) https://doi.org/10.1007/s11548-020-02171-6

Author contributions: David García Mato was responsible for data acquisition, data analysis, and writing the paper. All authors were responsible for conceptualizing the framework, writing, editing, and reviewing the paper.

Contribution partially included in chapter 4.

[2] **D. García-Mato**, M. García-Sevilla, S. Ochandiano, C. Navarro-Cuéllar, J. V. Darriba-Allés, R. García-Leal, J. Pascau. Structured Light Scanning for Morphometric Analysis in Craniosynostosis Reconstruction Surgery. *In: CARS 2019 - Computer Assisted Radiology and Surgery Proceedings of the 33rd International Congress and Exhibition, Rennes, France, June 18–21, 2019. Int J CARS 14, 1–194* (2019) https://doi.org/10.1007/s11548-019-01969-3

Author contributions: David García Mato was responsible for data acquisition, data analysis, and writing the paper. All authors were responsible for conceptualizing the framework, writing, editing, and reviewing the paper.

Contribution partially included in chapter 4.

[3] **D. García-Mato**, M. García-Sevilla, S. Ochandiano, C. Navarro-Cuéllar, J. V. Darriba-Allés, R. García-Leal, J. Pascau. Morphometric Analysis in Craniosynostosis Reconstruction Surgery based on Structured Light Scanning. *18th meeting of the International Society of Craniofacial Surgery (ISCFS) 2019, Paris, France. Plastic and Reconstructive Surgery - Global Open: August 2019 - Volume 7 - Issue 8S-2 - p 196.* https://doi.org/10.1097/01.GOX.0000583984.37423.9c

Author contributions: David García Mato was responsible for data acquisition, data analysis, and writing the paper. All authors were responsible for conceptualizing the framework, writing, editing, and reviewing the paper.

Contribution partially included in chapter 4.

[4] R. Moreta-Martinez, **D. García-Mato**, M. García-Sevilla, S. Ochandiano, R. García-Leal, R. Pérez-Mañanes, J. A. Calvo-Haro, J. I. Salmerón, J. Pascau. Augmented reality for bone fragment positioning during craniosynostosis reconstruction surgery. *In: CARS 2020 - Computer Assisted Radiology and Surgery Proceedings of the 34th International Congress and Exhibition, Munich, Germany, June 23–27, 2020. Int J CARS 15, 1–214* (2020) https://doi.org/10.1007/s11548-020-02171-6

Author contributions: David García Mato was responsible for data acquisition and writing the paper. All authors were responsible for conceptualizing the framework, writing, editing, and reviewing the paper.

Contribution partially included in chapter 6.

[5] S. Ochandiano, **D. García-Mato**, E. Bullejos, J. V. Darriba-Allés, R. García-Leal, J. Pascau, J. I. Salmerón. Intraoperative Navigation in Craniosynososis based on Virtual Surgical Planning and an "In-House" Technique. *18th meeting of the International Society of Craniofacial Surgery (ISCFS) 2019, Paris, France. Plastic and Reconstructive Surgery - Global Open: August 2019 - Volume 7 - Issue 8S-2 - p 176* https://doi.org/10.1097/01.GOX.0000583852.46832.e8

Author contributions: David García Mato was responsible for software development, data acquisition, data analysis, and writing the paper. All authors were responsible for conceptualizing the framework, writing, editing, and reviewing the paper.

Contribution partially included in chapter 5.

[6] G. Arenas, **D. García-Mato**, M. Tousidonis, P. Montes, J. Pascau, S. Ochandiano. Open Source Navigation System and CAD-CAM Technology in Surgical Treatment of Craniosynostosis. *European Association for Cranio-Maxillo-Facial Surgery 201*8, Munich, Germany.

Author contributions: David García Mato was responsible for software development, data acquisition, data analysis, and writing the paper. All authors were responsible for conceptualizing the framework, writing, editing, and reviewing the paper.

Contribution partially included in chapter 5.

The material from these sources included in this thesis are not singled out with typographic means and references.

TABLE OF CONTENTS

ABSTRACT

Craniosynostosis is a congenital defect defined as the premature fusion of one or more cranial sutures. This fusion leads to growth restriction and deformation of the cranium, caused by compensatory expansion parallel to the fused sutures. Surgical correction is the preferred treatment in most cases to excise the fused sutures and to normalize cranial shape. Although multiple technological advancements have arisen in the surgical management of craniosynostosis, interventional planning and surgical correction are still highly dependent on the subjective assessment and artistic judgment of craniofacial surgeons. Therefore, there is a high variability in individual surgeon performance and, thus, in the surgical outcomes.

The main objective of this thesis was to explore different approaches to improve the surgical management of craniosynostosis by reducing subjectivity in all stages of the process, from the preoperative virtual planning phase to the intraoperative performance.

First, we developed a novel framework for automatic planning of craniosynostosis surgery that enables: calculating a patient-specific normative reference shape to target, estimating optimal bone fragments for remodeling, and computing the most appropriate configuration of fragments in order to achieve the desired target cranial shape. Our results showed that automatic plans were accurate and achieved adequate overcorrection with respect to normative morphology. Surgeons' feedback indicated that the integration of this technology could increase the accuracy and reduce the duration of the preoperative planning phase.

Second, we validated the use of hand-held 3D photography for intraoperative evaluation of the surgical outcome. The accuracy of this technology for 3D modeling and morphology quantification was evaluated using computed tomography imaging as gold-standard. Our results demonstrated that 3D photography could be used to perform accurate 3D reconstructions of the anatomy during surgical interventions and to measure morphological metrics to provide feedback to the surgical team. This technology presents a valuable alternative to computed tomography imaging and can be easily integrated into the current surgical workflow to assist during the intervention.

Also, we developed an intraoperative navigation system to provide real-time guidance during craniosynostosis surgeries. This system, based on optical tracking, enables to record the positions of remodeled bone fragments and compare them with the target virtual surgical plan.

Our navigation system is based on patient-specific surgical guides, which fit into the patient's anatomy, to perform patient-to-image registration. In addition, our workflow does not rely on patient's head immobilization or invasive attachment of dynamic reference frames. After testing our system in five craniosynostosis surgeries, our results demonstrated a high navigation accuracy and optimal surgical outcomes in all cases. Furthermore, the use of navigation did not substantially increase the operative time.

Finally, we investigated the use of augmented reality technology as an alternative to navigation for surgical guidance in craniosynostosis surgery. We developed an augmented reality application to visualize the virtual surgical plan overlaid on the surgical field, indicating the predefined osteotomy locations and target bone fragment positions. Our results demonstrated that augmented reality provides sub-millimetric accuracy when guiding both osteotomy and remodeling phases during open cranial vault remodeling. Surgeons' feedback indicated that this technology could be integrated into the current surgical workflow for the treatment of craniosynostosis.

To conclude, in this thesis we evaluated multiple technological advancements to improve the surgical management of craniosynostosis. The integration of these developments into the surgical workflow of craniosynostosis will positively impact the surgical outcomes, increase the efficiency of surgical interventions, and reduce the variability between surgeons and institutions.

LIST OF FIGURES

LIST OF TABLES

LIST OF ABBREVIATIONS AND ACRONYMS

2D: Two-Dimensional

3D: Three-Dimensional

AR: Augmented Reality

CAD: Computer-Aided Design

CAM: Computer-Aided Manufacturing

CT: Computed Tomography

FOA: Fronto-Orbital Advancement

ICV: Intracranial Volume

IFA: Interfrontal Angle

IGS: Image-Guided Surgery

LFL: Left Frontal Landmark

MFB: Minimal Frontal Breadth

MRI: Magnetic Resonance Imaging

MSL: Metopic Suture Landmark

PCA: Principal Component Analysis

PLA: Polylactic Acid

RFL: Right Frontal Landmark

RGB: Red Green Blue

RMSE: Root-Mean-Square Error

SLAM: Simultaneous Localization and Mapping

STL: Stereolithography

TFW: Transverse Forehead Width

TRE: Target Registration Error

VR: Virtual Reality

VSP: Virtual Surgical Planning

1

INTRODUCTION

1.1. Craniosynostosis

Cranial sutures are the fibrous tissues uniting the cranial bones and the major growth centers of bone tissue during craniofacial development (**Figure 1.1**) [1]. These sutures enable the skull deformation during passage through the birth canal and calvarial growth caused by the expansion of the rapidly developing brain during the first years of life [2]. In a newborn, the brain typically doubles its size during the first six months, quadruples by the first year, and reaches 80% of its adult size by the second year of life [3].

Craniosynostosis is a congenital defect defined as the premature fusion of one or more cranial vault sutures [4]. According to prevalence studies, this condition affects approximately one in 2000-2500 live births worldwide [5], [6]. Although approximately 90% of the cases occur as an isolated event and unrelated to syndromic or genetic causes (*nonsyndromic craniosynostosis*), craniosynostosis can also be associated with a syndrome (*syndromic craniosynostosis*) [7], being Muenke's, Apert's, Crouzon's, Pfeiffer's, Saethre-Chotzen, and Carpenter's the most common ones [8].

The fusion of the sutures causes growth restriction and deformation of the cranium. As the brain develops, volume expansion results in compensatory growth parallel to the fused sutures causing morphological abnormalities in the cranial vault and often facial asymmetry. Deformation of the cranium caused by craniosynostosis provides information about which suture or sutures are affected. According to Virchow's law, calvarial growth is disrupted in the perpendicular plane to that of the fused suture, while compensatory growth occurs in the parallel plane [9]. Therefore, craniosynostosis can be classified in terms of the affected sutures

and the resulting malformation as follows: sagittal (scaphocephaly), metopic (trigonocephaly), coronal (anterior plagiocephaly), and lambdoid (posterior plagiocephaly) (**Figure 1.2**)[8].

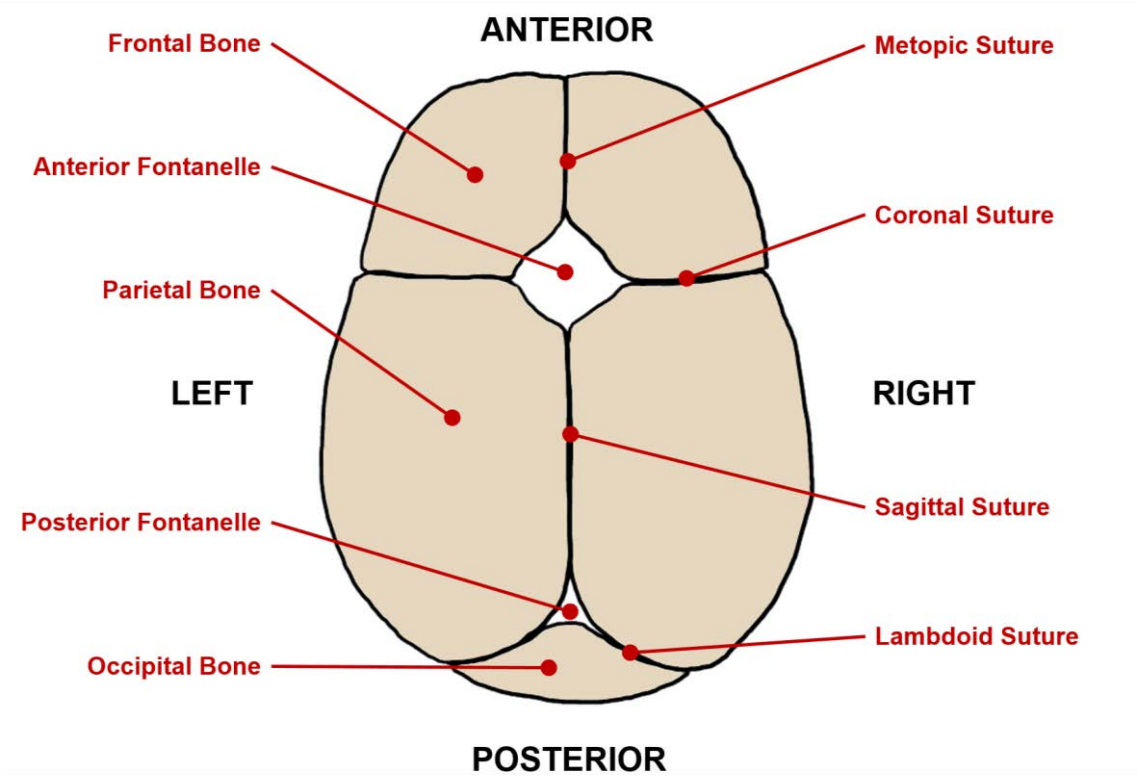

Figure 1.1. Anatomy of the cranium: bones and sutures.

1.1.1. Types of craniosynostosis

Sagittal craniosynostosis is the most common type of craniosynostosis, with an incidence of 1 in 2000 infants (40% of all nonsyndromic craniosynostosis) [8]. It affects the sagittal suture, producing restricted growth in the biparieto-temporal areas, sagittal ridging, and overcompensatory antero-posterior growth resulting in scaphocephaly, which consists of frontal bossing and occipital protrusion [7].

Metopic craniosynostosis is caused by the premature closure of the metopic suture, often resulting in a lateral growth restriction of the frontal bones leading to trigonocephaly. This malformation is characterized by a wedge-shaped forehead, a bony midline ridge, and a shortening of the anterior fossa [10]. Multiple studies indicate a remarkable increase in the number of diagnoses of this condition during the last decades, and confirm that metopic craniosynostosis is now the second most frequently seen type of craniosynostosis (27% of all nonsyndromic cases) [6].

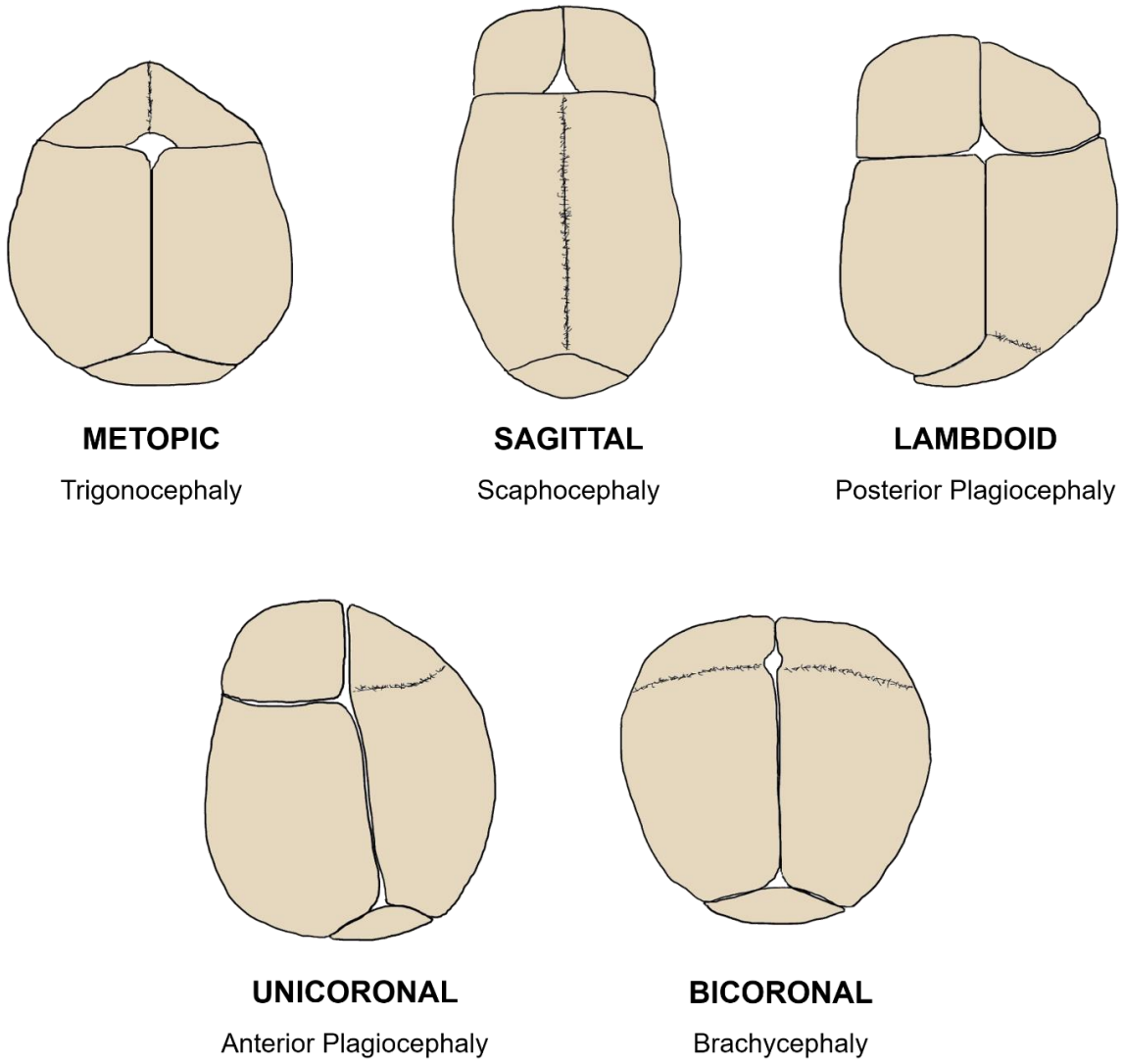

Figure 1.2. Types of craniosynostosis.

Unicoronal craniosynostosis is caused by the premature fusion of one of the coronal sutures, resulting in anterior plagiocephaly. This deformity is characterized by fronto-orbital asymmetry with ipsilateral forehead flattening, elevation and anterior displacement of the ear, deviation of the nasal root to the affected side, and an elevated and recessed supraorbital bar [11]. When both coronal sutures are affected, bicoronal craniosynostosis occurs. The fusion of both sutures results in a shortening of the cranium in the anterior-posterior direction and a widening of the forehead. Coronal craniosynostosis affects 1 in 10000 infants (20% of all nonsyndromic craniosynostosis).

Lambdoid craniosynostosis is a very rare condition (0-3% of all non-syndromic craniosynostosis). It is caused by the premature fusion of one of the lambdoid sutures at the

posterior part of the cranium. This condition, known as posterior plagiocephaly, is phenotypically characterized by an ipsilateral occipital flattening, ipsilateral frontal bossing, contralateral parietal and occipital bossing, and inferior and posterior displacement of the ear on the affected side [12].

1.1.2. Functional issues in craniosynostosis

The premature fusion of the cranial sutures may restrict the normal growth and development of the brain, resulting in the manifestation of functional issues. Increased intracranial pressure has been extensively documented in children with craniosynostosis due to a disparity between cranial vault volume and brain size [8]. Although this problem is more frequent in syndromic patients (30-40% incidence), it has also been reported in patients with single suture craniosynostosis (15-20% incidence) [13].

In addition, multiple studies have demonstrated that vision function is frequently impaired by craniosynostosis, and that the severity of visual problems is related to the type of craniosynostosis [14]. The morphological abnormalities of the orbital area and the displacement of the ocular structures may result in exorbitism, ocular dysmotility, optic atrophy, and blindness.

1.2. Diagnosis

An early diagnosis of craniosynostosis is crucial for management, prevention of complications, and consideration for early surgical correction [7]. Preoperative assessment of a patient with an abnormal cranial shape should include reviewing the medical history, physical examination, and the acquisition of any necessary diagnostic imaging studies.

Although the fusion of sutures is a clear indication of craniosynostosis, an evaluation of the cranial shape abnormality is crucial to determine the need for surgical correction. However, there are no objective methods available in the clinical practice to quantify cranial malformations, making the diagnosis and the surgical planning highly dependent on the surgeon's expertise [15].

Computed tomography (CT) imaging is the standard diagnostic tool for investigating potential craniosynostosis due to its ability to display bone tissue with high spatial resolution. CT enables the acquisition of fast and accurate three-dimensional (3D) reconstructions of the

anatomy and the evaluation of cranial morphological abnormalities and the state of the cranial sutures (**Figure 1.3**) [16].

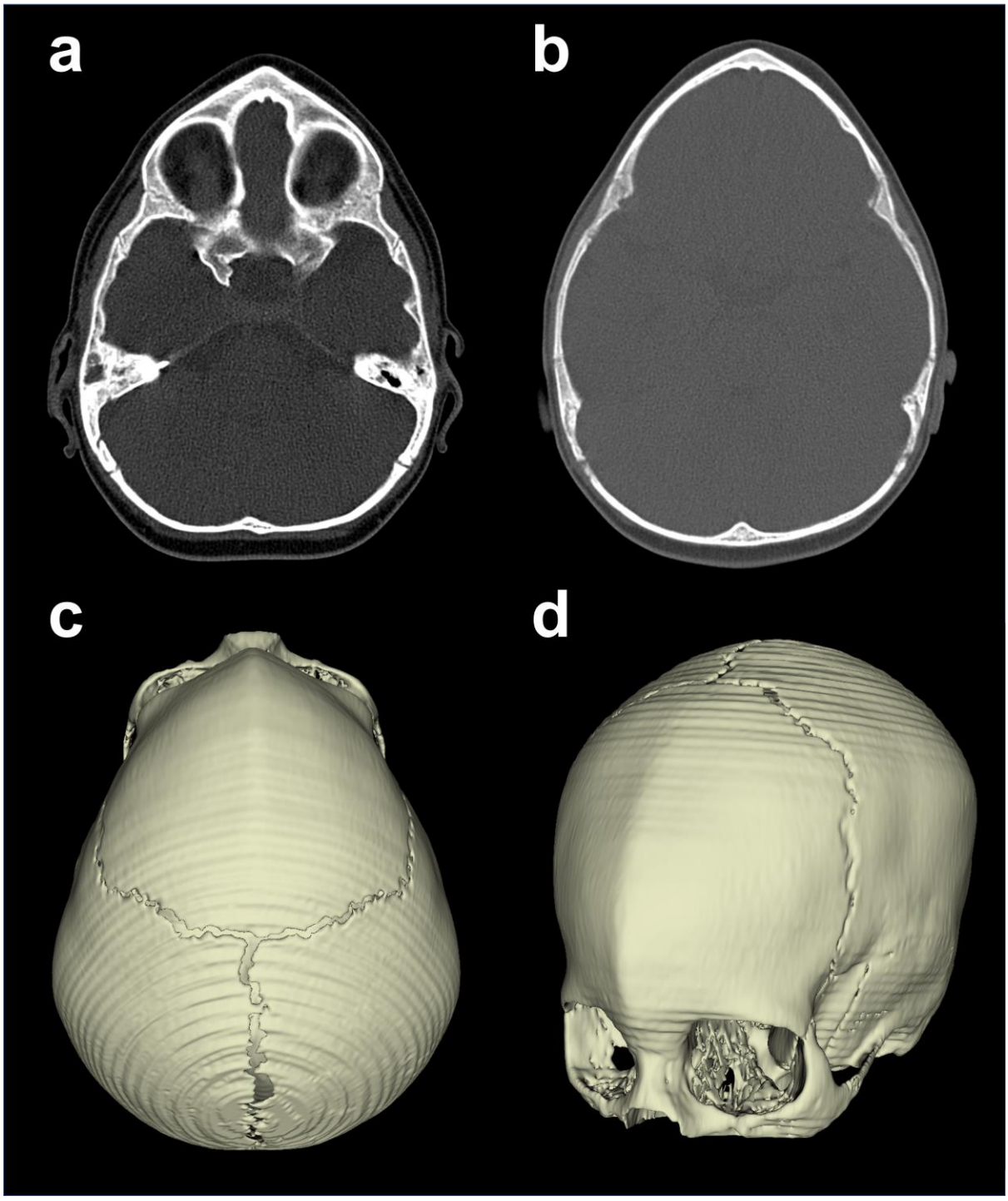

Figure 1.3. Axial CT slices and 3D reconstruction of the cranium of a patient with metopic craniosynostosis. The fusion of the metopic suture and severe trigonocephaly deformation can be observed.

The analysis of the preoperative morphology is the most critical step when planning surgery [17]. A 3D reconstruction of the preoperative imaging may not be sufficient for an accurate diagnosis. A comparison of the patient's anatomy with a normal (healthy) morphology is essential to comprehend the cranial malformations and determine the best approach for surgical correction. In this context, several methods based on statistical shape models have been proposed to eliminate subjectivity and to increase reproducibility during diagnosis and planning. The idea of these approaches is to define the normal cranial shape from a dataset of normative subjects and compare it with the subject's pathological shape under evaluation to provide a patient-specific diagnosis and reference for planning.

Saber et al. [18] generated a library of normative pediatric skulls from CT scans of 103 normative subjects. Each CT scan was segmented, and a set of reference points was distributed onto the outer surface of the skull. Then, all 3D models were aligned and an average composite skull, "super-skull", was created from the data of all 103 patients providing an estimation of what a normal child cranium looks like. For each new subject with craniosynostosis, the composite skull model can be scaled to their age and head circumference to obtain an appropriate normative reference shape for that subject. This approach requires age stratification and suffers from the limitation of defining landmark correspondence.

Later, Mendoza et al. [19] presented a statistical shape model of normal anatomy constructed via principal component analysis (PCA). Each new subject under study is projected into the PCA shape space, and its closest normal cranial shape is computed through similarity metrics in the PCA space. Moreover, age-invariance is achieved using a registration algorithm that aligns and scales the subject's cranial shape with the reference normal shape only considering the anatomy at the base of the skull, where pathological deformations during craniosynostosis are negligible [20]. This methodology presents an improvement in comparison with previous approaches [18], [21], which were based on population averages or age-matched templates, and accounts for normal variations in healthy anatomy (e.g. due to sex or ethnicity [22]).

Comparison of the cranial shape of a patient with a normative reference shape, computed from statistical shape models, can be used to discriminate pathological shape abnormalities from healthy phenotypes. The malformation field for each subject can be computed by measuring the Euclidean distance from each vertex of the subject's skull surface

mesh to the closest vertex in the normative reference mesh. Local malformation values in the different regions of the cranium can then be visualized using a color map (**Figure 1.4**).

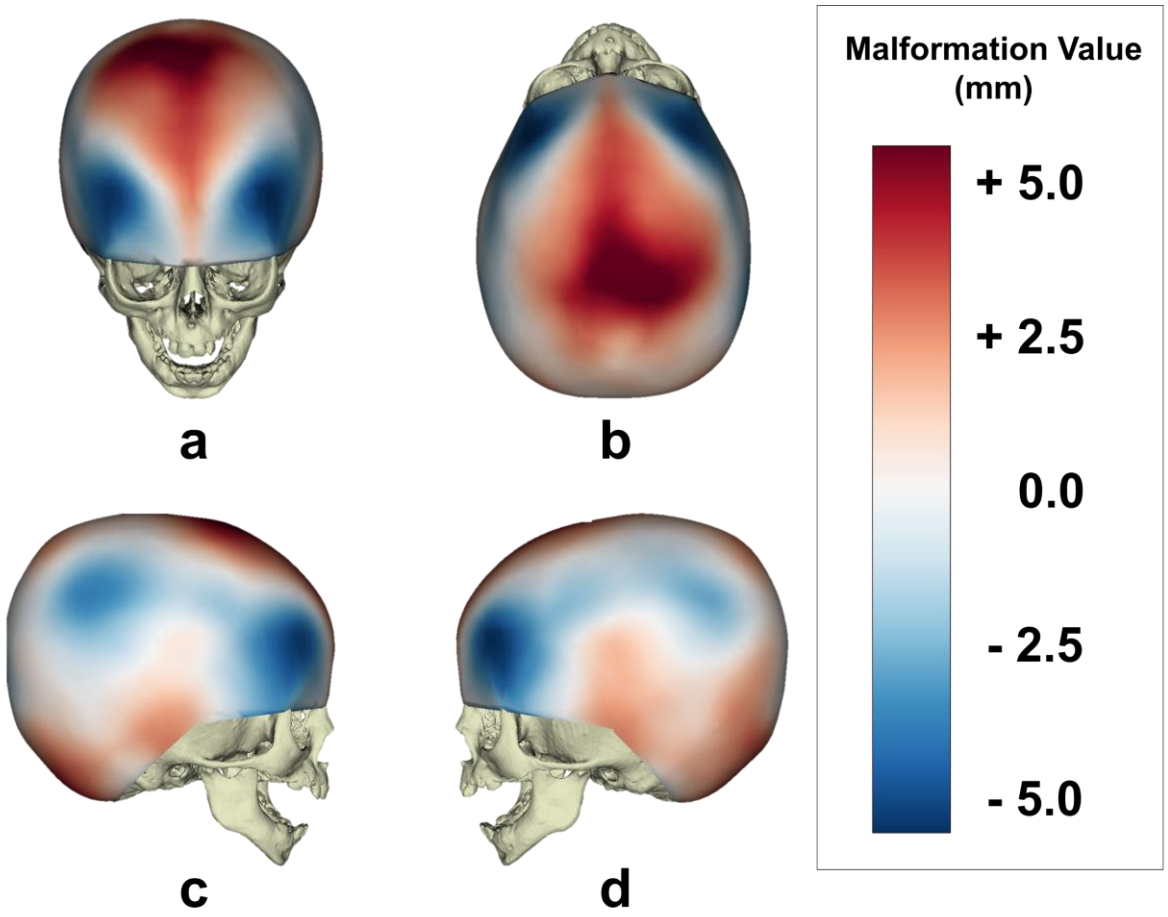

Figure 1.4. Malformation field of a patient with metopic craniosynostosis computed by comparing the preoperative cranial shape with a patient-specific normative reference shape: (a) anterior view, (b) superior view, (c) right view, and (d) left view.

Malformation fields provide valuable information on the degree of morphological abnormality and can be used for automatic diagnosis. Mendoza et al. [23] used a dataset of 18 patients with metopic craniosynostosis to identify three robust landmarks for diagnosis and characterization of trigonocephaly. The malformation field for each patient in the dataset was averaged across metopic craniosynostosis subjects and represented on a template of normal anatomy. Then, optimal landmarks were defined on the points of maximum average malformation on the frontal bone region. Wood et al. [24] demonstrated that the interfrontal angle value, measured using these three optimal landmarks, presented significantly different values in metopic craniosynostosis patients and healthy phenotypes. They obtained an accuracy of 98% for the diagnosis of metopic synostosis using this methodology. Similar approaches

have been proposed for the quantification of other types of craniosynostosis, such as unicoronal [25] or sagittal [26].

Most methods for quantitative evaluation of cranial shape are based on 3D reconstructions generated from CT scans. However, this technique involves the exposure of the infants to ionizing radiation and frequently requires sedation or anesthesia. For these reasons, CT imaging is rarely used for postoperative evaluation of surgical outcomes and patient follow-up [27].

Due to the limitations of CT imaging, 3D photography has been introduced for the evaluation of cranial malformations. The validity and reliability of this technology to obtain craniofacial anthropometric measurements have already been demonstrated [28]–[30]. In particular, Porras et al. [31] showed how 3D photography discriminates between patients with and without craniosynostosis with a sensitivity above 94%. Other authors have shown that it is possible to calculate intracranial volume with this technique [32].

3D photography followed by statistical shape analysis provides a powerful tool for fast, non-invasive, and radiation-free quantification of cranial shape, presenting a valuable alternative to CT imaging. This technology enables the visualization and quantification of global and regional cranial malformations without exposure to ionizing radiation. Besides, the acquisition of 3D photographs is very fast (below 1 second), avoiding the need for sedation or anesthesia of the infant. Multiple 3D photographs can be acquired for diagnosis and postoperative evaluation of the surgical outcomes. The main limitation of 3D photography is the difficulty in capturing hair. This issue is easily solved by covering the patient's hair during the acquisition with a tight nylon skull cap to avoid artifacts [33]. A suboptimal covering of the hair may cause bumps on the surface that will affect cranial shape quantification.

1.3. Surgical treatment

Once a patient is diagnosed with craniosynostosis, surgical correction is the standard of care for most moderate to severe deformities. The objective of surgical correction is to release the fused suture and to normalize calvarial shape.

Minimally invasive techniques (endoscopic, linear craniectomy) have been proposed as an alternative to open surgery [34]. These procedures are usually followed by postoperative helmet-molding therapy to facilitate appropriate changes in the cranial morphology [35].

However, these limited approaches are typically reserved for the treatment of mild-to-moderate deformities affecting young patients (less than six months old) [8].

Another alternative for surgical correction is distraction osteogenesis, which has been accepted by many surgeons [36]. This technique involves the application of graduated tension to the bone tissue using external fixation devices. The main advantage of this procedure is the reduced invasiveness in comparison with open cranial vault remodeling, since the dissection of the dura is limited [37]. However, it shows limitations such as long treatment duration and, in some cases, secondary surgical interventions.

The most common approach for surgical correction is open cranial vault remodeling, which aims to normalize the calvarial shape to increase intracranial volume and reduce the risk of elevated intracranial pressure. Typical cranial vault remodeling involves an osteotomy, division of the affected bone region into multiple fragments, and a reconfiguration of those fragments to achieve a normal cranial morphology. Finally, the remodeled bone fragments are transferred to the patient and rigidly fixed and secured using resorbable plates [38], [39]. This operation is typically performed before the first year of life to maximize reossification and benefit from the malleability of bone tissue [2].

1.3.1. Fronto-orbital advancement

Fronto-orbital advancement (FOA) is a surgical procedure used to treat those types of craniosynostosis causing malformations in the fronto-orbital region of the cranium (i.e. metopic craniosynostosis, unicoronal craniosynostosis, and bicoronal craniosynostosis). The objective of FOA is to release the fused metopic suture and normalize the calvarial shape by remodeling and advancing the fronto-orbital region.

First, a bicoronal S-shaped incision is performed to expose the surface of the fronto-orbital region. Then, subperiosteal skin flaps are created and elevated until the entire frontal bone, nasofrontal junction, and supraorbital ridge are exposed (**Figure 1.5a**).

After exposure of the cranial surface, the osteotomy lines are outlined with a marking pen (**Figure 1.5b**). Then, surgeons perform a bifrontal craniotomy to remove the frontal bones and fronto-orbital osteotomies to separate the supraorbital bandeau **(Figure 1.5c** and **Figure 1.5d**). Tenon extensions are created bilaterally to facilitate advancement and subsequent fixation of the bone tissue fragments in the supraorbital bar. Although multiple techniques have

been proposed, the most common surgical approach is to divide the supraorbital bar into four fragments and the frontal bone into two fragments [40].

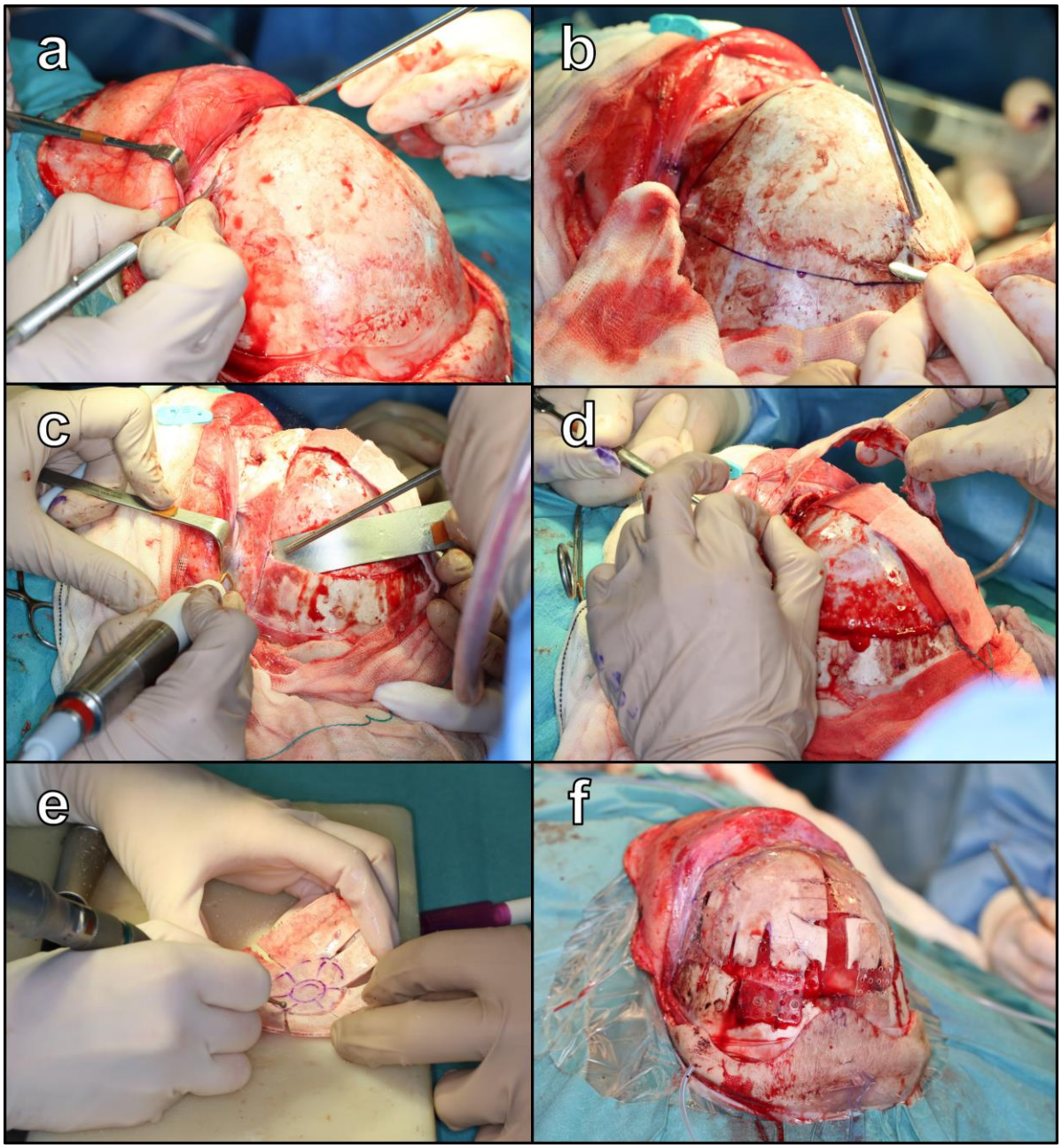

Figure 1.5. Surgical workflow for FOA: (a) exposure of fronto-orbital bone surface, (b) osteotomy lines marked in the bone tissue surface, (c) osteotomy of the left tenon extension of the supraorbital bar, (d) removal of the supraorbital bar, (e) remodeling of the bone fragments on a sterile table, and (f) fixation and stabilization of bone fragments with resorbable plates and screws.

The supraorbital bar is taken to a sterile table where it is cut and reshaped to achieve the desired target shape. The two halves of the supraorbital bar are typically separated and opened to increase the bitemporal width and the central angle. Moreover, closing wedge osteotomies are placed laterally in the bandeau to enable the bone tissue to curve at the tenon

extension for lateral continuity [41]. Multiple bony segments of bandeau are fixed and stabilized into the patient's final position using resorbable plates and screws. After fixation of the supraorbital bar, the bifrontal coronal bone flap is typically cut, bent, and reshaped to match the outline of the bandeau and to achieve the desired cranial shape (**Figure 1.5e**). The remodeled bifrontal coronal flap is fixed and stabilized using resorbable plates and screws (**Figure 1.5f**). Finally, skin closure is carried out by approximating the pericranial flaps and secured with sutures.

1.4. Technologies to improve surgical outcome

Nowadays, surgical correction of craniosynostosis is still highly dependent on the subjective assessment and artistic judgment of the surgeons [42], [43]. Multiple technologies have been evaluated and integrated into surgical workflows to improve the accuracy and reproducibility of craniosynostosis surgical interventions. Technological advancements have been focused on providing tools to facilitate intervention planning and intraoperative decision making.

1.4.1. Computer-assisted planning

The objective of the surgical correction is to remodel the affected bone tissue to create a normal cranial shape. However, “normal” cranial shape is usually defined through mental constructions by experienced craniofacial surgeons, and is thus highly subjective. Therefore, determining the best approach to restore normal shape remains a subjective surgical art, leading to a less reliable prediction of the surgical outcome for each patient.

Virtual surgical planning (VSP) has been proposed to enhance the accuracy, efficiency, and reproducibility of craniosynostosis surgeries [17], [44]. Surgery can be simulated preoperatively on a computer workstation, reducing the time-consuming intraoperative decision making. During VSP, osteotomies are defined and bone fragments are configured to achieve the desired target cranial morphology and features (**Figure 1.6)**. However, most reported techniques for VSP are based on free-hand approaches requiring extensive manual human interactions [44]–[46]. Furthermore, “normal” cranial shapes to target are usually subjectively defined by craniofacial surgeons through mental constructions. Therefore, these approaches are still highly subjective and dependent on the physicians’ judgment and experience.

The accuracy of VSP can be improved using statistical shape models of normal anatomy constructed from the cranial shapes of normative subjects [19]. These models can provide a normative reference shape to target during surgical treatment personalized to each patient, providing a valuable reference during the planning stage. Therefore, fragments can be virtually configured to achieve the desired target shape defined by the statistical shape model [47], [48].

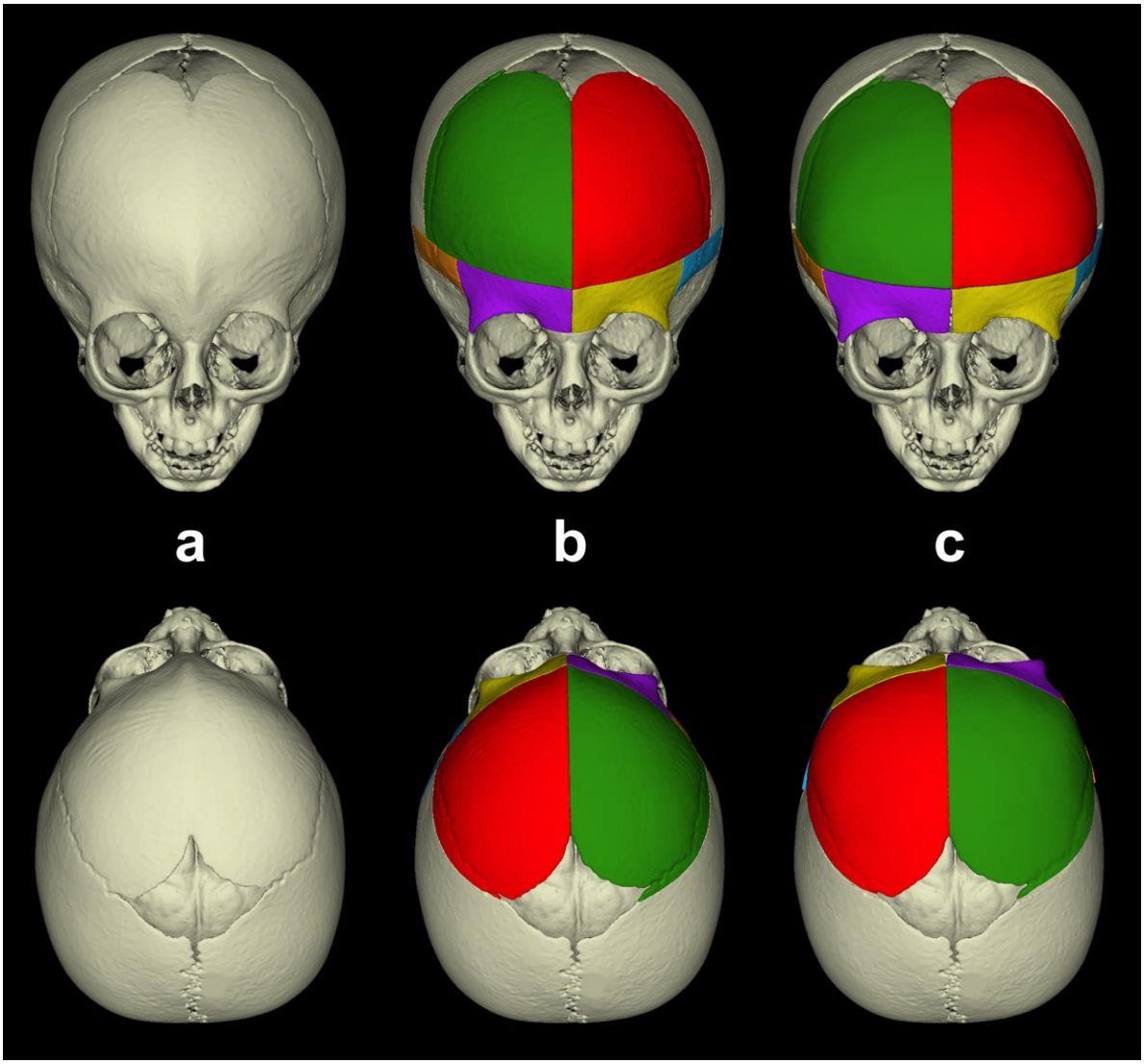

Figure 1.6. VSP of open cranial vault remodeling for correction of metopic craniosynostosis: (a) 3D model of the cranium obtained from preoperative CT scan, (b) definition of osteotomy lines and fragments, and (c) reconfiguration of bone fragments to achieve desired postoperative cranial shape.

1.4.2. Computer-aided design and manufacturing

Transforming the preoperative virtual plan into a reality is a challenging endeavor highly dependent on surgical experience. Computer-aided design and manufacturing (CAD/CAM) enables the fabrication of patient-specific cutting guides and shaping templates

that can be used during surgery to guide osteotomy and remodeling according to the preoperative virtual plan [44].

Surgical cutting guides are designed to fit into the affected anatomical region using a 3D reconstruction of the cranial surface as a reference (**Figure 1.7a**) and to guide the location of osteotomies as defined during the planning stage (**Figure 1.7b**) [49]. Besides, shaping templates can also be designed to assist during the intraoperative remodeling of the cranial vault [39], [43]. These templates enable the configuration of the resected bone fragments following the shape predefined during VSP. Each of the fragments is fitted into their corresponding position on the template (**Figure 1.7c** and **Figure 1.7d**) and rigidly fixed using resorbable plates and screws.

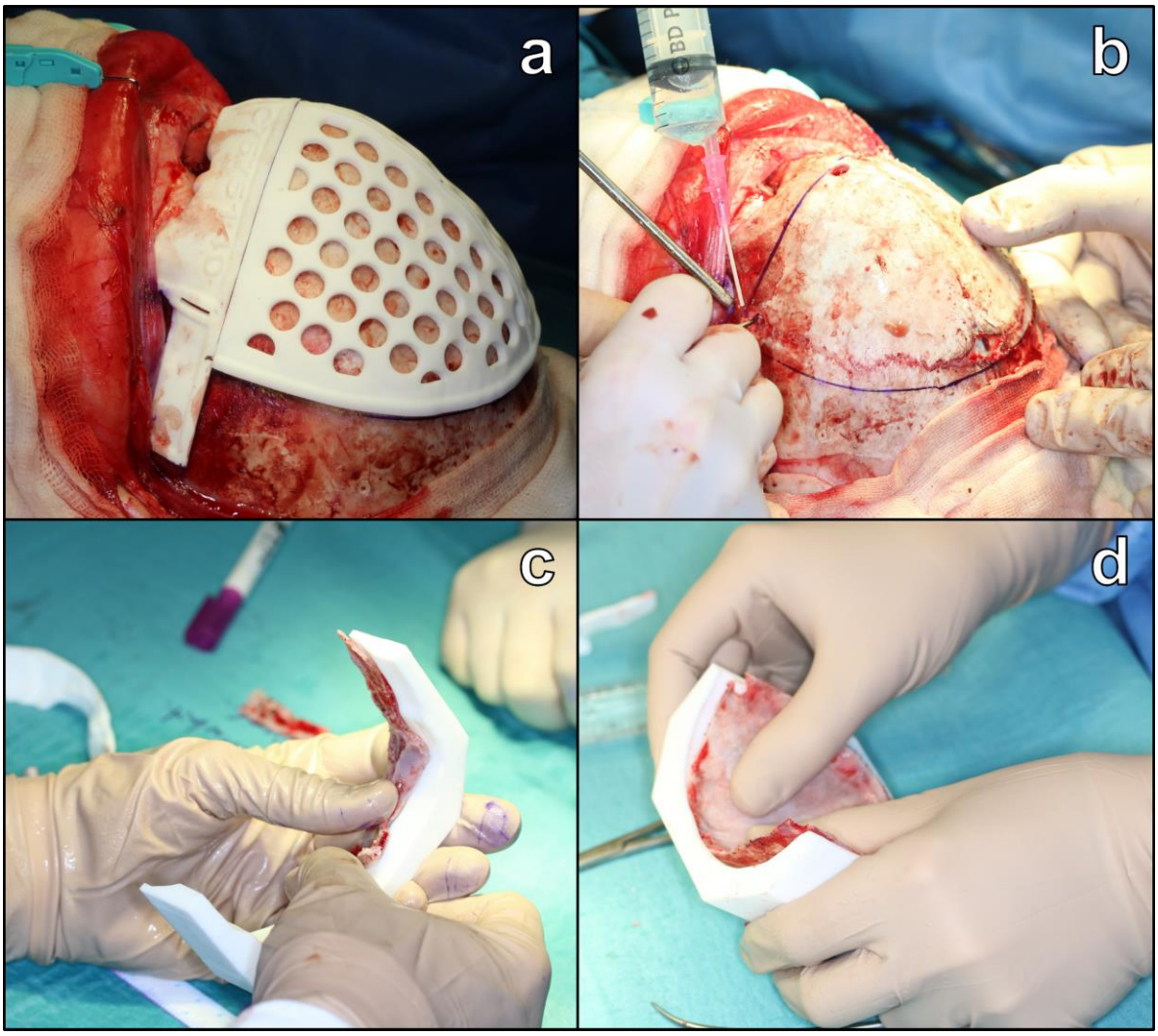

Figure 1.7. Cutting guides and templates used during FOA for surgical correction of a patient with metopic craniosynostosis. (a) Placement of surgical cutting guides on the calvarium, (b) marking of planned osteotomies on the calvarium, (c) shaping template for supraorbital bar remodeling, and (d) shaping template for frontal bone remodeling. Image adapted from [49].

Accurate 3D reconstructions of the cranium are required to ensure optimal design and application of CAD/CAM guides and templates. CT imaging is the standard technique used to generate 3D models of the cranium prior to surgery. However, a new magnetic resonance imaging (MRI) technique called “black bone” has already been validated as a reference for CAD/CAM craniosynostosis surgery [50]. Therefore, MRI could be used to avoid CT scans and infants' exposure to ionizing radiation.

Fabrication of the patient-specific surgical cutting guides and templates must ensure a fast availability and safe sterilization without the risk of deformation. For this reason, manufacturing is commonly performed with selective laser sintering and polyamide material [49]. Other approaches have proposed the use of stainless steel templates [42]. Both types of materials can be sterilized before surgery using standard autoclave protocols [43].

Several studies have demonstrated the advantages of combining VSP and CAD/CAM guides and templates for craniosynostosis surgery [39], [44], [51], [52]. This technology has been applied to single-suture [49] and multiple-suture craniosynostosis [53]. Results indicate improved surgical outcomes and reduced operative time. These technologies could also reduce the experiential gap between younger and veteran craniofacial surgeons by accelerating the learning curve of future trainees. Overall, these studies demonstrate that the inclusion of this technology in the surgical workflow improves the efficiency, accuracy, and reproducibility of the interventions.

1.4.3. Image-guided surgery

Patient-specific CAD/CAM guides and templates enable cutting the affected bone tissue and remodeling of the bone fragments as defined during the VSP. However, after remodeling, reshaped bone tissue must be manually placed and fixed to the patient. In most cases, the reshaped bone tissue placement is assessed visually, and the final position may differ from the preoperative plan. Therefore, surgical outcomes can be compromised by slight positional and rotational variations of the remodeled bone tissue position.

In this context, different methodologies have been reported to assist during bone fragment placement. Hochfeld et al. [54] proposed using a stereotactic frame and Schanz screws to control the fragments' position during the remodeling phase. Individual bone fragments are attached to the Schanz screws by bone brackets and configured based on a reference cranial shape obtained from a statistical shape model. Then, the frame is assembled

in the surgical field to confirm fragment positions, and, finally, the remodeled fragments are rigidly fixed to each other by resorbable plates.

Later on, Kobets et al. [55] described a guidance system to confirm bone fragment placement through intraoperative CT imaging. First, remodeling of the cranial vault is performed exclusively based on the subjective assessment of the surgeons. An intraoperative CT imaging scan is then acquired and aligned with the preoperative plan for comparison and analysis (**Figure 1.8**). Finally, any necessary corrections in the bone fragment positions are applied before surgery is completed.

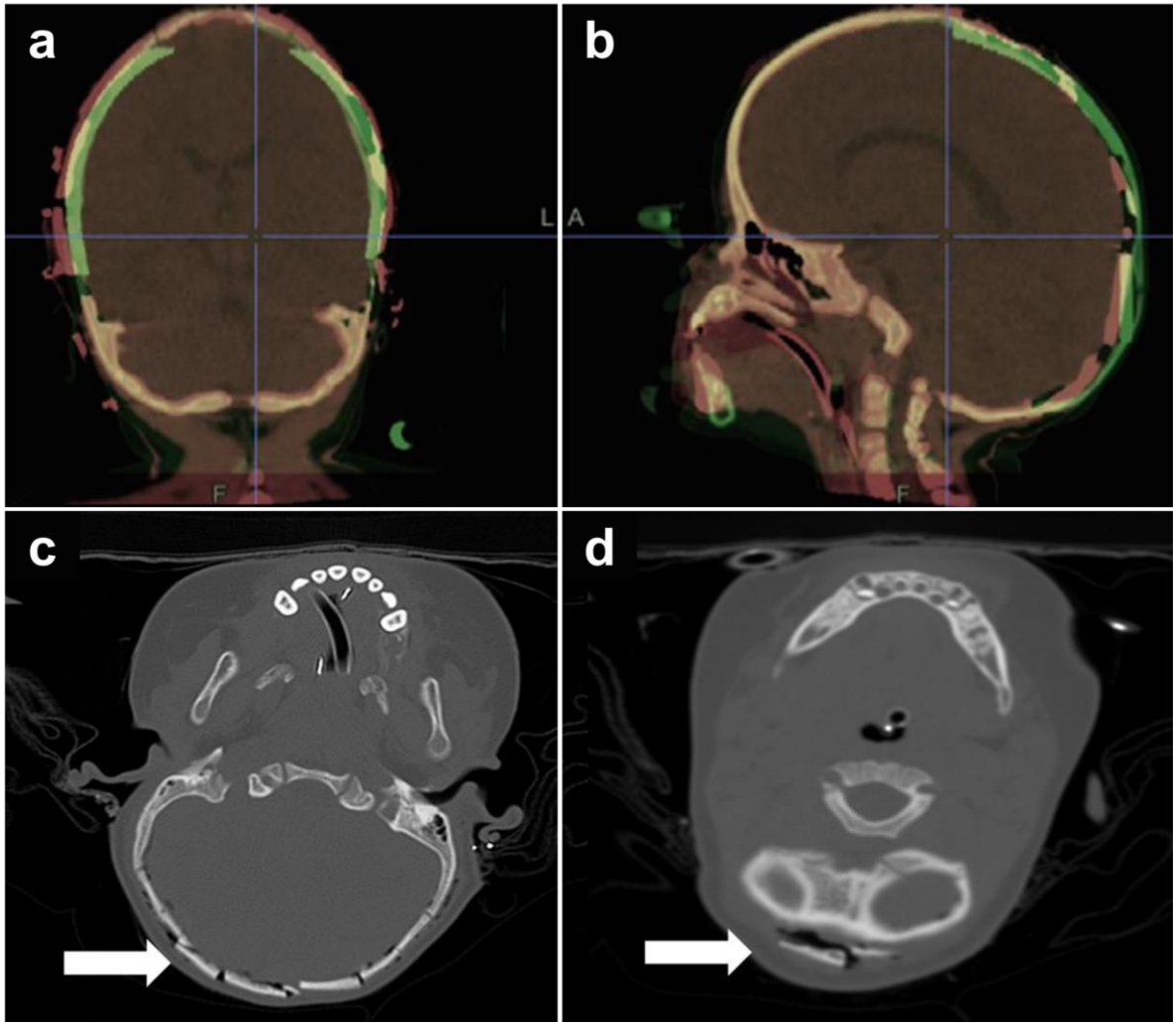

Figure 1.8. Intraoperative CT scan acquired during surgical correction of a patient with sagittal craniosynostosis. VSP is overlaid in green in the coronal (a) and sagittal (b) slices of the CT scan for comparison. Axial slices show misplaced bone fragments in the suboccipital region (c and d). Image adapted from [55] (figure reprinted with permission from the copyright holder, Springer Nature).

Although image-guided surgery technology could assist surgeons during craniosynostosis surgical interventions, there are no standard methodologies used in routine clinical practice. New technological advancements are still required to overcome the limitations of existing techniques and to further reduce the subjectivity and variability in craniosynostosis surgery.

The content of this chapter has been published as a chapter of the book "Craniosynostosis – New Perspectives of Prevention and Treatment":

D. García-Mato, J. Pascau, S. Ochandiano. "New Technologies to Improve Surgical Outcome during Open-Cranial Vault Remodeling". In: Craniosynostosis - New Perspectives of Prevention and Treatment. IntechOpen, 2020.

2

MOTIVATION AND OBJECTIVES

2.1. Motivation

Nowadays, interventional planning and surgical correction of craniosynostosis are still highly dependent on the subjective assessment and artistic judgment of surgeons [49]. As a result, there is high variability in surgeons' performance and, thus, in the surgical outcomes. Although the more experienced craniofacial surgeons may achieve optimal surgical results, more complications may arise among the less experienced [42]. Several studies evaluating the long-term postoperative results after surgical correction between 1987 and 2013 have reported complication rates varying between 2% and 23.3%, and reoperation rates as high as 10% to 36% [56]–[62]. In addition, these studies reported that between 9.9% and 36% of the patients presented moderate-to-severe malformations after surgical treatment, causing suboptimal aesthetic outcomes (Whitaker class III/IV). Therefore, there is a clinical need to improve the reproducibility of surgical outcomes and reduce inter-surgeon variability in craniosynostosis surgery.

During the last years, preoperative VSP has become a standard practice in many hospitals. This technology enables the craniofacial surgeons to simulate multiple treatment strategies and determine the best approach for cranial vault remodeling. Although several software platforms have been specifically developed for craniosynostosis surgical planning, most of them require manual interactions to define the optimal configuration of bone fragments

and, thus, are still highly dependent on the subjective judgment of the surgeons. Recently, new algorithms have been proposed to automatically compute a normative reference shape personalized to each patient using a statistical shape atlas [18], [19]. Bone fragments can then be automatically configured to match the desired normal shape [47], [48].

However, previous methodologies for automatic planning have been validated using only a few generic osteotomy templates that did not include bilateral tenon extensions of the supraorbital bar, which are important during FOA to facilitate advancement and subsequent stabilization of the remodeled fragments. In addition, long-term postoperative follow-up studies of craniosynostosis patients have shown inadequate cranial development after surgical correction [63]. Therefore, targeting a statistically normal cranial shape does not guarantee optimal long-term aesthetic and functional outcomes. In this context, many authors have reported that an overcorrection must be performed in anticipation of relapse or lack of growth [51], [59], [62], [64], [65]. There are no methodologies for automatic planning of craniosynostosis that consider and apply overcorrection during the virtual configuration of the fragments.

Furthermore, transforming the preoperative VSP into reality during the surgical intervention is crucial to ensure optimal surgical outcomes. However, this step is challenging and highly dependent on the experience and judgment of the surgeons. The objective is to replicate the virtual osteotomies and reconfiguration of the fragments in the actual surgery. CAD/CAM technology is currently being used by many hospitals to fabricate customized surgical guides and templates that can assist surgeons during osteotomy and reshaping of the bone fragments. However, the final step involves the placement and fixation of the bone tissue fragments to the patient’s anatomy. This process is typically performed manually, and slight mismatches with respect to the VSP can compromise the patient's aesthetic outcome. There are no standard techniques to accurately control bone fragment positioning during craniosynostosis surgeries.

The use of intraoperative CT imaging for guidance was described and evaluated by Kobets et al. [55]. Although this technique provides accurate 3D reconstructions of the patient’s anatomy during surgery, it requires the exposure of the infant to ionizing radiation, increases operative time, and does not enable real-time adjustment of bone fragments position to achieve the desired surgical outcome. Therefore, its application into the standard clinical practice is limited.

Another approach for intraoperative guidance was proposed by Hochfeld et al. [54]. This methodology is based on the use of a stereotactic frame and Schanz screws to control the position of bone fragments. This technique has been evaluated in 14 patients with craniosynostosis, and the reported results are positive. However, the incorporation of this technique into the standard clinical practice is limited by the increased surgical time, complexity, and invasiveness associated with the fixation of the frame to the patient's anatomy.

Standard navigation systems have not been used for guidance during craniosynostosis surgical correction due to the risk, invasiveness, and discomfort associated with head immobilization and the attachment of landmarks for intraoperative registration. The thickness and fragility of infants' cranial bone tissue are not suitable for invasive head immobilization or the attachment of navigation reference frames [66]. Therefore, cranial fixation is rarely used in patients under two years of age due to the potential risk of skull and brain injury from pin fixation [67].

New advancements in image-guided surgery are still required to develop surgical navigation systems suitable for intraoperative guidance during open cranial vault remodeling.

2.2. Objectives

The main objective of this thesis is to explore different approaches to improve the surgical management of craniosynostosis by reducing subjectivity in all stages of the process, from the preoperative virtual planning phase to the intraoperative performance. These improvements will lead to increased accuracy and reproducibility of the surgical outcomes and reduced inter-surgeon variability. The objectives of this work are the following:

(1) To develop a new framework for automatic interventional planning of craniosynostosis surgery estimating optimal osteotomy locations, calculating the transformation of each fragment to achieve a statistically normal cranial shape, and including overcorrection into the plan to ensure accurate long-term surgical outcomes.

(2) To study 3D photography for the radiation-free and non-invasive evaluation of the surgical outcome during open cranial vault remodeling, providing valuable feedback and enabling surgeons to perform corrections in the bone fragment positions in order to achieve the desired surgical outcomes.

(3) To design and evaluate an optimal workflow for intraoperative navigation to guide the placement and fixation of bone fragments during open cranial vault remodeling without requiring the immobilization of the patient's head or the invasive fixation of external markers prior to surgery.

(4) To explore the use of augmented reality visualization for intraoperative guidance in open cranial vault remodeling.

The work presented in this thesis has been carried out in Universidad Carlos III de Madrid in collaboration with the Department of Oral and Maxillofacial Surgery and the Department of Neurosurgery of Hospital General Universitario Gregorio Marañón in Madrid, Spain. Moreover, an extensive collaboration has been established with the Sheikh Zayed Institute for Pediatric Surgical Innovation at Children's National Hospital in Washington, DC, United States.

3

COMPUTER-ASSISTED PLANNING

3.1. Introduction

Surgical correction of metopic craniosynostosis is typically performed by open cranial vault remodeling with FOA. The objective of the surgery is to release the fused suture and to normalize the calvarial shape. FOA consists of three main steps: (1) removal of the affected bone tissue in the fronto-orbital region, (2) reshaping of the bone tissue into the most appropriate shape for the patient, and (3) placement and fixation of the remodeled bone fragments [38].

All these steps of the surgical procedure rely on the subjective judgment of the surgeon to determine the osteotomy locations and the most optimal configuration of the fragments to achieve the desired target cranial shape. As a result, although the more experienced surgeons can achieve optimal surgical outcomes, it is more open to error in the less experienced [42].

Computer-assisted surgical planning has been proposed to increase accuracy, efficiency, and reproducibility of craniosynostosis surgeries [17], [44]. VSP enables to define osteotomies and to reconfigure the fragments according to the desired shape and features. During VSP, surgeons can compare multiple treatment strategies and determine the best overall correction approach. Besides, VSP can be combined with CAD/CAM surgical guides and templates to facilitate the translation of the planning into the operating room. Several studies

have demonstrated a decrease in operative time and improved postoperative cranial morphology when using VSP [68], [69].

Multiple approaches for VSP are available in the literature. However, most reported techniques for interventional planning are based on manual interactions to define osteotomies and reconfiguration of fragments required to achieve the desired target shape [44]–[46]. Furthermore, most of the available virtual planning methodologies do not include references of normative cranial shape to target, so experienced craniofacial surgeons usually define "normal" cranial shapes through mental constructions. Therefore, these approaches are still highly subjective and dependent on the physician's experience.

Only a few automatic surgical planning techniques have been developed to determine the optimal shape to target during FOA [47], [48]. These algorithms are based on statistical shape models generated from databases of normative subjects. Learning from normative data, the methods determine the optimal cranial shape to target during surgical treatment, personalized to each subject. An optimization approach is then employed to rearrange the bone fragments in the most appropriate configuration that minimizes cranial malformations with respect to the optimal normal shape.

However, these automatic planning frameworks present limited clinical applicability due to the definition of the bone fragments required for cranial vault remodeling. These algorithms were validated using only a few surgical templates that did not include bilateral tenon extensions of the supraorbital bar, which are important during FOA to facilitate advancement and subsequent stabilization of the remodeled fragments.

It is important to note that although significant head shape improvements have been quantified after surgical treatment [31], long-term postoperative follow-up evaluations of craniosynostosis patients have demonstrated an abnormal cranial development following surgery [63]. Therefore, achieving a statistically normal cranial shape may not be sufficient to ensure optimal long-term aesthetic and functional outcomes.

In this context, many authors have reported that an overcorrection must be performed in anticipation of relapse or lack of growth, and factored into the VSP [51], [59], [62], [64], [65]. To our knowledge, there are no methods for automatic surgical planning of craniosynostosis that incorporate overcorrection during the virtual configuration of the fragments [70].

3.2. Objective

This work aims to present and evaluate a new approach for automatic planning of fronto-orbital advancement to treat metopic craniosynostosis. Our method follows the standard surgical approach and includes overcorrection to ensure optimal long-term outcomes for the patients. This framework has been integrated into a customized software that enables surgeons to introduce manual corrections into the VSP according to their surgical needs and preferences.

3.3. Methods

In this section, we first describe the database of patients used in this study. Then, we detail the methodology for cranial shape evaluation, bone fragment estimation, and virtual remodeling. Finally, we describe the metrics used for the assessment of our planning software. A summary of the proposed workflow for automatic planning is presented in **Figure 3.1**.

3.3.1. Database

Our automatic planning framework was evaluated on 9 patients (mean age 10.68 ± 1.73 months; range 8-13 months; 4 girls and 5 boys) with metopic craniosynostosis. All patients were treated with an open cranial vault remodeling with FOA in our center. Available data for each patient includes a preoperative CT scan and a manual VSP performed by experienced craniofacial surgeons. Manual VSP includes virtual osteotomies and reconfiguration of fronto-orbital bone fragments according to the surgeon's clinical judgment. This manual VSP was used as a reference during surgical intervention.

In addition, we used a database including CT scans of 201 subjects without cranial disease (mean age, 23 ± 20 months; range, 0-72 months; 89 girls and 112 boys) to build a statistical shape atlas of the normative cranial shape [31]. One normative subject was selected as a reference template to establish a common coordinate system for evaluation.

3.3.2. Preoperative Cranial Shape Evaluation

Comprehensive, 3D volumetric analysis of the patient's cranial anatomy compared with normal morphology is crucial to determine the severity of the malformations and the best approach for surgical correction. To quantify malformation, we followed the procedure described in [19]. First, a statistical shape model was built from the CT scans of the 201

normative subjects. Then, we aligned each subject with metopic craniosynostosis in our database with the reference template in the atlas and computed a patient-specific, normative reference cranial shape. Finally, cranial malformations were quantified as the local Euclidean distance between the normative reference calculated from the multi-atlas and the patient's cranial shape.

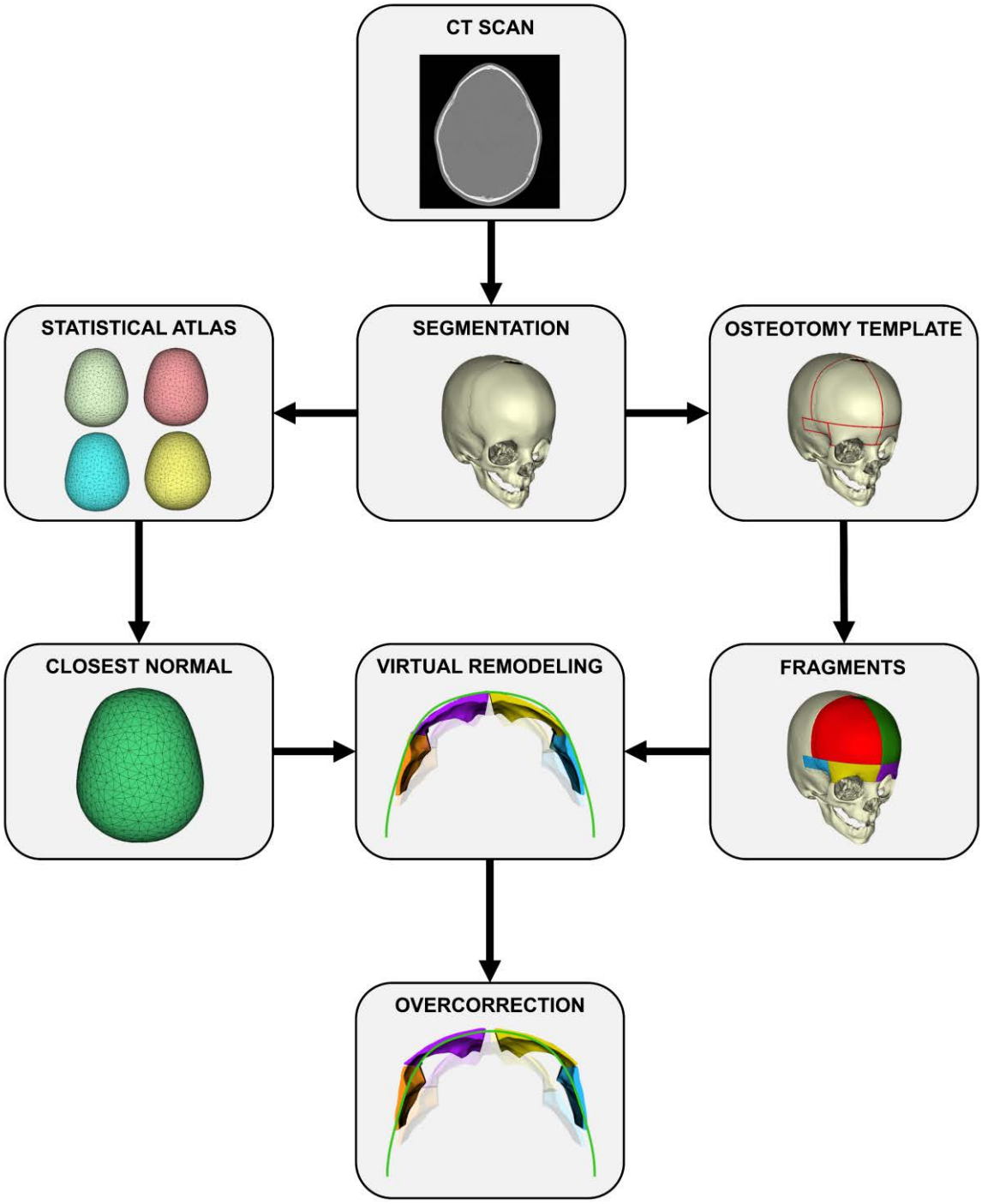

Figure 3.1. Proposed workflow for automatic surgical planning of FOA.

3.3.3. Osteotomy Planning

An osteotomy template was manually defined by specialized craniofacial surgeons based on their previous experience in craniosynostosis VSP. A total of eight cutting planes were defined in the fronto-orbital region of the reference template (normative subject) in the atlas, using the Frankfurt plane as a reference (**Figure 3.2**). The supraorbital axial, frontozygomatic, inferior temporal, and frontonasal planes are parallel to the Frankfurt plane. The coronal, sphenofrontal, posterior temporal, and midsagittal planes are perpendicular to the Frankfurt plane.

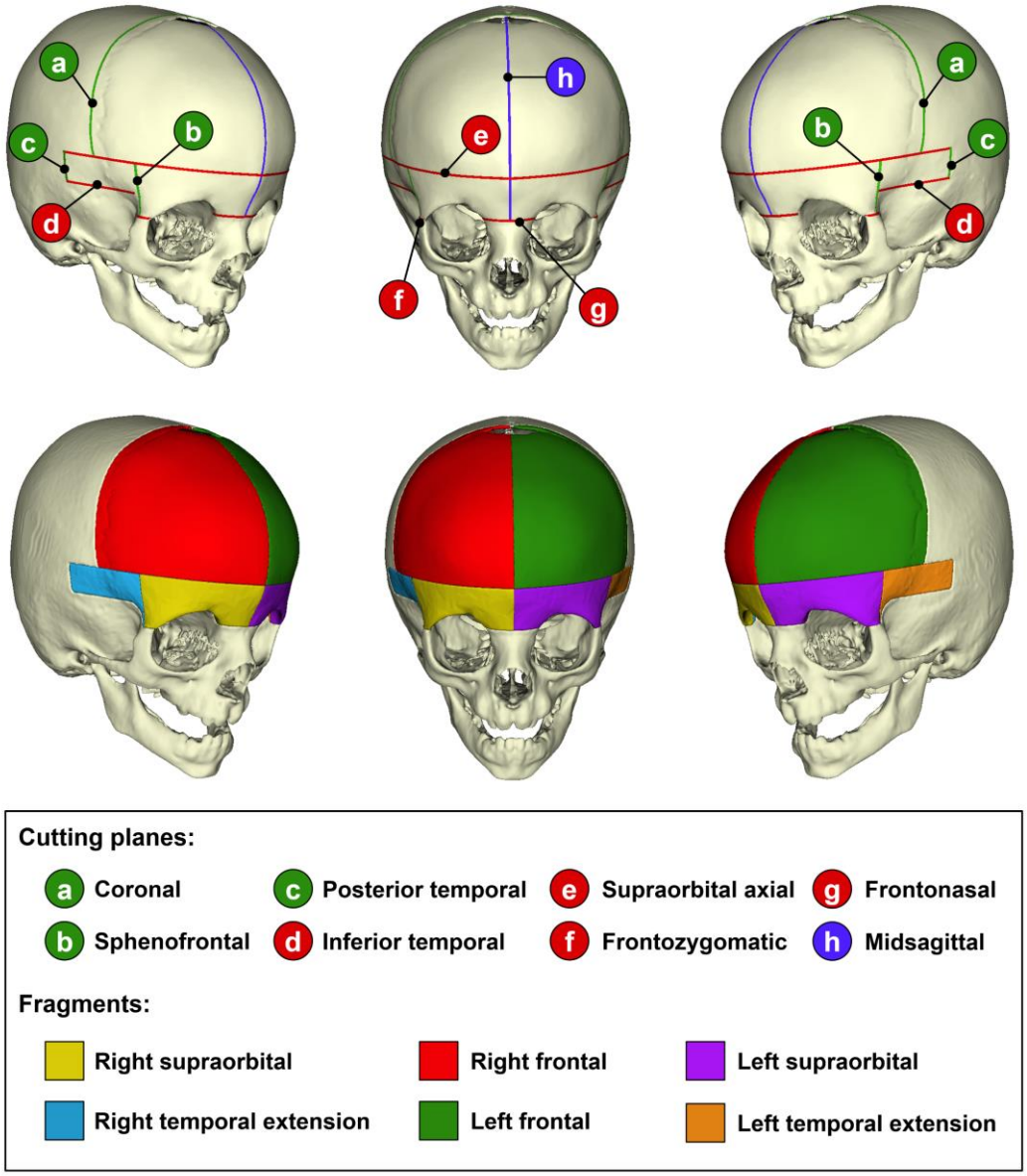

Figure 3.2. VSP of fronto-orbital advancement: cutting planes (top) and fragments for cranial vault remodeling (bottom).

Fragments were automatically estimated for all 9 subjects in our database using the osteotomy template. For each subject, the preoperative CT image was aligned with the reference template using the anatomy of the cranial base, and the eight cutting planes in the osteotomy template were directly projected onto the subject's coordinate space. Finally, the projected cutting planes were used to simulate osteotomies in the fronto-orbital region and to generate six bone fragments to be used for FOA: four fragments in the supraorbital bar and two fragments in the frontal area (**Figure 3.2**).

3.3.4. Automatic Cranial Vault Remodeling

For virtual cranial remodeling, fragments in the fronto-orbital region were reconfigured to achieve the desired target shape (**Figure 3.3**). The target shape was obtained following the steps described in Section 3.3.2. Our algorithm estimated the necessary transformation (i.e., translation, rotation, and bending) required for each of the fragments to achieve the target cranial shape considering the constraints imposed by the clinical protocol of FOA, as explained next.

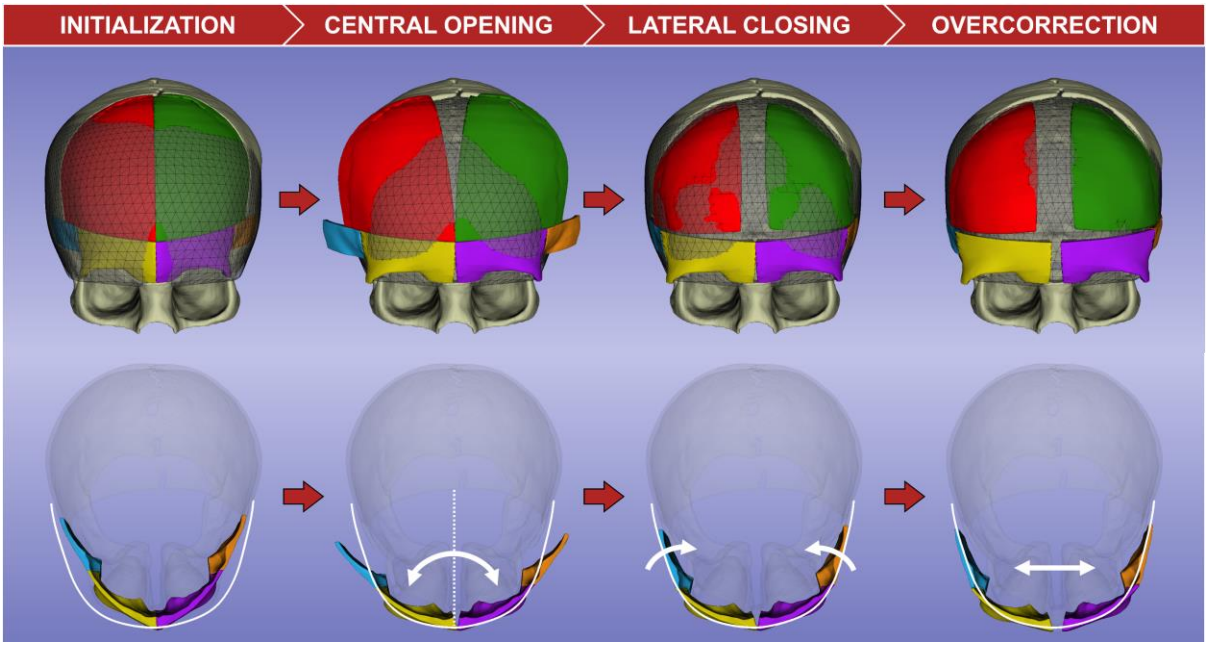

Figure 3.3. Workflow for the simulation of fronto-orbital advancement using a patient-specific normative reference obtained from a statistical shape model. The normative reference is displayed as a triangulated mesh in the top diagram, and as a white curve in the bottom diagram.

First, the two halves of the supraorbital bar and both frontal fragments are rotated parallel to the Frankfurt plane to increase the bitemporal width and the central angle. We refer

to this step as the central opening. Optimal rotation is computed by minimizing the surface-to-surface distance between the left and right supraorbital fragments and the target shape. The rotation angle computed for each supraorbital fragment is applied to each ipsilateral frontal fragment.

Then, bilateral temporal fragments of the bandeau are rotated parallel to the Frankfurt plane to ensure lateral continuity with the healthy bone tissue. In addition, left and right frontal fragments are deformed to match the target shape by means of an affine model-to-model registration. Finally, overcorrection is applied to further increase the interfrontal angle and the bifrontal width over the target normative shape.

3.3.5. Planning Software

A software application called CranioPlan was developed as an extension for the 3D Slicer open-source platform [71] to automatically plan FOA. The software enables to import patient's CT imaging studies or 3D models of the cranium. If CT images are imported, intensity-based segmentation can be performed to generate a 3D model of the patient's anatomy. Our software platform enables a semi-automatic segmentation of the bone tissue, which combines an initialization based on global thresholding with region growing [72].

The planning software incorporates the necessary tools for the automatic estimation of the bone fragments in the fronto-orbital region using the osteotomy template and reconfiguration of these fragments to achieve a normalization of the calvarial shape. Complete automated planning is possible, but the software enables the surgeons to include manual modifications of the VSP at any point according to their surgical needs and preferences.

CranioPlan enables the quantification of morphological metrics commonly used by craniofacial surgeons during diagnosis, surgical planning, and evaluation of surgical outcomes. These metrics include the interfrontal angle (IFA) [73], the transverse forehead width (TFW) [74] and minimal frontal breadth (MFB) [63]. These morphological metrics were measured from a set of landmarks defined in the reference template of our statistical shape model, which are projected onto the coordinate space of each new metopic subject under evaluation. Landmarks for the computation of IFA and TFW were computed as previously described in [23], while the landmarks for MFB were manually selected at the frontotemporale points on both sides of the reference cranium. Morphological metrics can be computed at any step during

the VSP to compare the simulated surgical outcome with the preoperative and normative reference cranial shapes.

In addition, CranioPlan can automatically apply overcorrection to increase the interfrontal angle and the bifrontal width over the normative values. Two predefined levels of overcorrection can be selected by the user: (1) *mild overcorrection*, which increases minimal frontal breadth by 7 mm, and (2) *severe overcorrection*, which increases minimal frontal breadth by 15 mm as recommended by Fearon et al. [63]. However, surgeons can manually input the desired overcorrection degree into the planning software according to their surgical preferences and clinical judgment.

3.3.6. Performance Evaluation

The performance of our software was evaluated by automatically planning FOA in all 9 patients with metopic craniosynostosis in our database. CranioPlan was used to estimate cutting planes and fragments using the osteotomy template, and to virtually arrange the fragments into the most appropriate postsurgical shape according to the target normative reference shape. Three different treatment strategies were computed for each patient: without overcorrection (OC-0mm), mild overcorrection (OC-7mm), and severe overcorrection (OC-15mm). Optimal post-surgical cranial shapes determined by our software for each subject were compared with the manual VSP performed by experienced craniofacial surgeons and the personalized normative reference shape using the following metrics: IFA, TFW, MFB, intracranial volume (ICV) of the fronto-orbital region, and malformations in the fronto-orbital region (i.e. Euclidean distances between the patient's cranial shape and the normative reference). In addition, the processing time required for automatic planning was measured for each subject. Finally, three experienced craniofacial surgeons evaluated the usability and performance of the different steps of the automatic planning framework.

3.4. Results

Evaluation of automatic VSP outcomes indicated a correct normalization of the cranial shape for all 9 patients (**Table 3.1**). All postoperative IFA values were within the range reported in the literature for normative patients: 136.7 ± 6.2 degrees; minimum, 123.8 degrees; maximum, 169.9 degrees [24]. The average processing time required to complete the automatic planning was 19.22 ± 3.25 seconds.

Table 3.1. Mean and standard deviation of morphometric and volumetric values for preoperative cranial shapes, normative reference shapes, manual surgical plans performed by experienced craniofacial surgeons, and automatic plans. Automatic plans were computed with CranioPlan software with three different degrees of overcorrection: no overcorrection (OC-0mm), mild overcorrection (OC-7mm), and severe overcorrection (OC-15mm).

	Metric			
	IFA (º)	**TFW (mm)**	**MFB (mm)**	**Front. ICV (cm^3)**
Preoperative	115.05 ± 5.26	69.12 ± 5.21	77.87 ± 4.54	161.18 ± 38.44
Normative	129.63 ± 3.89	78.51 ± 4.49	85.77 ± 3.92	190.22 ± 39.38
Manual VSP	133.48 ± 4.64	81.04 ± 4.17	88.87 ± 3.48	203.29 ± 36.46
Auto OC-0mm	129.10 ± 3.85	78.04 ± 4.75	87.86 ± 4.74	191.47 ± 39.74
Auto OC-7mm	132.39 ± 4.05	81.08 ± 4.46	92.40 ± 4.95	205.59 ± 42.20
Auto OC-15mm	138.59 ± 3.18	85.87 ± 4.42	100.36 ± 5.46	235.80 ± 47.10

Results without overcorrection (OC-0mm) demonstrate an accurate matching with the normative reference shape, showing an average absolute error of 0.93º in IFA, 0.66 mm in TFW, 2.16 mm in MFB, and 1.25 cm^3 in frontal ICV. In addition, local malformations in the fronto-orbital region were significantly reduced from 2.73 ± 0.88 mm to 0.45 ± 0.09 mm, representing an average reduction of 82.01% (**Figure 3.4**). The average reduction was 80.95% and 82.48% in the supraorbital bar and frontal bone regions, respectively.

Automatic VSP with overcorrection showed increased IFA, TFW, MFB, and frontal ICV in all subjects (**Figure 3.4**). Manual VSP performed by craniofacial surgeons showed an average overcorrection of 7.75% in the frontal ICV. Average volumetric overcorrection over the normative values was 0.66%, 8.16%, and 24.19% for OC-0mm, OC-7mm, and OC-15mm, respectively.

Automatic mild overcorrection (OC-7mm) demonstrated a strong resemblance with manual VSP for all patients, with an average difference of 2.32º in IFA, 1.28 mm in TFW, 3.74 mm in MFB, and 12.81 cm^3 in frontal ICV (**Table 3.2**). Automatic VSP presented a reduced variability in comparison with manual VSP.

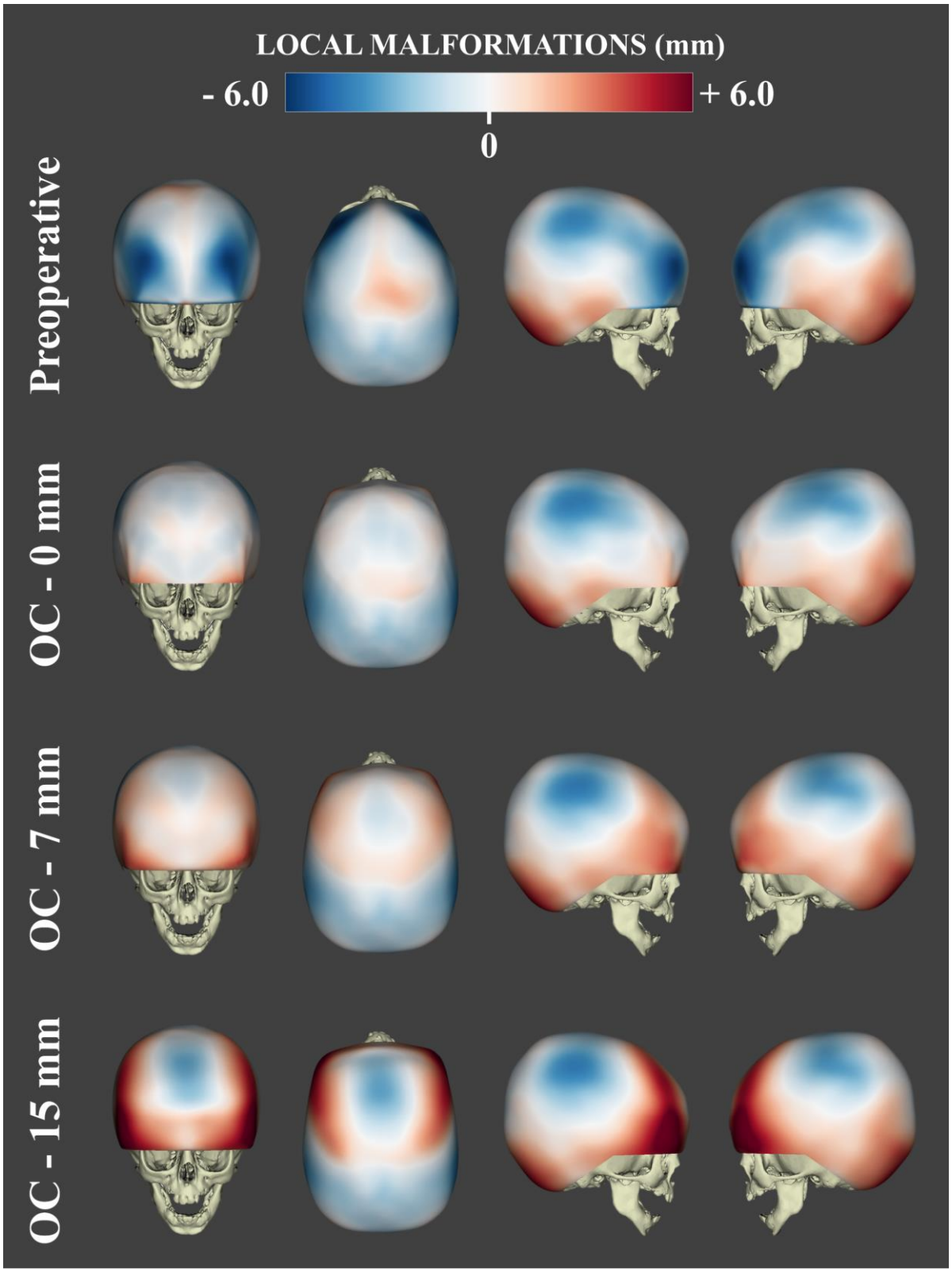

Figure 3.4. Local malformations of the cranium of a metopic craniosynostosis patient before planning (preoperative), after automatic planning without overcorrection (OC-0mm), after automatic planning with an overcorrection of 7 mm in minimal frontal breadth (OC-7mm), and after automatic planning with an overcorrection of 15 mm in minimal frontal breadth (OC-15mm).

Table 3.2. Percentage of overcorrection of manual and automatic virtual surgical plans with respect to normative values.

	Percentage of Overcorrection			
	IFA (%)	**TFW (%)**	**MFB (%)**	**Front. ICV (%)**
Manual VSP	2.97 ± 2.12	3.27 ± 2.39	3.69 ± 3.62	7.75 ± 8.93
Auto OC-0mm	-0.41 ± 0.76	-0.61 ± 0.84	2.41 ± 1.73	0.66 ± 0.50
Auto OC-7mm	2.13 ± 0.80	3.29 ± 0.64	7.71 ± 1.84	8.16 ± 2.19
Auto OC-15mm	6.93 ± 1.25	9.42 ± 1.33	16.99 ± 2.38	24.19 ± 3.07

CranioPlan software was successfully used to compute an automatic interventional plan for FOA in all 9 patients in our database. Feedback from three experienced craniofacial surgeons indicated that the automatic estimation of osteotomies was accurate and provided a suitable initialization for VSP. The orientation of the coronal cutting plane was manually modified in two patients to avoid intersection with the coronal suture. In the rest of the patients, no manual modifications were required, and all automatically estimated fragments were suitable for VSP (**Figure 3.5**).

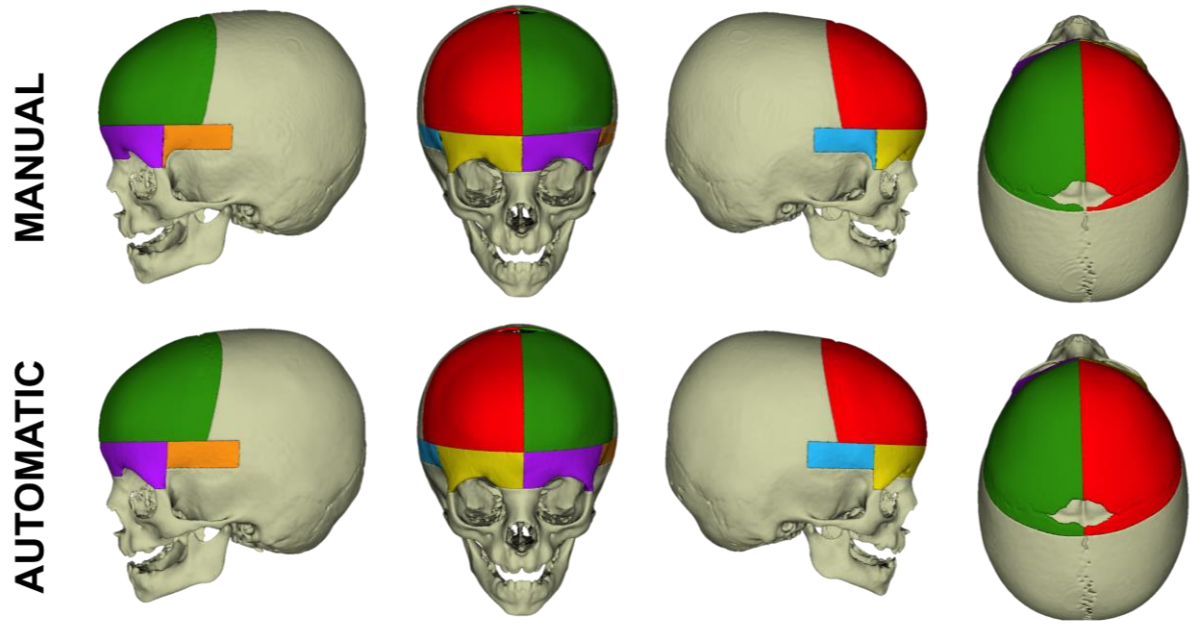

Figure 3.5. Fronto-orbital bone fragments defined during manual VSP (top) and estimated using the osteotomy template during automatic VSP (bottom) in one patient with metopic craniosynostosis.

In addition, surgeons consider that the automatic interventional plans including mild overcorrection, computed using CranioPlan software, were suitable for surgical deployment. While the duration of manual VSP ranged between 40 and 75 minutes, automatic VSP was completed in less than 30 seconds for all patients in our database. Surgeons' feedback suggests that the use of CranioPlan software will improve the repeatability and reduce the duration of the preoperative planning stage.

3.5. Discussion and conclusion

Existing methods for automatic planning of FOA do not incorporate overcorrection, which has shown to be essential to ensure optimal long-term surgical outcomes [63]. In this work, we presented an automatic method for the interventional planning of FOA that enables surgeons to quantify and incorporate the desired overcorrection degree into the VSP.

Our approach is based on statistical shape models of the healthy cranium used to calculate patient-specific normative reference shapes. With these, we can define the most appropriate cranial shape to target during interventional planning. This approach eliminates the subjective determination of the normal cranial shape presented by previous techniques [44]–[46]. Therefore, the use of normative references with VSP can reduce the variability of surgical outcomes across different surgeons and institutions.

In addition, our method introduces an osteotomy template to automatically estimate the optimal bone fragments for FOA. This template includes the bilateral tenon extensions of the supraorbital bar, which are important during FOA to facilitate advancement and subsequent stabilization of the remodeled fragments. The results of this study indicate that the automatic estimation of osteotomies is accurate and provides a valuable and objective tool to improve repeatability and reduce the duration of the preoperative planning stage.

Reconfiguration of fronto-orbital bone fragments was virtually simulated to achieve the desired cranial shape for each patient. The average processing time for virtual remodeling was below 20 seconds. Postoperative cranial shapes of 9 patients reconstructed with our approach significantly reduced malformations in the fronto-orbital region by 82% and presented IFA values within the range reported in the literature for normative patients [24].

Multiple studies have highlighted the importance of performing overcorrection during craniosynostosis treatment to avoid relapse or lack of growth [59], [62], [64], [65]. Our

planning software automatically estimates overcorrected postoperative cranial shapes based on morphological metrics and including the suggestions from previous studies [63]. CranioPlan provides two predefined overcorrection degrees: mild and severe overcorrection. Moreover, surgeons can manually input the desired amount of overcorrection considering the patient clinical history and surgical preferences. This overcorrection can be quantified for later use in surgical outcome analysis. To our knowledge, this is the first solution to consider and apply overcorrection for craniosynostosis VSP.

Importantly, our framework for the simulation of osteotomies and cranial remodeling is integrated into a software application, i.e., CranioPlan. Although this automatic planning tool provides objective metrics and references, it is not meant to replace the surgeon's clinical judgment or technical skills. Therefore, our software enables surgeons to perform a completely automatic VSP based on the personalized data of the patient and to perform modifications in any step of the process according to their surgical needs and preferences.

The limitations of the current study are related to the automatic reconfiguration of the bone fragments during simulated FOA. Our approach estimates a transformation for each fragment, which may lead to potential overlaps between fragments during the virtual remodeling. However, the defined physical constraints of FOA avoid overlaps, so we did not encounter any challenges with the data presented in this paper. However, these constraints may not be suitable for simulating other types of open cranial vault remodeling techniques. To expand our work to other surgical approaches, we will integrate global registration algorithms into our framework to account for bone fragment interactions during simulation [47].

The presented method for VSP can be combined with other technologies to further improve the surgical management of craniosynostosis. Patient-specific normative references could be used to perform quantitative evaluation of the local malformations, assisting physicians during diagnosis [19] or postoperative monitorization of surgical outcomes [31].

Virtual surgical planning of cranial vault remodeling based on statistical shape models has demonstrated to be an accurate, automatic, and objective tool to improve the surgical management of craniosynostosis. The use of normative references of the cranium enables the definition of optimal patient-specific shapes to target during preoperative planning. Our solution enables the estimation of osteotomy locations in the fronto-orbital regions, the automatic configuration of the bone fragments to minimize cranial malformations, and the integration of overcorrection to ensure optimal long-term surgical outcomes. The use of this

technology could lead to a reduction of inter-surgeon variability and an improvement in surgical outcomes.

The content of this chapter is currently under review for publication in the journal Plastic and Reconstructive Surgery:

D. García-Mato, A. R. Porras, S. Ochandiano, G. F. Rogers, J. Pascau, M. G. Linguraru. "Automatic Planning of Fronto-Orbital Advancement for the Surgical Correction of Metopic Craniosynostosis". Plast. Reconstr. Surg. (2021) [submitted]

4

INTRAOPERATIVE 3D PHOTOGRAPHY

4.1. Introduction

Accurate characterization of cranial morphology is essential for diagnosis, treatment planning, and monitorization of surgical outcomes in patients with craniofacial abnormalities [21]. In craniosynostosis, the evaluation of the cranial shape compared with normal morphology is essential to comprehend the basis of the malformations and determine the best approach for surgical correction.

Although multiple morphological metrics are available for cranial shape evaluation, IFA [73] and TFW [74] are the most commonly used by the surgeons during diagnosis, surgical planning, and outcome evaluation of craniosynostosis patients with malformations in the frontal area. These two metrics are strongly related to the severity of the malformation and the effect on the harmony and balance between the face and cranial vault in metopic craniosynostosis patients. However, accurate measurement of these metrics can only be achieved with a 3D analysis of the cranial vault and with an optimal and standardized anatomical landmark definition.

In the past, cranial anthropometry has been limited to direct measurements of the anatomy during examination using traditional instruments (e.g. calipers or angle meters). This methodology enables a simple, non-invasive, and inexpensive quantification of cranial shape. Normative databases of direct anthropometric measurements are available in the literature [75],

providing references that can be compared with specific patients. However, this methodology requires training for reliable performance and is time-consuming. Another significant limitation is the inability to store craniofacial surface morphology for further analysis [28].

Later, two-dimensional (2D) images have been proposed to overcome the limitations of direct anthropometry [76]. The main advantages of this methodology are fast acquisition, simplicity, low cost, noninvasiveness, and storage capabilities [28]. However, 2D images do not enable users to make volume and topographic measurements, which are essential for many applications [77]. In addition, it has been demonstrated that the reliability of this methodology is highly dependent on multiple factors, such as subject-camera relative position, head orientation, or lighting. Therefore, variable measurements are expected when images are acquired by several users under different conditions.

In this context, 3D imaging has emerged to provide accurate and reproducible quantification of cranial morphology. In craniosynostosis, CT scans have become the standard for evaluating the cranium due to its ability to display bone tissue with high spatial resolution [16]. CT imaging enables to detect the fusion of the cranial sutures and to generate accurate 3D reconstructions for diagnosis, shape analysis, and surgical planning. However, this technique is limited by the exposure of the subjects to ionizing radiation and the frequently required sedation or anesthesia for the infants to remain steady during acquisition. For these reasons, CT imaging is rarely used for postoperative evaluation of surgical outcomes and patient follow-up [27].

The limitations of CT imaging have led to the use of 3D photography for cranial anthropometry. This technology is based on the acquisition of images of the subject from multiple angles and the alignment of those images to reconstruct a 3D surface. Several studies have demonstrated the validity and reliability of 3D photography for craniofacial anthropometry [28]–[30]. In addition, 3D photography has been used to evaluate cranial malformations and surgical outcomes in craniosynostosis with accuracy similar to CT imaging [31].

The devices used in previous works to acquire 3D photographs of craniosynostosis patients are mostly stationary, based on several synchronized cameras obtaining images from multiple angles to reconstruct the 3D scene (**Figure 4.1**). The main advantage of these devices is the near-instantaneous image capture, which minimizes motion artifacts and enables the acquisition of images without sedation or anesthesia of the infants. However, these systems

require a dedicated room with highly specialized equipment for the acquisition, and trained personnel to acquire and process the images [26].

Figure 4.1. The 3dMDface System (3dMD, Atlanta) consists of four geometric and two texture cameras that acquire synchronized images of the subject to create a single 3D image. Image adapted from [78] (figure reprinted with permission from the copyright holder, Elsevier).

Hand-held 3D scanners are not a common tool in biomedical applications, but they are widely employed in other areas, such as industrial design or architecture [79], [80]. Within the medical field, mobile devices have been mostly applied for facial scanning [81] or objective evaluation in plastic surgery [82]. Few studies report the use of hand-held 3D photographs for postoperative evaluation of patients with craniosynostosis [26], [33]. These scanners are moved around the area of interest to acquire 3D images from multiple angles and reconstruct the 3D surface.

Although the acquisition time is higher than in stationary devices, the portability of hand-held 3D scanners enables its use inside the operating room for surgical outcome evaluation [83]. However, the use of this technology for the intraoperative evaluation of the surgical outcome during open cranial vault remodeling has not been reported, and its accuracy has not been evaluated yet.

4.2. Objective

This study aims to evaluate the feasibility of using a hand-held 3D photography device for noninvasive and radiation-free intraoperative morphometric cranial vault analysis during metopic craniosynostosis surgery. We assessed the accuracy of this technology for intraoperative reconstruction of the cranial vault surface and the measurement of morphological metrics (IFA and TFW). Additionally, we recorded the time required for intraoperative scanning and gathered feedback from several specialized surgeons to investigate the feasibility of integrating this technology into the current surgical workflow.

4.3. Materials and methods

In this section, we first describe the subjects included in this study. Then, we present the methodology and the hardware required to acquire intraoperative 3D photographs. Later, we describe the evaluation of the intraoperative scanning process and the accuracy for 3D reconstruction and morphometry. Finally, a methodology for automatic registration of intraoperative 3D photographs is presented and evaluated.

4.3.1. Subjects

Data from five patients with metopic craniosynostosis were included in this study: a 9-month-old boy, a 15-month-old (corrected age is 12 months) girl, a 16-month-old (corrected age is 13 months) boy, a 10-month-old girl, and a 10-month old boy. These patients suffered from isolated, non-syndromic metopic craniosynostosis, and surgical corrections were performed through FOA assisted by patient-specific cutting guides, remodeling templates, and intraoperative navigation. The parent or legal guardian of the patients signed an informed consent for study participation. The study was approved by the Research Ethics Committee at Hospital General Universitario Gregorio Marañón (Madrid, Spain) and performed in accordance with the principles of the 1964 Declaration of Helsinki as revised in 2013.

A 3D printed phantom was designed and manufactured to produce a realistic scenario for surgical simulation and performance evaluation. The design of the phantom was based on patient 2, presenting metopic craniosynostosis. Polylactic acid (PLA) and silicone (Smooth-On, PA, USA) materials were used to simulate bone and soft tissue, respectively. A total of 15 reference points were attached to the simulated bone tissue surface for error computation

purposes. This phantom was used for the evaluation of the automatic registration of 3D photographs. More details are provided in section 4.3.6.

In addition, we used a database from Children's National Hospital (Washington, DC, United States) including CT scans of 201 normative subjects (mean age, 1.93 ± 1.69 years; range, 0 to 6 years; 89 girls and 112 boys) and 34 patients diagnosed with metopic craniosynostosis (mean age, 5.46 ± 4.32 months; range, 0 to 14 months; 11 girls and 23 boys). The normative subjects were used to build a statistical shape atlas [19]. The 34 patients with metopic craniosynostosis were used to compute the average malformation field to estimate optimal anatomical landmarks for morphology quantification, following the methodology described by Mendoza et al. [23]. More details are provided in section 4.3.5.

4.3.2. Preoperative CT scanning

A preoperative cranial CT scan was acquired as part of the standard of care for all five patients with a Philips Mx8000 scanner before the intervention. The axial in-plane pixel size ranged between 0.24 and 0.28 mm, the slice thickness ranged between 1 and 1.3 mm, and the spacing between slices ranged between 0.5 and 0.6 mm for all cases.

Intensity-based segmentation of the CT scans was performed using the 3D Slicer platform [84], generating 3D models of the skin and the bone tissue of each subject (**Figure 4.2**). Segmentation of the skin tissue was performed using an automatic method based on Otsu thresholding and extracting the outer surface. Bone tissue was segmented semi-automatically combining an initialization based on global thresholding with region growing [72].

After segmentation, skin and bone tissue models were post-processed to eliminate unconnected regions and fill holes, ensuring continuity in the final mesh. No additional post-processing (e.g. smoothing) was performed. These models served as a reference for preoperative VSP and as a gold-standard for 3D photography performance evaluation.

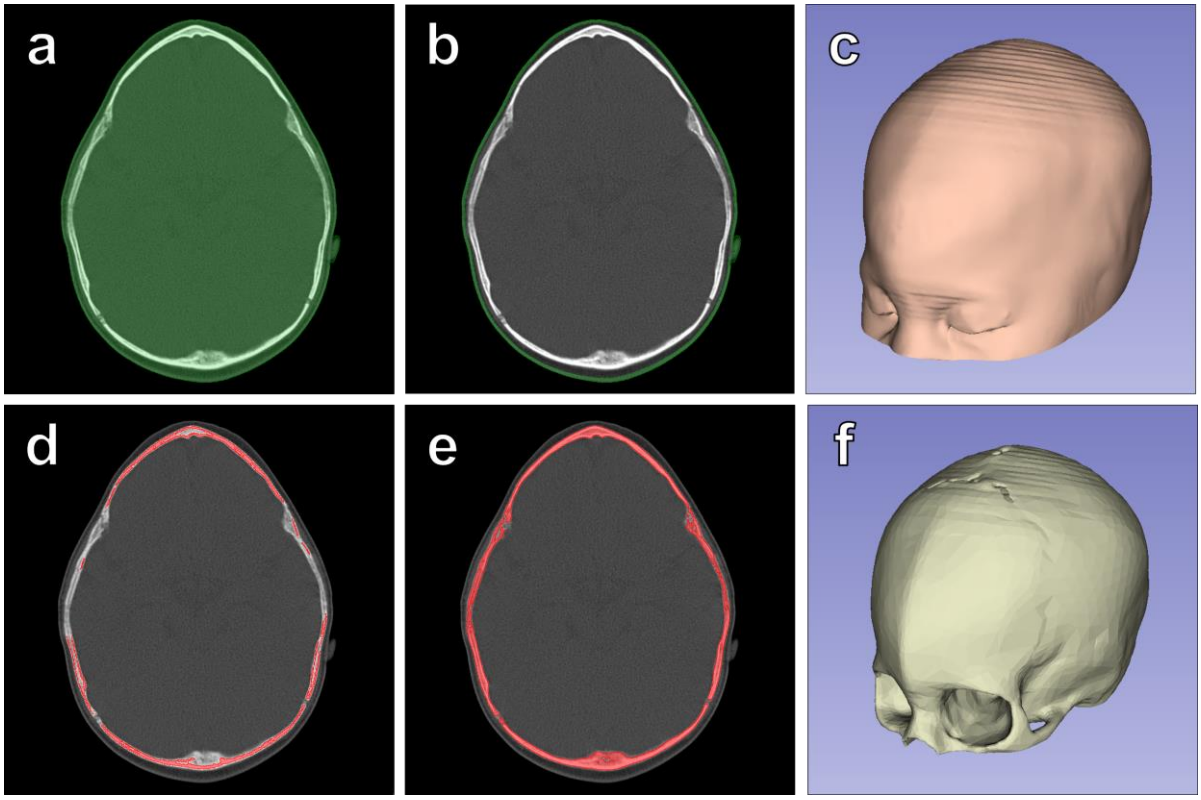

Figure 4.2. Segmentation of skin and bone from preoperative CT scan of subject 1. (a) Segmentation of skin tissue surface using Otsu thresholding. (b) Extraction of the outer surface of the segment. (c) 3D model of skin tissue. (d) Initialization of bone segmentation using global thresholding. (e) Segmentation of bone tissue using region growing. (f) 3D model of bone tissue.

4.3.3. Intraoperative 3D photography

3D photographs were acquired using the Artec EVA® (Artec Group, Luxembourg) structured light scanner during surgery to obtain skin and bone tissue surfaces. This hand-held device illuminates the surgical area with striped patterns of bright white light and computes a 3D surface mesh from the deformation of these patterns captured by two cameras included in the scanner. The process does not involve any harmful radiation. In addition, a third internal camera obtains color texture information.

During the scanning process, the device was moved around the region of interest at a distance range of 0.4-1.0 meters for 3D frame acquisition (**Figure 4.3**), taking into account that a minimum safety margin of 30 centimeters must be maintained between unsterile personnel and the sterile surgical field [85].

Figure 4.3. Acquisition of an intraoperative 3D photograph of the cranial vault during craniosynostosis surgery using the hand-held structured light scanner.

Intraoperative 3D photographs of the cranial vault were acquired at three different stages of the surgical correction (**Figure 4.4**): skin tissue surface before incision (preoperative skin), bone tissue surface before osteotomy (preoperative bone), and bone tissue surface after remodeling (postoperative bone). After scanning, the acquired 3D images were aligned and fused using geometry and texture information with Artec Studio® software. Processing steps include global registration, outlier removal, smooth fusion, and texture mapping. The final 3D surface, texture, and mapping information were exported in Wavefront Object (.obj), Joint Photographic Experts Group (.jpg), and Material Template Library (.mtl) file formats, respectively. The time required for scanning and processing steps was measured for each surgery.

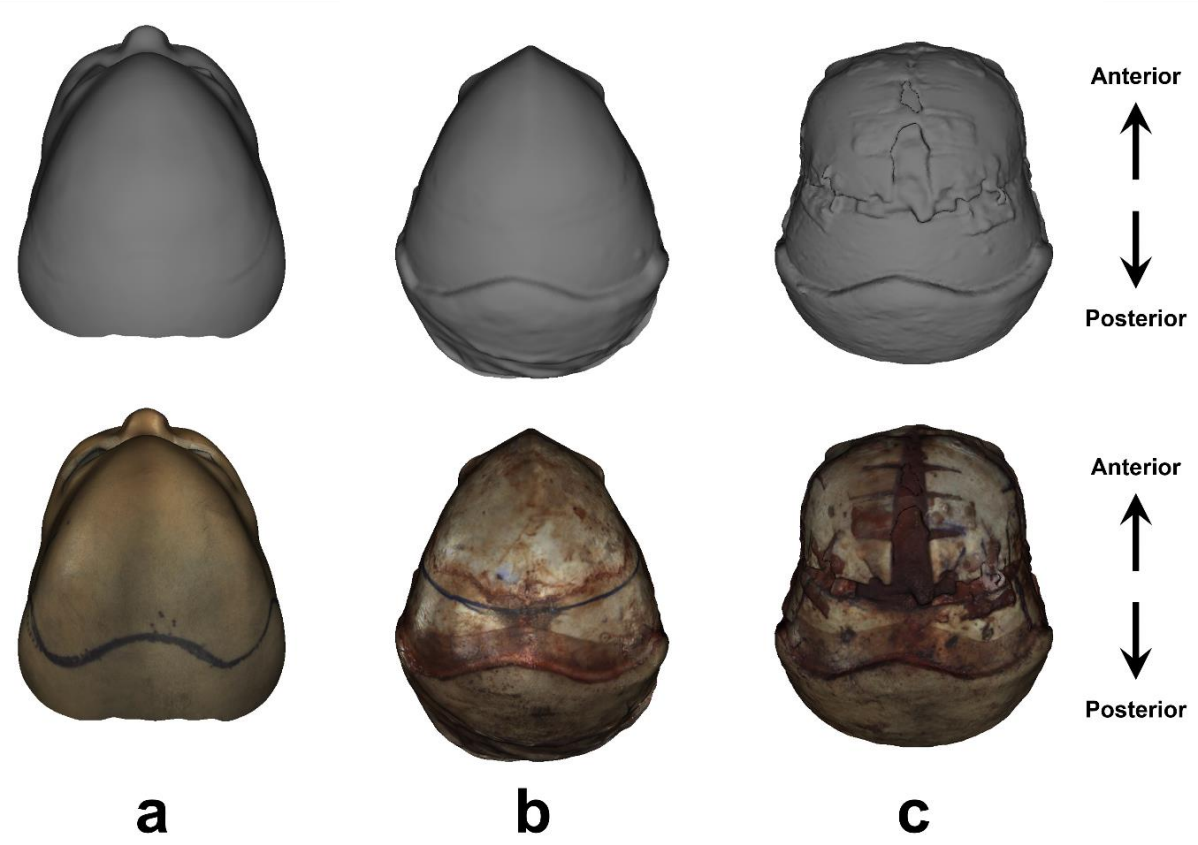

Figure 4.4. Superior view of intraoperative 3D photographs without (first row) and with texture information (second row) of the cranial vault of subject 1 at different phases of the surgical correction: (a) skin tissue surface before incision, (b) bone tissue surface before osteotomy, and (c) bone tissue surface after remodeling.

4.3.4. Accuracy evaluation

The accuracy of intraoperative 3D photography was evaluated using the preoperative photographs of skin and bone tissue (before cranial vault remodeling), and taking the 3D models of skin and bone surfaces obtained from the preoperative CT as gold-standard. The iterative closest point algorithm [86] was used to align the acquired 3D surfaces with the segmented reference models. Once aligned, 3D photography accuracy was measured as the average surface distance, i.e. the Euclidean distance between each vertex of the source mesh to the closest vertex in the target mesh. A Student t-test was applied to investigate the existence of significant differences in accuracy between the skin and bone tissue scanning.

4.3.5. Morphometry analysis

We evaluated the feasibility of quantifying morphological metrics from 3D photography data for the evaluation of cranial deformity in craniosynostosis patients using three anatomical landmarks in the cranial vault. For the automatic computation of robust landmarks, we followed a similar methodology to the one proposed by Mendoza et al. [23] and previously validated for discrimination of pathological shape abnormalities from healthy phenotypes [24].

First, each of the 34 subjects with metopic craniosynostosis in our database was aligned with a reference healthy subject (template). Then, a patient-specific normative reference cranial shape was computed for each subject using a statistical shape atlas built from the CT scans of the 201 normative subjects. This normative reference is used to calculate the malformation field of each metopic subject, which represents the local malformation values of each subject with respect to the normal shape.

Finally, all malformation fields were combined to compute an average absolute malformation field where the three points of maximum average malformation were identified at the left frontal bone (LFL), at the right frontal bone (RFL), and along the metopic suture (MSL) (**Figure 4.5**). These points follow the clinical observations in the diagnosis procedure to identify the morphological abnormalities associated with trigonocephaly: recession of the frontal bones and protrusion of the metopic suture area. The manual identification of these points using anatomical landmarks is not possible, and their identification relies on the registration of the preoperative CT scan with the reference template.

For each of the 5 subjects in our study, the preoperative CT scan was aligned with the reference template and the three maximum average malformation landmarks (LFL, RFL, and MSL) were projected on the cranial vault of each subject (**Figure 4.5**). Intraoperative 3D photographs were aligned with the preoperative CT scan, and the three landmarks were projected on the surface for intraoperative morphology quantification. IFA and TFW morphological metrics were calculated from the projected landmarks of each subject: IFA was defined as the angle formed by the left frontal segment (LFL-MSL) and right frontal segment (RFL-MSL), and TFW was measured as the distance between the two most lateral landmarks (LFL and RFL).

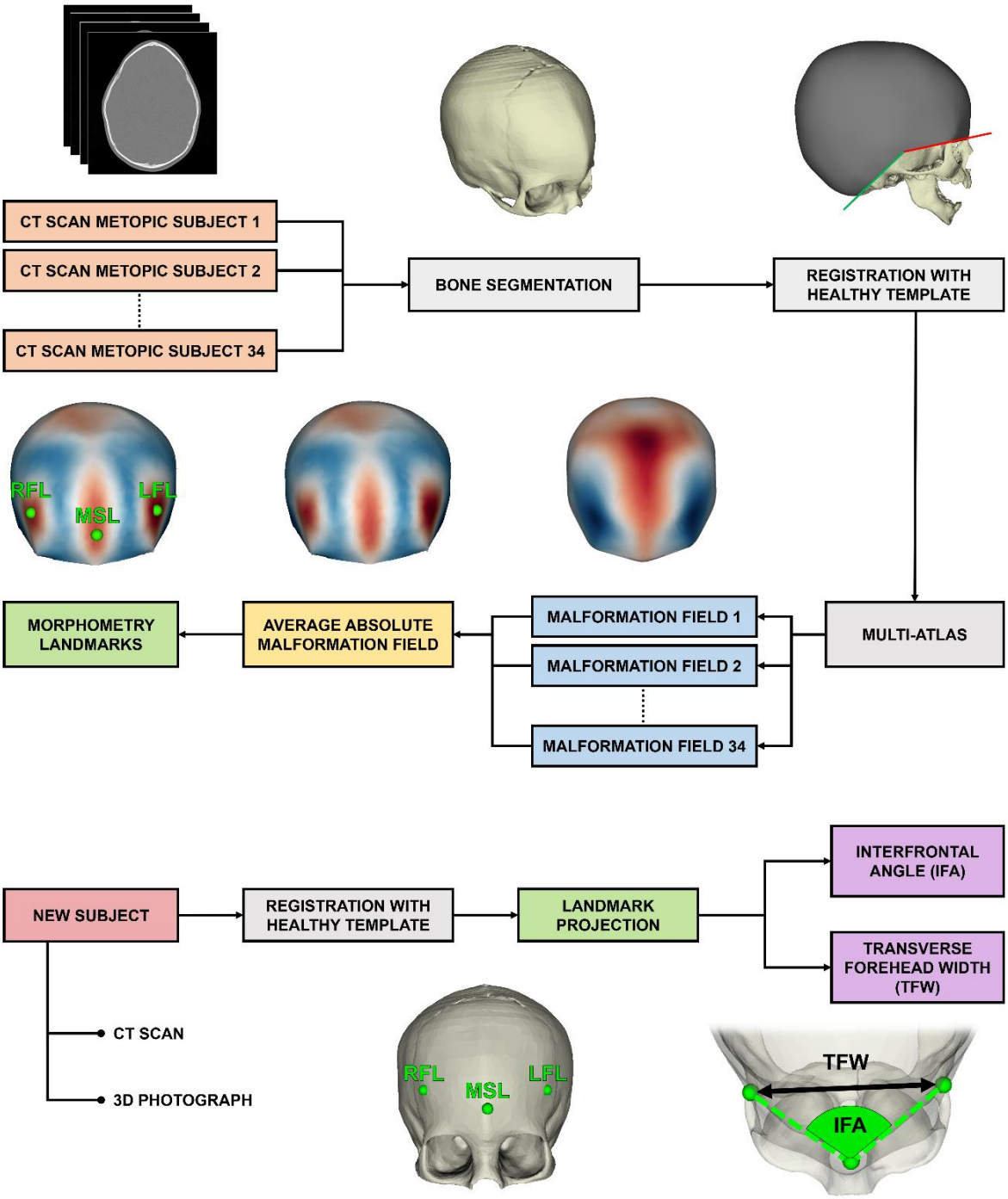

Figure 4.5. Methodology for computation of IFA and TFW morphological metrics of a metopic subject using an average malformation field computed from a database of 34 metopic subjects. Individual malformation fields are generated from a multi-atlas of normative cases. The three points with the maximum average malformation (LFL, RFL, and MSL) are computed and used for the computation of morphological metrics of every new subject.

These two metrics were calculated on the skin and bone tissue models obtained from the preoperative CT scan and on the intraoperative 3D photographs acquired during surgery for each of the 5 patients. Morphological metrics computed on the preoperative 3D photographs (before cranial vault remodeling) were compared to the IFA and TFW values computed using the preoperative CT scans, and the difference was considered as the morphometry error. A Student t-test was performed to investigate the existence of significant differences between the values measured in 3D photographs and CT scans. In addition, morphological metrics were also computed on the intraoperative 3D photographs acquired after cranial vault remodeling and on the normative reference shapes of each subject. These values were used to evaluate and compare the surgical outcomes with normal (healthy) morphology, computed from the statistical shape atlas of normative cases.

4.3.6. Automatic registration

We propose a novel approach for the automatic registration of bone tissue 3D photographs based on the attachment of 3D printed color markers to the bone surface (**Figure 4.6**). Three squared color markers were used: blue, green, and magenta. Color markers consist of a top layer made of PLA material containing the color information to be automatically identified in the 3D photographs, and a bottom layer made of resin, which will be in contact with the bone tissue and contains holes for rigid fixation using resorbable pins.

These markers are attached to the healthy tissue surrounding the reconstruction area before cranial vault remodeling. These markers can then be automatically identified in the intraoperative 3D photographs by applying color filtering over the texture data. Once markers are detected, the center of mass is extracted from each one and subsequent 3D photographs can be aligned using fiducial-based registration. It must be noted that the color markers must be in a fixed position during cranial vault remodeling to ensure optimal registration accuracy

This methodology for automatic registration was evaluated in the 3D printed phantom to assess the accuracy of the alignment for different spatial configurations of the markers and different illumination conditions. Color markers were attached to the simulated bone tissue surface into five spatial configurations, and 3D photographs were acquired under three different illumination conditions (homogeneous, dim, and unidirectional lights) (**Figure 4.7**). For each case, the target registration error (TRE) was measured at 15 reference points distributed along the surface of the 3D printed phantom. Finally, the complete workflow for automatic

registration was tested on a real surgery to assess the attachment of the markers to real bone tissue and the accuracy for automatic identification in the surgical field.

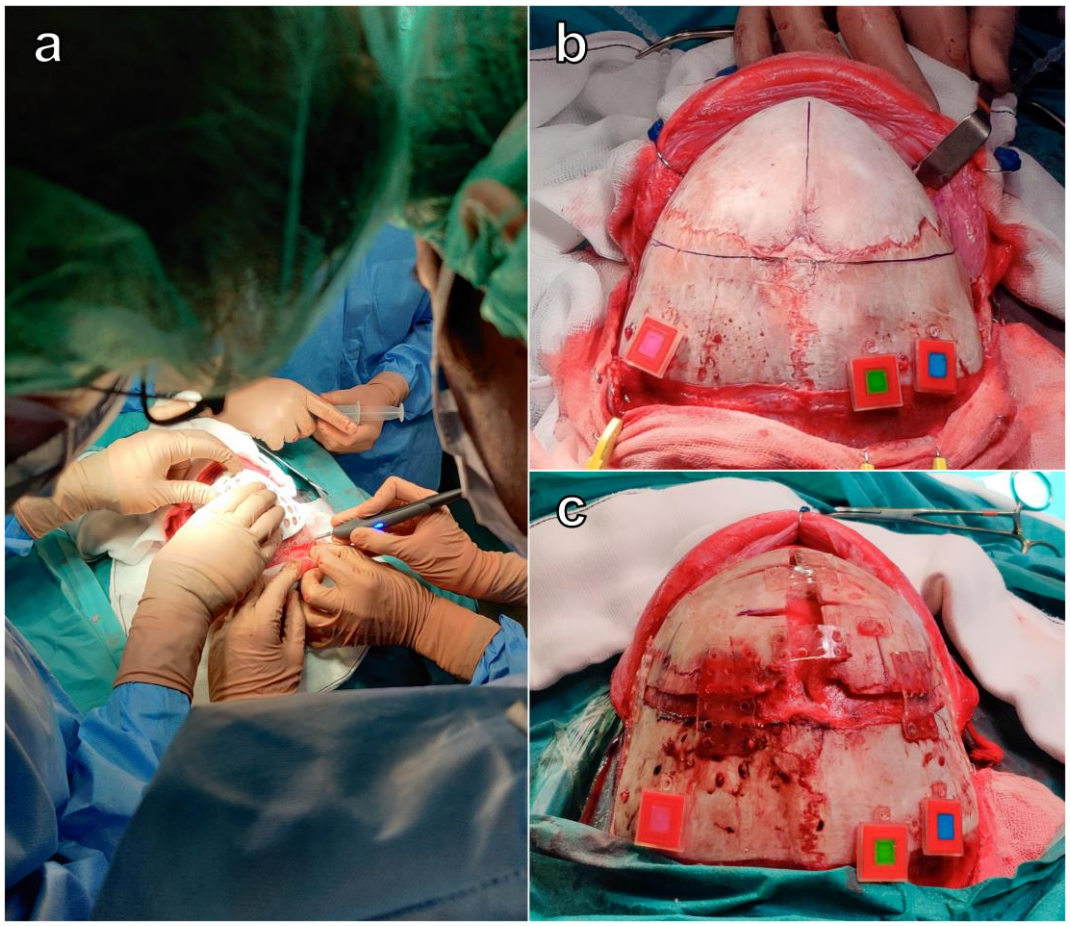

Figure 4.6. (a) Attachment of registration color markers to bone tissue using resorbable pins. (b) Surgical field before cranial vault remodeling with color markers attached. (c) Surgical field after cranial vault remodeling with color markers attached.

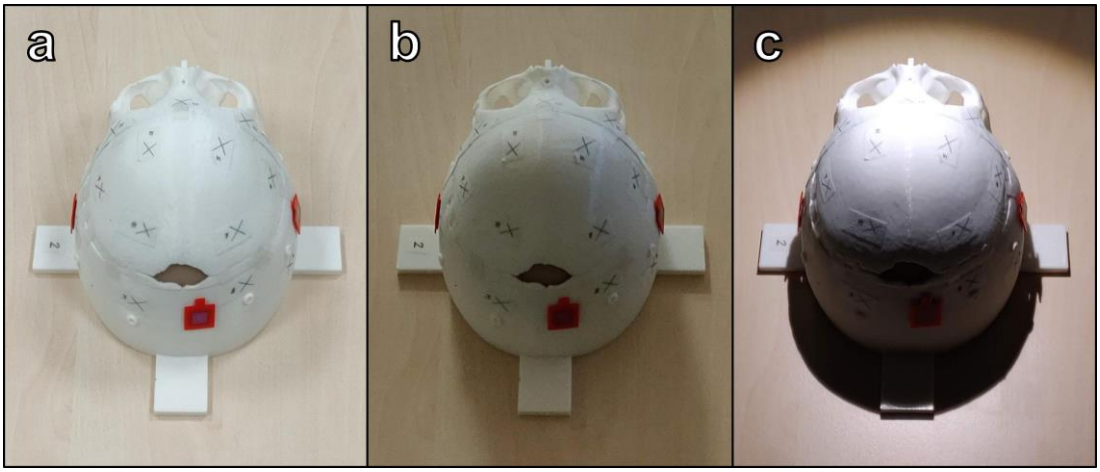

Figure 4.7. Simulation phantom during 3D photograph acquisition under three different illumination conditions: (a) homogeneous light, (b) dim light, and (c) unidirectional light.

4.3.7. Usability evaluation

Feedback from specialized surgeons was obtained to assess the usability of intraoperative 3D photography in craniosynostosis surgical correction, compare the use of 3D photography with other approaches, and determine the feasibility of integrating this technology into the current surgical workflow. A questionnaire survey was filled-in by six surgeons (three from the Department of Oral and Maxillofacial Surgery and three from the Department of Neurosurgery) involved in the craniosynostosis correction surgeries after the completion of the last case. Questions were scored on a 5-point Likert scale (**Figure 4.8**). The results are presented in the following section.

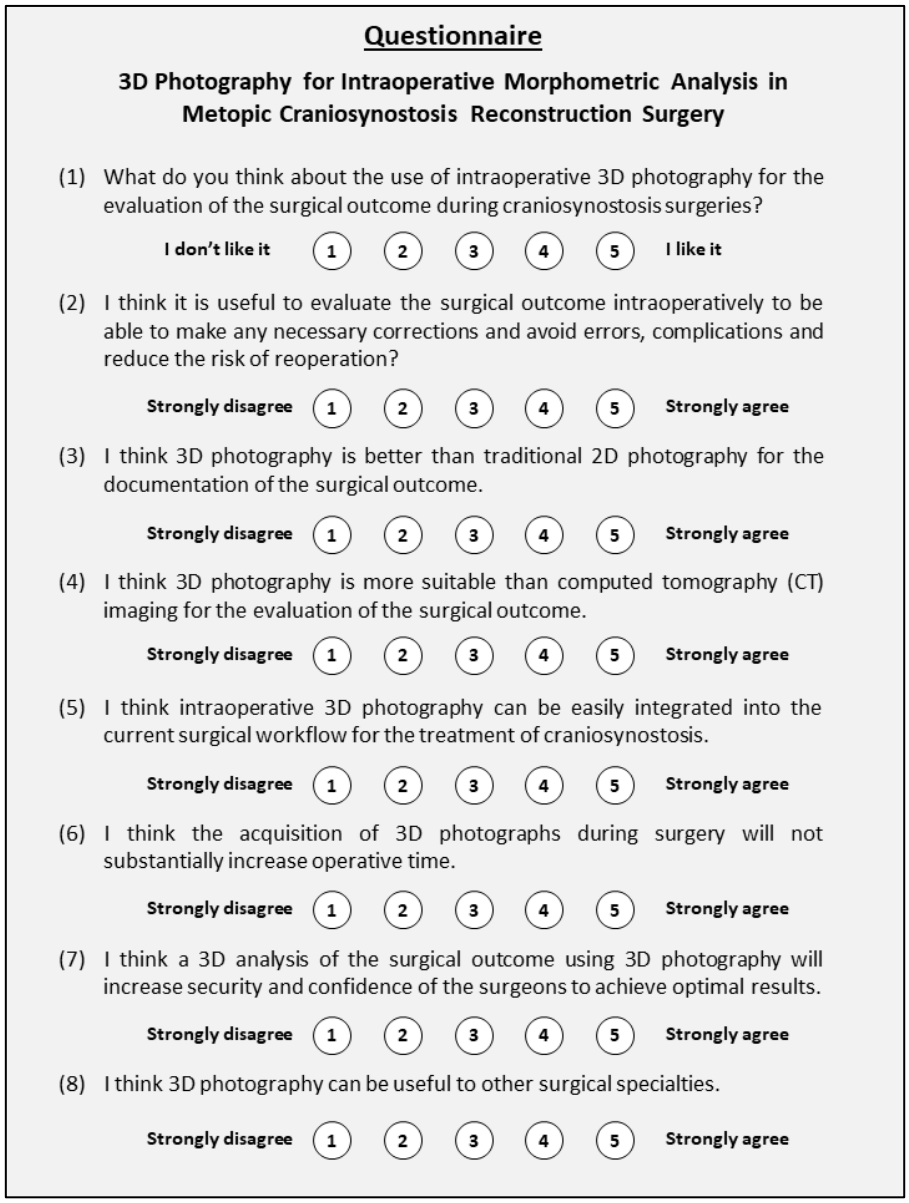

Questionnaire

3D Photography for Intraoperative Morphometric Analysis in Metopic Craniosynostosis Reconstruction Surgery

(1) What do you think about the use of intraoperative 3D photography for the evaluation of the surgical outcome during craniosynostosis surgeries?

I don't like it (1) (2) (3) (4) (5) I like it

(2) I think it is useful to evaluate the surgical outcome intraoperatively to be able to make any necessary corrections and avoid errors, complications and reduce the risk of reoperation?

Strongly disagree (1) (2) (3) (4) (5) Strongly agree

(3) I think 3D photography is better than traditional 2D photography for the documentation of the surgical outcome.

Strongly disagree (1) (2) (3) (4) (5) Strongly agree

(4) I think 3D photography is more suitable than computed tomography (CT) imaging for the evaluation of the surgical outcome.

Strongly disagree (1) (2) (3) (4) (5) Strongly agree

(5) I think intraoperative 3D photography can be easily integrated into the current surgical workflow for the treatment of craniosynostosis.

Strongly disagree (1) (2) (3) (4) (5) Strongly agree

(6) I think the acquisition of 3D photographs during surgery will not substantially increase operative time.

Strongly disagree (1) (2) (3) (4) (5) Strongly agree

(7) I think a 3D analysis of the surgical outcome using 3D photography will increase security and confidence of the surgeons to achieve optimal results.

Strongly disagree (1) (2) (3) (4) (5) Strongly agree

(8) I think 3D photography can be useful to other surgical specialties.

Strongly disagree (1) (2) (3) (4) (5) Strongly agree

Figure 4.8. Questionnaire about the use of 3D photography.

4.4. Results

4.4.1. Acquisition time

Intraoperative 3D photographs of skin and bone tissue were successfully acquired in all five surgeries. The mobile scanner was easily moved around the surgical field to obtain 3D images of the cranial vault from different angles. The average scanning duration was 74.67 ± 14.78 and 87.79 ± 39.62 seconds for the skin and bone 3D photographs, respectively (mean ± standard deviation). The fastest scan was obtained in 53 seconds and the slowest in 191 seconds. The average time to process the acquired scans was 63.92 ± 23.37 seconds for skin tissue and 92.54 ± 37.99 seconds for bone tissue. Processing 3D photographs of bone tissue after remodeling presented an increased duration compared with those acquired before cranial remodeling. Recorded scanning and processing time required for each subject are shown in **Table 4.1**.

Table 4.1. Scanning and processing time of intraoperative 3D photographs of the cranial vault acquired using the Artec Eva scanner.

	Scanning time (s)			Processing time (s)		
Subject ID	**Skin**	**Bone (Pre)**	**Bone (Post)**	**Skin**	**Bone (Pre)**	**Bone (Post)**
1	60.82	90.45	190.55	46.20	75.80	198.70
2	85.18	109.00	87.36	105.30	90.50	94.10
3	75.73	87.64	52.82	74.60	53.30	89.10
4	95.64	90.18	41.00	46.50	72.10	86.70
5	56.00	73.73	55.18	47.00	64.20	100.90
Mean	74.67	90.20	85.38	63.92	71.18	113.90
SD	14.78	11.24	54.78	23.37	12.36	42.68

4.4.2. Accuracy evaluation

The average error of intraoperative 3D photography for the reconstruction of the patient's anatomy was 0.30 ± 0.29 mm. An average surface distance of 0.45 ± 0.36 mm and 0.17 ± 0.12 mm was obtained for the skin and bone tissue scans, respectively. In the case of skin tissue scanning, larger error values were found in ocular and nasal regions, which may be caused by soft tissue displacements and misalignments with the preoperative CT scan. For bone

tissue, higher errors were found in the anterior fontanel region due to its low density and reduced visibility in the CT scan (**Figure 4.9**). Significant differences ($p < 0.001$) were found between the accuracies of skin and bone tissue scanning consistently in all subjects, demonstrating a higher accuracy of the technique for the reconstruction of the bone tissue surface.

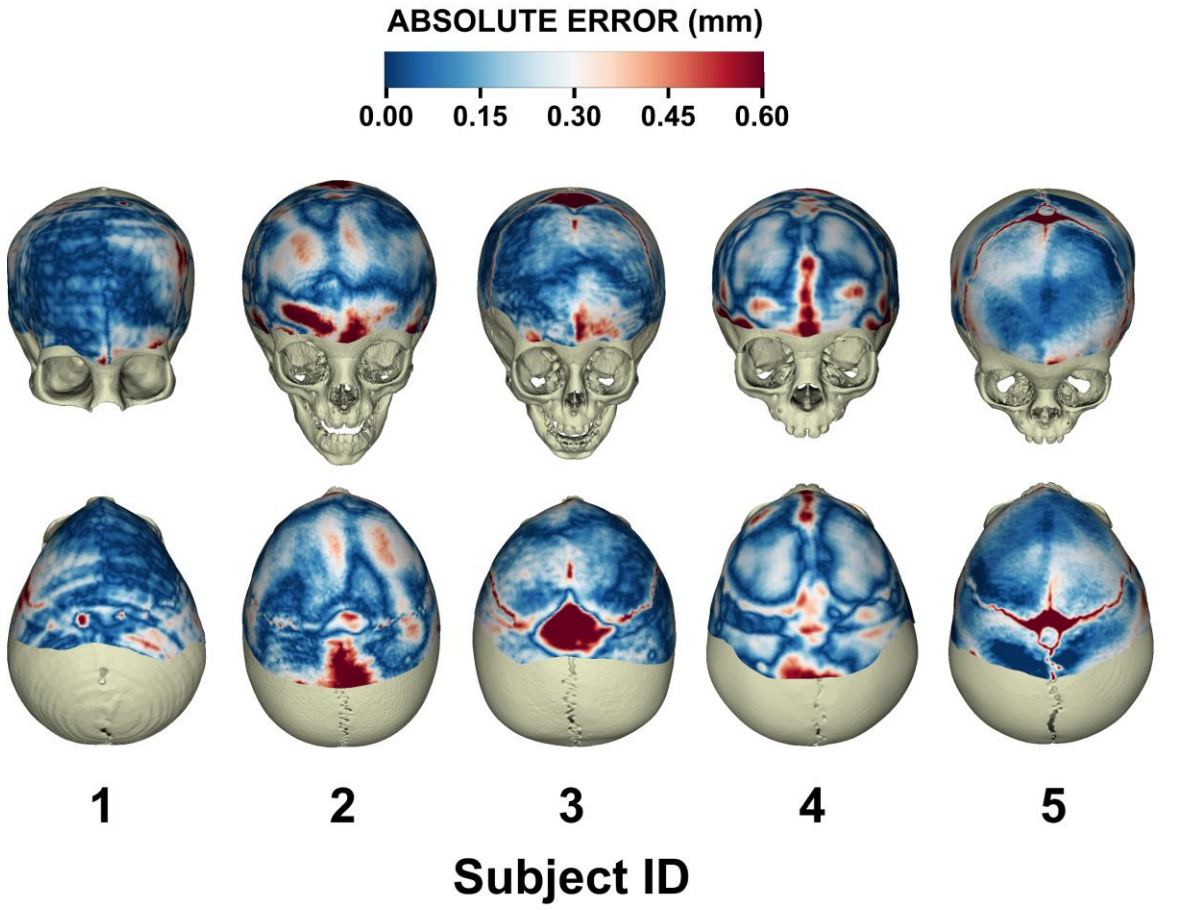

Figure 4.9. 3D models of the cranial surface with a color representation of the local surface distance between intraoperative 3D photographs and reference models of the cranium obtained from preoperative CT scans. Red color represents those areas of the cranial vault with increased error and blue color represents those areas with a lower error.

4.4.3. Morphometry analysis

Computed morphological metrics before cranial vault remodeling and the corresponding errors are shown in **Table 4.2**. The average absolute error in IFA estimation was 0.72 ± 0.46 degrees. An absolute morphometry error of 0.62 ± 0.42 degrees and 0.82 ± 0.47 degrees was obtained for skin and bone tissue scanning, respectively. No significant differences

($p > 0.9$) were found between IFA measured in the 3D photographs and the preoperative CT scans. In addition, all measured values for the IFA are within the range reported in the literature for patients with metopic craniosynostosis: 116.5 ± 5.8 degrees; minimum, 106.8 degrees; maximum, 126.6 degrees [24].

TFW presented an average morphometry error of 0.62 ± 0.44 mm (0.42 ± 0.42 mm for skin tissue and 0.81 ± 0.36 mm for bone tissue scanning). No significant differences ($p > 0.9$) were found between the TFW measured in the 3D photographs and the CT scans.

Table 4.2. Preoperative measurements of interfrontal angle and transverse forehead width in intraoperative 3D photographs before remodeling and reference preoperative CT scans.

		IFA (°)			TFW (mm)		
Subject ID	**Tissue**	**3D photograph**	**CT scan**	**Error**	**3D photograph**	**CT scan**	**Error**
1	Skin	107.85	107.58	0.26	70.37	69.78	0.59
	Bone	106.86	105.67	1.18	66.41	67.45	1.04
2	Skin	117.57	116.14	1.43	84.22	84.17	0.06
	Bone	117.17	118.72	1.54	80.76	79.87	0.89
3	Skin	120.43	121.02	0.59	72.49	72.56	0.07
	Bone	121.29	121.00	0.29	69.95	69.68	0.26
4	Skin	116.46	116.06	0.40	71.03	71.27	0.24
	Bone	118.76	119.22	0.46	68.12	68.67	0.55
5	Skin	114.99	114.57	0.42	78.75	77.59	1.16
	Bone	112.26	112.88	0.62	72.36	71.06	1.30

Morphological metrics measured in the postoperative 3D photographs show an average reduction of the forehead malformations of 87%, using the normative shape of each subject as a reference (**Table 4.3**). Postoperative values of IFA are within the range defined in the literature for normative patients: 136.7 ± 6.2 degrees; minimum, 123.8 degrees; maximum, 169.3 degrees [24]. In addition, postoperative values of TFW indicate an overcorrection of the bifrontal width by an average of 2.07 mm over the normal values of each subject.

Table 4.3. Measurements of interfrontal angle and transverse forehead width in intraoperative 3D photographs of the bone surface before (pre-op) and after (post-op) cranial vault remodeling. Normal values correspond with the morphological metrics of the normative reference shape of the subject computed from the multi-atlas of 201 normative cases.

Subject ID	IFA (°)			TFW (mm)		
	Pre-Op	Normal	Post-Op	Pre-Op	Normal	Post-Op
1	106.86	127.00	133.55	66.41	78.49	84.07
2	117.17	125.86	125.08	80.76	86.50	88.27
3	121.29	137.46	136.92	69.95	77.54	77.84
4	118.76	129.76	127.82	68.12	73.37	74.63
5	112.26	127.12	127.10	72.36	80.16	81.59

4.4.4. Automatic registration

Average TRE for the different spatial configurations of markers and illuminations conditions are shown in **Table 4.4**. A higher registration error was found in configurations 1 and 2, where color markers were attached close to each other in a specific side of the cranial vault (avg. marker distance below 24 mm). A lower error was found in configurations 3, 4 and 5, where color markers were distributed separately and surrounding the cranial vault (avg. marker distance above 87 mm).

Regarding the illumination conditions, lower registration errors can be observed in most of the cases when 3D photographs were acquired with homogeneous light conditions. However, no significant differences were found between the registration error of 3D photographs acquired under the three different illumination conditions investigated.

During the real surgery, color markers were successfully sterilized and attached to the bone tissue surface using resorbable pins. In addition, automatic identification of color markers was accurately performed under the illumination conditions of the operating room, and automatic alignment and evaluation of the intraoperative photographs could be performed.

Table 4.4. Target registration error for five different spatial configurations of color markers and three different illumination conditions.

Configuration of markers		Target registration error (mm)			
ID	**Avg. marker distance (mm)**	**Homogeneous light**	**Dim light**	**Unidirectional light**	**Avg.**
1	23.30	0.29	0.50	0.52	0.44
2	23.05	0.85	0.42	0.33	0.53
3	88.78	0.31	0.43	0.38	0.37
4	102.06	0.23	0.40	0.40	0.34
5	88.08	0.22	0.22	0.24	0.22
Avg.	65.05	0.38	0.39	0.37	

4.4.5. Usability evaluation

From the scores of the questionnaire (**Table 4.5**), it can be observed that surgeons support the integration of intraoperative 3D photography for evaluation of the surgical outcome during open cranial vault remodeling to correct craniosynostosis (avg. score = 4.8). Besides, surgeons believe that the intraoperative assessment of the surgical outcome with this technology will enable them to make necessary corrections during the intervention to ensure optimal outcomes, reducing the risk of complications and reoperation (avg. score = 4.8) and increasing the security and confidence of the surgeons (avg. score = 4.8).

All surgeons agree that using this technology in the operating room is feasible and can be integrated into the surgical workflow (avg. score = 5.0). Moreover, they consider that intraoperative 3D photography will not substantially increase the operative time (avg. score = 5.0). Participants believe that 3D photography is preferred over traditional 2D photography for documenting surgical outcomes (avg. score = 5.0) and more suitable than CT imaging for evaluation since it avoids exposing children to unnecessary radiation (avg. score = 4.7). Finally, they agree that 3D photography can be useful for the intraoperative 3D reconstruction and analysis of the anatomy in other surgical specialties (avg. score = 4.8).

Table 4.5. Questionnaire scores given by the surgeons regarding the use of intraoperative 3D photography for craniosynostosis surgery.

Question	Individual scores (per surgeon)						Avg. score
	1	2	3	4	5	6	
3D photography for outcome evaluation	5	5	5	4	5	5	4.8
Usefulness of intraoperative evaluation	5	4	5	5	5	5	4.8
More suitable than 2D photography	5	5	5	5	5	5	5.0
More suitable than CT imaging for evaluation	5	4	5	4	5	5	4.7
Does not substantially increase operative time	5	5	5	5	5	5	5.0
Increases security and confidence of surgeons	5	4	5	5	5	5	4.8
Feasible integration into surgical workflow	5	5	5	5	5	5	5.0
Applicable to other surgical specialties	5	4	5	5	5	5	4.8
Avg. score	5.0	4.5	5.0	4.7	5.0	5.0	

4.5. Discussion and conclusion

Intraoperative acquisition of 3D photographs was successfully tested in five patients who underwent open cranial vault remodeling for the correction of trigonocephaly. The average duration of intraoperative scanning performed with the Artec Eva hand-held scanner was below 91 seconds and the processing time was less than 114 seconds. An increased duration in the scanning of bone tissue can be noticed. This tissue involves a more challenging 3D image acquisition due to the presence of blood and the increased complexity of the scene after skin flap elevation, a step required to expose the bone surface.

In addition, intraoperative 3D photographs of the bone tissue acquired after cranial remodeling required longer processing times. This may be caused by the irregular bone tissue surface, which is built from multiple fragments joined by resorbable plates and screws. After testing in the surgical room, the surgeon's feedback suggests that this technology can be integrated into the current surgical workflow for craniosynostosis correction without substantially increasing surgical time. Furthermore, surgeons agreed that 3D photography is more suitable than CT imaging to evaluate the surgical outcome since it will avoid the exposure of children to unnecessary radiation and reduce image acquisition time. Although increased

acquisition and processing times can be noticed in the first subject, a substantial reduction can be observed in subsequent subjects. Therefore, we believe that 3D photography acquisition and processing duration could be further reduced with experience. Nevertheless, this duration is one of the limiting factors to consider when introducing 3D photography into the surgical workflow, especially if the process has to be repeated several times during the intervention.

The accuracy of 3D photography for cranial vault surface reconstruction was below 0.5 mm for both skin and bone tissue scanning. Bone tissue scanning was found to be significantly more accurate than skin tissue scanning presenting an average accuracy of 0.17 mm, which correlates with the 0.1 mm 3D point accuracy indicated in the technical specifications of the Artec Eva scanner. Higher errors in soft tissue scanning may be caused by tissue displacements and misalignments with the preoperative CT scan. Moreover, our results of the accuracy of the Artec Eva scanner for intraoperative 3D reconstruction are consistent with those reported by Modabber et al. [81] for 3D facial scanning using the same hand-held device.

A robust framework for morphological metric computation in intraoperative 3D photographs was proposed. This methodology, based on a statistical shape atlas, enables the automatic computation of three landmarks in the frontal region of the cranium and does not require manual identification of anatomical landmarks by physicians, thus eliminating the intra- and inter-rater variability. The results of the present study demonstrate that the IFA and the TFW can be automatically computed with an average error below 0.9 degrees and 0.9 mm, respectively. These errors are caused by the resolution of the structured light scanner, which produces slight variations in the surface mesh of 3D photographs with respect to the gold-standard (preoperative CT scans). No significant differences were found between the metrics measured in the 3D photographs and the gold-standard. The average error for IFA computation is almost one order of magnitude smaller than the standard deviation of the IFA values reported in the literature [24] for each of both diagnostic groups: metopic craniosynostosis patients (116.5 ± 5.8 degrees) and controls (136.7 ± 6.2 degrees). We believe this accuracy is sufficient for the evaluation of the surgical outcome and the discrimination of pathological shape abnormalities from healthy phenotypes.

Morphology quantification of preoperative and postoperative 3D photographs of the cranial surface indicates optimal surgical outcomes for all five subjects included in this study (i.e. Whitaker class I). IFA values demonstrate an adequate correction of trigonocephaly and normalization of the forehead shape in all cases. In addition, TFW values indicate an average

overcorrection of 2 mm above the normative reference for each subject. Overcorrection of the bifrontal width is typically included in the surgical plans to compensate for subnormal cranial growth following surgery and ensure optimal long-term aesthetic and functional outcomes [63]. Therefore, intraoperative 3D photography would enable the objective evaluation of the surgical outcomes in craniosynostosis by obtaining precise 3D reconstruction of the cranial vault. This technology will enable physicians to evaluate and compare different surgical approaches and determine the most optimal approach, proving the best long-term aesthetic and functional outcome.

Current intraoperative 3D photography acquisition requires moving the mobile scanner around the surgical field to acquire images from multiple viewpoints. The main limitation of this procedure is the presence of cables between the mobile scanner and the computer, which may difficult the user's movement during acquisition and restrict the range of motion. However, in craniosynostosis procedures, the surgical field is relatively small, and optimal scanning can be performed without an extensive rotation around the patient’s anatomy. This limitation could be easily overcome using wireless structured light scanners, which enable complete freedom of movement during acquisition.

Accurate alignment of preoperative, intraoperative, and postoperative 3D photographs is essential to perform shape analysis and surgical outcome evaluation. A novel methodology for the automatic registration of intraoperative 3D photographs was described and evaluated in the present study. This methodology enables the automatic alignment of 3D photographs by identifying a set of color markers, attached to the bone tissue surface, in the texture data. The results of this study indicate that the accuracy of the registration can be reduced below 0.4 mm when color markers are distributed around the cranial vault region.

Although in this study we only acquired one single intraoperative 3D photograph after cranial vault remodeling, multiple 3D photographs can be acquired to provide valuable feedback to surgeons. Acquired 3D photographs can be processed, aligned, and visualized inside the operating room without substantially increasing surgical time. Each 3D photograph will enable the comparison of the current surgical outcome with the normative reference shape or VSP of each patient, indicating surgeons if bone fragment positions must be corrected to match the desired surgical outcomes.

The results of the present study demonstrate that 3D photography could be used not only for diagnosis [31] and patient follow-up [87] but also for intraoperative evaluation and

surgical guidance avoiding ionizing radiation from CT. Moreover, those surgical workflows requiring the design and manufacturing of cutting guides and remodeling templates could substitute CT imaging with MRI to further reduce the infants' exposure to harmful radiation [50].

To conclude, hand-held 3D photography and quantitative head shape analysis provide accurate, automatic, and objective tools for the intraoperative evaluation of the surgical outcome. These tools avoid children's exposure to radiation, generate accurate 3D morphological metrics, and do not substantially increase the operative time. This methodology can be easily integrated into the surgical workflow to reduce the subjective component of the intervention, improving the reproducibility of the surgical reconstruction, and ensuring optimal surgical outcomes.

The content of this chapter has been published in the International Journal of Computer-Assisted Radiology and Surgery (IJCARS):

D. García-Mato, M. García-Sevilla, A.R. Porras, S. Ochandiano, J.V. Darriba-Allés, R. García-Leal, J.I. Salmerón, M.G. Linguraru, J. Pascau. "Three-Dimensional Photography for Intraoperative Morphometric Analysis in Metopic Craniosynostosis Surgery". Int J CARS (2021)

5

INTRAOPERATIVE NAVIGATION

5.1. Introduction

Image-guided surgery (IGS), also known as surgical navigation or computer-assisted surgery, is an evolving technology used to assist during medical procedures by displaying the position of surgical instruments with respect to the patient's anatomy. IGS can be used to accurately transfer the preoperative virtual plan into the operating room, to check the surgical outcomes intraoperatively, and to identify important anatomical structures [88]. This technology has been applied in many fields (e.g. neurosurgery, orthopedic surgery, maxillofacial surgery) to improve the performance, speed, and safety of surgical procedures [89].

The main component of an IGS system is the tracking device, which computes the position of the surgical instruments with respect to the patient's anatomy during the intervention. Although multiple technologies are available for tracking, infrared optical tracking systems are widely used in clinical applications because of their high accuracy and large working volume [90]. These devices use cameras covering the working area to track the position of specially designed optical markers. Surgical instruments can be tracked by attaching a minimum of three optical markers arranged in a unique geometry. Then, the optical tracking system can estimate the 3D position and orientation of the surgical instruments from each camera projection. However, visualizing the position of surgical instruments with respect to

the patient’s anatomy during a surgical intervention requires the registration or alignment of the preoperative images with the patient’s position in the operating room.

Accurate patient-to-image registration is essential for successful IGS. The estimation of the spatial transformation relating the preoperative image data with the patient’s position in the operating room is based on recording the position of matching reference locations in both geometries. Techniques used for registration can be classified into two categories: surface-matching registration, and point-matching registration [91].

Surface-matching methods are usually based on laser scanners that reconstruct the patient's 3D surface intraoperatively and align that surface with the preoperative image data. However, these techniques are limited by the lack of robustness and accuracy in some scenarios [92]. Point-matching technique is the most common registration method in clinical practice. This approach is based on identifying and recording the position of a set of corresponding points in both the image and patient spaces. A minimum of three points is needed for registration. These registration points can be intrinsic, extrinsic, or a combination of both. Intrinsic points are derived from the patient's anatomy (e.g. anatomical landmarks), while extrinsic points are provided by artificially attached markers (e.g. skin adhesive markers) [93]. Since optimal anatomical landmarks are not always available for registration during IGS applications, artificial markers or fiducials attached to the skin or bone tissues are commonly used. However, these markers need to be in-place before preoperative image acquisition with a proper distribution to minimize target registration error during navigation [94]. For skin-adhesive markers, their main limitations are the time-consuming attachment, the patient's discomfort, and the loss of registration accuracy when markers move or fall off from original positions. Markers can be rigidly attached to the bone tissue to minimize errors, and it has been demonstrated that bone-mounted markers provide a higher registration accuracy than skin-adhesive markers [95]. However, the use of these markers in clinical practice is limited due to their invasiveness [91].

Patient-to-image registration establishes the relationship between the preoperative image data and the patient’s position in the operating room. However, if the patient moves during the surgical intervention, the registration must be repeated to realign the patient’s anatomy with the IGS system. Therefore, IGS systems usually rely on the patient's immobilization (e.g. stereotactic frames) [88] or the attachment of a dynamic reference frame

with optical markers to the patient's anatomy to compensate for possible movements (**Figure 5.1**) [96]. Both approaches usually involve rigid fixation to the bone tissue using screws.

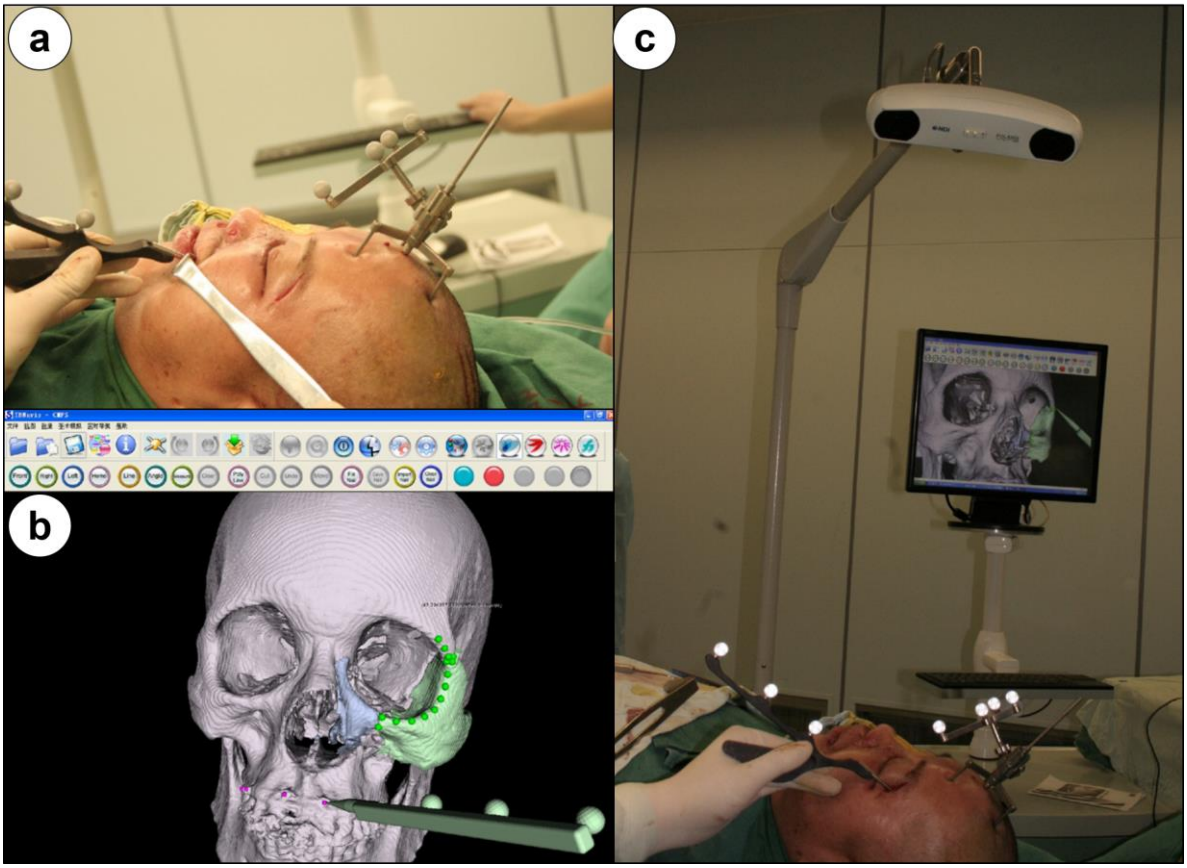

Figure 5.1. Intraoperative navigation system used for orbital floor reconstruction. (a) Dynamic reference frame fixed rigidly to the patient's skull. (b) Recording of the position of five positioning screws attached preoperatively to the maxillary alveolar bone for patient-to-image registration. (c) Navigation of surgical tool using an optical tracker. Image adapted from [96] (figure reprinted with permission from the copyright holder, Elsevier).

IGS based on real-time tool tracking has not been applied yet to craniosynostosis surgical correction owing to the risk, invasiveness, and discomfort associated with head immobilization and the attachment of landmarks for intraoperative registration. Although an adult's skull can support an invasive head immobilization or reference fixation using screws, the infant's skull is thin and fragile [66]. Cranial fixation is rarely used in patients under two years of age due to the potential risk of skull and brain injury from pin fixation. Some complications derived from fixation pins in infants include cranial fractures, cerebrospinal fluid leak, and epidural and subdural hematomas [67].

Nowadays, craniosynostosis surgical correction is still highly dependent on the subjective assessment and artistic judgment of craniofacial surgeons. Therefore, there is a large

variability in the performance of multiple surgeons and, thus, the surgical outcomes are not reproducible. Although the more experienced craniofacial surgeons may achieve optimal surgical results, more complications may arise among the less experienced.

Several methodologies have been proposed to reduce the subjectivity and improve the surgical outcomes in craniosynostosis surgery. Hochfeld et al. [54] proposed the use of a stereotactic frame and Schanz screws to control the position of the fragments during the remodeling phase. Although the preliminary results obtained with this frame-based remodeling approach are positive, the incorporation of this technique into the standard clinical practice is limited by the increased surgical time, complexity, and invasiveness associated with the fixation of the frame to the patient.

Later on, Kobets et al. [52] described a guidance system to confirm bone fragment placement through intraoperative CT imaging, to evaluate the surgical outcome, and to make corrections in bone fragment positions if necessary. However, this technique requires the exposure of the infant to ionizing radiation, increases operative time, and does not enable real-time adjustment of bone fragments position to achieve the desired surgical outcome. Therefore, its application into the standard clinical practice is also limited.

IGS based on real-time tool tracking could assist during osteotomy and guide the positioning of the remodeled bone fragments to achieve the desired target shape. This technology will significantly benefit craniosynostosis surgery by reducing the subjectivity associated with the current surgical workflow. IGS could enable surgeons to accurately translate the preoperative VSP into the operating room and achieve optimal and reproducible outcomes.

5.2. Objective

In this study, we propose a new workflow for surgical correction of craniosynostosis based on intraoperative navigation and patient-specific 3D printed guides and templates. Our objective was to evaluate IGS for the positioning of remodeled bone fragments in craniosynostosis surgery. The proposed workflow was followed in five patients affected by common types of single-suture synostosis. Our workflow does not require head immobilization or preoperative attachment of registration landmarks, thus avoiding invasiveness and patient discomfort. To our knowledge, this is the first study to apply intraoperative navigation with IGS technology for the correction of craniosynostosis.

5.3. Materials and methods

We first describe the subjects included in this study. Then, we present the methodology used to design and manufacture patient-specific guides and templates for osteotomy and remodeling. Next, we describe the intraoperative navigation system and surgical procedure followed for remodeled bone positioning. Finally, an intraoperative 3D photography technique and methods for data analysis and evaluation are detailed. A summary of the proposed framework is presented in **Figure 5.2**.

5.3.1. Cases

The proposed workflow was followed in five patients: an 8-month-old girl with trigonocephaly, a 9-month-old boy with trigonocephaly, a 13-month-old girl with anterior plagiocephaly, a 15-month-old (corrected age is 12 months) girl with trigonocephaly, and a 16-month-old (corrected age is 13 months) boy with trigonocephaly. The patients were nonsyndromic, had not undergone prior craniofacial surgeries, and did not present hydrocephalus, intracranial hemorrhages, or craniofacial trauma. The parent or legal guardian of the patients signed an informed consent for study participation and a specific consent for publication of identifying images (patient 1).

The study was performed in accordance with the principles of the 1964 Declaration of Helsinki as revised in 2013 and was approved by the Research Ethics Committee at Hospital General Universitario Gregorio Marañón.

5.3.2. CT image acquisition and processing

A preoperative cranial CT scan was acquired for all patients with a Philips Mx8000 scanner. The axial in-plane pixel size ranged between 0.24 and 0.28 mm, the slice thickness ranged between 1 and 1.3 mm, and the spacing between slices ranged between 0.5 and 0.6 mm for all cases. CT imaging is the standard procedure in our center for confirming the diagnosis by evaluating the state of cranial sutures.

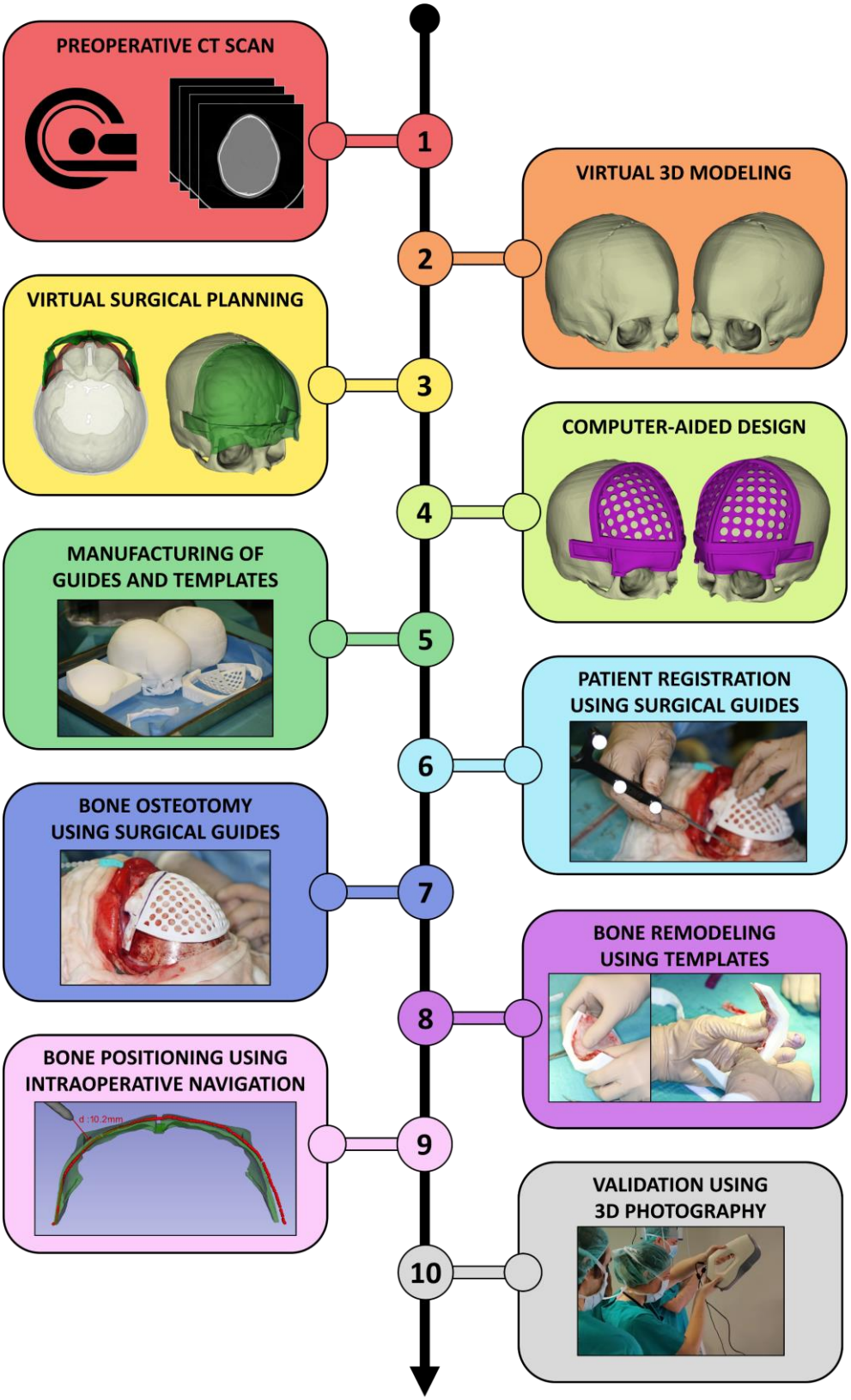

Figure 5.2. Proposed workflow for surgical correction of craniosynostosis

Bone tissue was segmented from CT images with intensity-based algorithms, and a 3D model of the skull was generated on 3D Slicer software [97]. The model was post-processed to eliminate unnecessary small-scale anatomical structures not 3D-connected with the region of interest. Then, the segmented model was smoothed using a Laplacian smoothing algorithm (iterations = 10, relaxation factor = 0.1) to remove stair-step artifact. Holes in the output mesh were filled to ensure continuity in the final mesh. The Surface Toolbox in 3D Slicer software was used in all post-processing steps. The final continuous 3D mesh was used as a reference for computer-assisted preoperative planning (**Figure 5.3a**).

5.3.3. Virtual surgical planning and computer-aided design

The standard procedure for FOA to treat metopic and unicoronal synostoses involves repositioning of the frontal bones and supraorbital bar [98]. Therefore, for the clinical cases evaluated in this study, VSP included osteotomies of the frontal bones and the supraorbital bar. Once the preoperative 3D virtual model of the skull was available, the surgeons performed virtual surgery on a computer workstation with the collaboration of biomedical engineers.

Specific CAD software (Freeform® Plus) was used for the following: (1) planning the surgical osteotomies (**Figure 5.3b**), (2) creating 3D models of patient-specific surgical cutting guides to assist during intraoperative osteotomies and including reference points for intraoperative navigation (**Figure 5.3c**), (3) simulating affected bone remodeling (**Figure 5.3d-e**), (4) generating 3D models of templates to assist during intraoperative bone remodeling (**Figure 5.3e**), and (5) generating postsurgical 3D models of the skull using the virtually remodeled bone fragments. All virtual models were exported in stereolithography (STL) file format.

Once the design was concluded, surgical guides and templates were manufactured using selective laser sintering (additive manufacturing) and polyamide material (KLS Martin Group, Tuttlingen, Germany). All 3D printed models were sterilized before surgery using standard autoclave protocols.

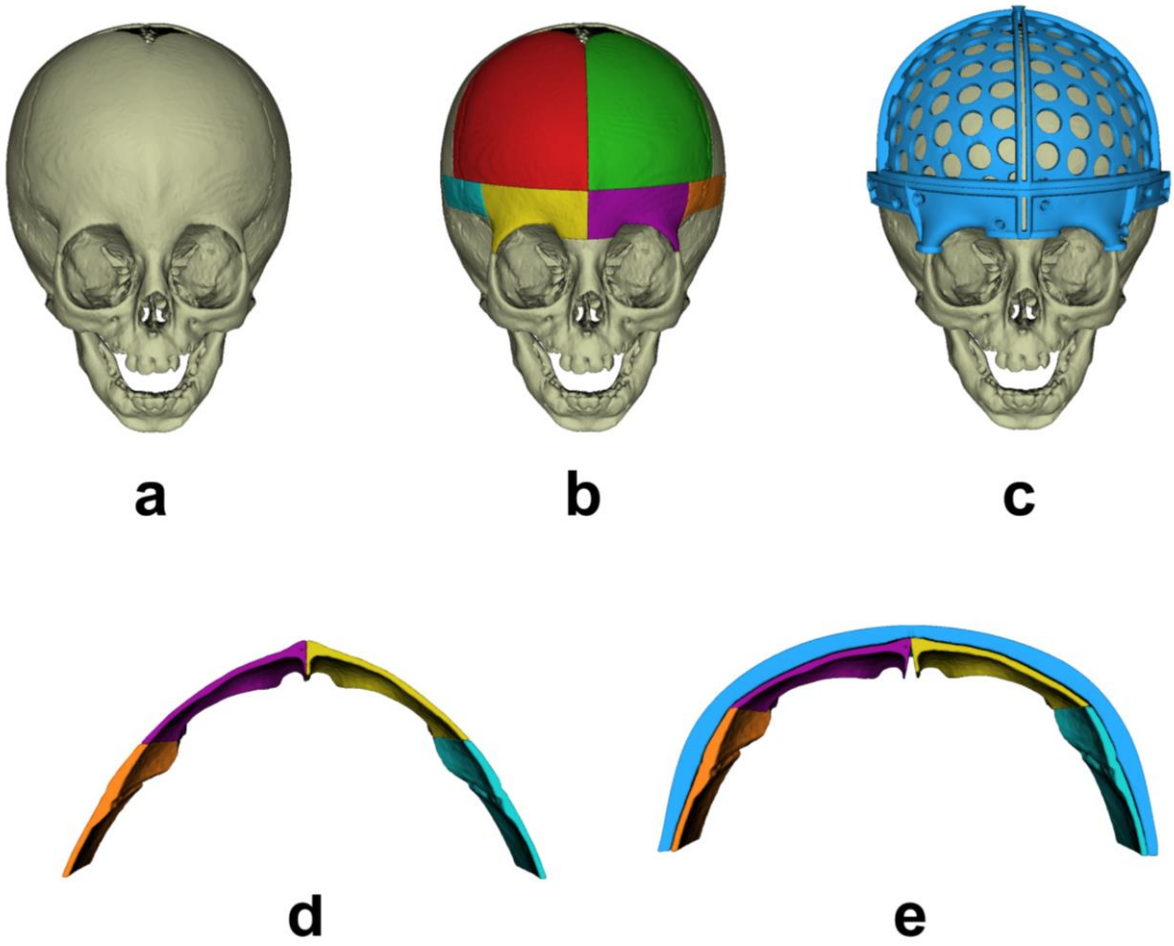

Figure 5.3. Virtual surgical planning: (a) preoperative skull model, (b) planned osteotomies, (c) designed cutting guides, (d) preoperative supraorbital bar, (e) remodeled supraorbital bar using a patient-specific template.

5.3.4. Intraoperative navigation

A software application called *CranioNav* was specifically developed as a module in the 3D Slicer platform [99] to assist surgeons during the procedures. *CranioNav* enables the importation of CT imaging studies, anatomical 3D models, and preoperative VSP.

A Polaris Spectra (NDI, Waterloo, Canada) optical tracking system was used for real-time tool positioning. The device was mounted on a tripod inside the operating room, and its position was adjusted to ensure that the field of view covered the surgical area. The optical tracker includes two infrared cameras and enables the tracking of instruments containing a configuration of three or more reflective optical markers. The IGS system uses a pointer tool, composed of four spherical optical markers, which is sterilized and used by the surgeon during

navigation. Positioning data from the tracking device are transferred to *CranioNav* using the PLUS toolkit [100] and the OpenIGTLink communication protocol [101].

Preoperative image data and the intraoperative physical anatomy were aligned using a two-step registration procedure based on patient-specific 3D printed surgical guides and external markers attached intraoperatively. This registration technique did not require the patient's head to be immobilized during surgery or markers to be attached to the patient's anatomy prior to CT imaging.

During the first step, once osteotomy guides were fitted to the patient's bone surface, predefined points of the 3D printed guides were recorded with the tracked pointer tool (**Figure 5.4a**). A *primary registration* was obtained using these landmarks. Then, a *secondary registration* was performed by recording the position of external markers attached intraoperatively to the bone (**Figure 5.4b**). The markers used were resorbable pins (SonicPins Rx, KLS Martin, Tuttlingen, Germany), which were inserted by drilling holes in the bone tissue surrounding the affected region. This two-step registration makes it possible to account for the position of the head since the secondary registration can be repeated at any time during the procedure.

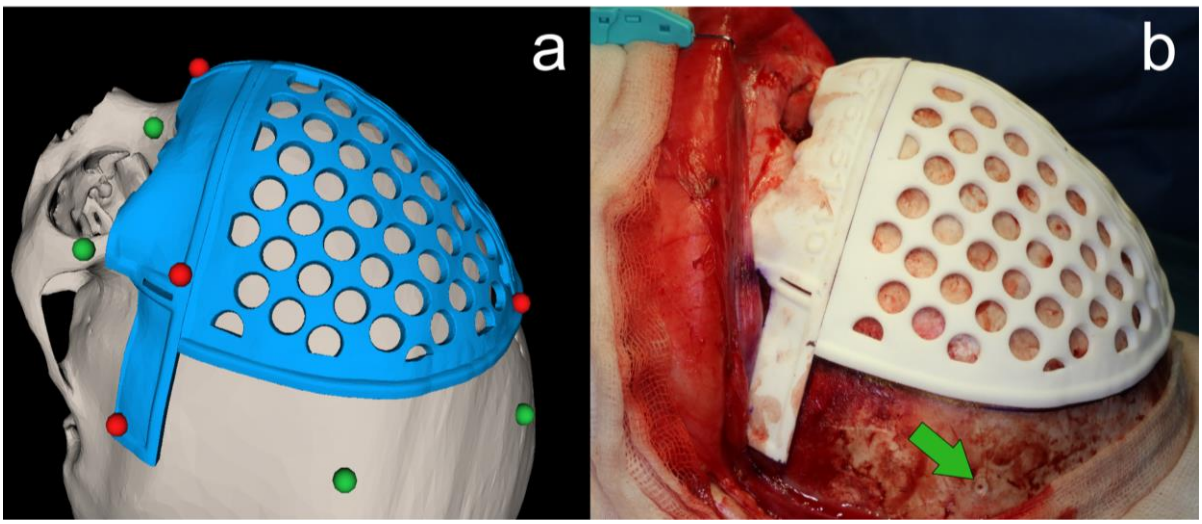

Figure 5.4. (a) Virtual models and distribution of registration landmarks for primary (red) and secondary registration (green). Landmarks for primary registration are included in the design of the surgical guides, while landmarks for secondary registration are intraoperatively attached and recorded using the tracked pointer tool. (b) Resorbable pin attached intraoperatively in the parietal region of the cranium for secondary registration.

CranioNav was displayed on a screen adjacent to the surgical field in order to guide the surgeons during the intraoperative navigation steps (**Figure 5.5**). First, it enabled the user to record registration points using the tracked pointer tool and to perform intraoperative registration. The software displayed registration errors and enabled the user to repeat the registration procedure when needed. Once registration had been performed, *CranioNav* displayed the real-time position of the tracked pointer with respect to the CT imaging data and virtual anatomical 3D models of the patient.

The application enabled the surgeon to visualize different 3D views of the scene, which can be defined preoperatively. Moreover, the system displayed the real-time distance from the tracked pointer tooltip to the VSP and anatomical regions of interest, thus providing visual and acoustic feedback to the surgeon. It is also possible to record point coordinates and perform geometrical measurements, which may be clinically relevant for the surgeon.

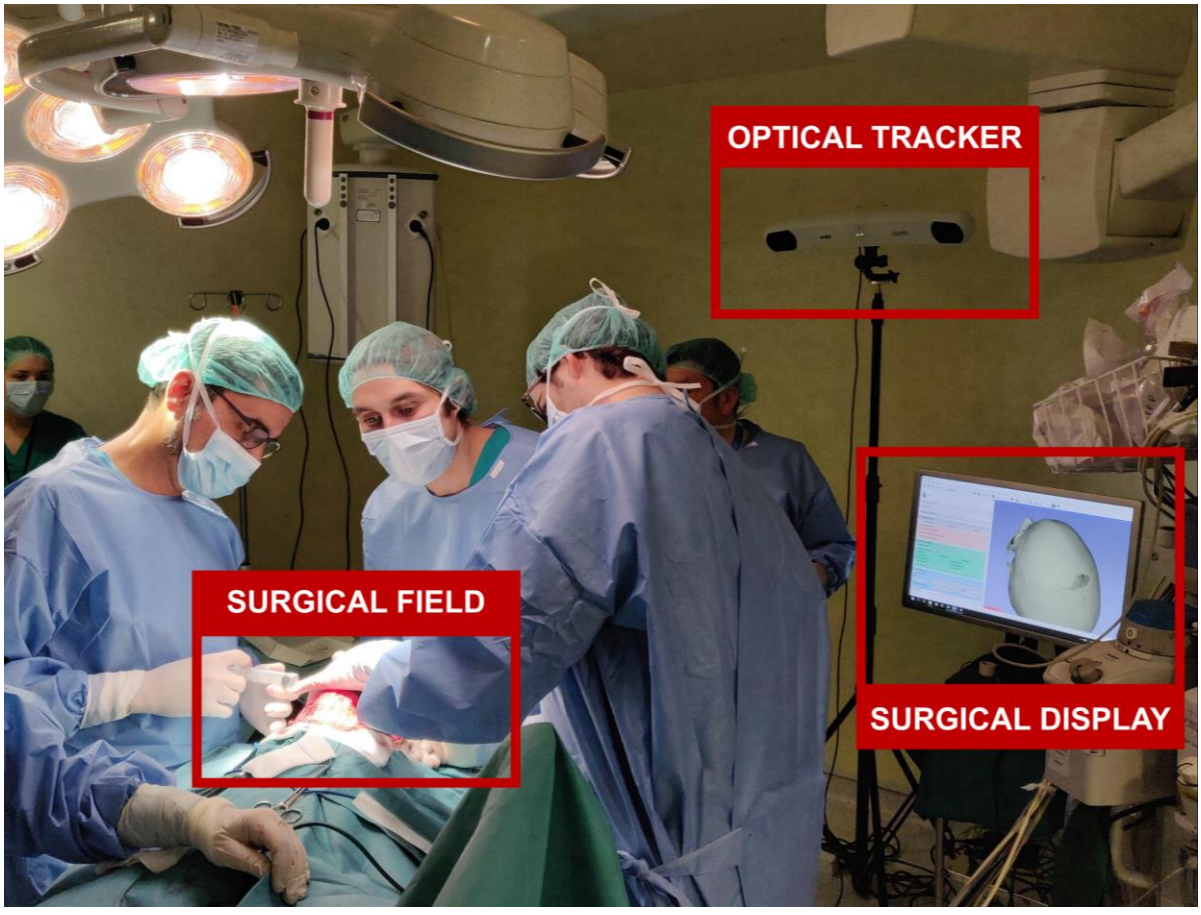

Figure 5.5. Setup for intraoperative navigation during craniosynostosis surgery. The NDI Polaris Spectra (NDI, Waterloo, Canada) optical tracking system is placed on a tripod. A surgical display is positioned adjacent to the surgical field to provide information to the surgeons.

5.3.5. Surgical procedure

A bicoronal S-shaped incision was made to expose the frontal and supraorbital regions. Once the bone surface was exposed, 3D printed patient-specific surgical guides were placed on the cranium, and the six resorbable registration pins were attached to the surface of the healthy bone outside the osteotomy region. Then, *primary registration* was performed by recording the position of six predefined characteristic points included in the surgical guides using the tracked pointer tool (**Figure 5.6a**). After primary registration, the positions of the resorbable pins were recorded for later usage during the *secondary registration* procedure.

Osteotomies of the frontal bone and supraorbital bar were performed following the edges of the cutting guides. The affected bone tissue was removed and then reshaped using the 3D printed patient-specific templates. Resorbable plates and pins were used to reinforce and reshape the bone tissue.

The next step was the placement and fixation of the remodeled bone over the exposed dura. First, secondary registration was performed by recording the position of the resorbable registration pins. Then, *CranioNav* displayed the position of the tracked pointer tooltip with respect to virtual anatomical models and CT images of the patient. The IGS system enabled the surgeon to verify that the reshaped bone has been placed in the location defined during preoperative VSP by recording the bone surface using the tracked pointer tool (**Figure 5.6**).

The final position of the bone fragments was obtained after an iterative process consisting of: (1) partially fixing the remodeled bone fragment to surrounding healthy bone using resorbable plates and screws, (2) recording bone fragment position using tracked pointer tool, (3) comparing recorded position with VSP, and (4) making corrections to match target position defined in planning based on the metrics provided by the navigation software and the surgeon's visual assessment. The patient's head was not immobilized during surgery, with the result that secondary registration was frequently repeated to minimize navigation error.

Once the optimal position had been achieved, the remodeled bone tissue was stabilized in place using additional resorbable plates and screws. The final surgical outcome was recorded by moving the tracked pointer tool along the surface of the reconstructed supraorbital bar and frontal bone.

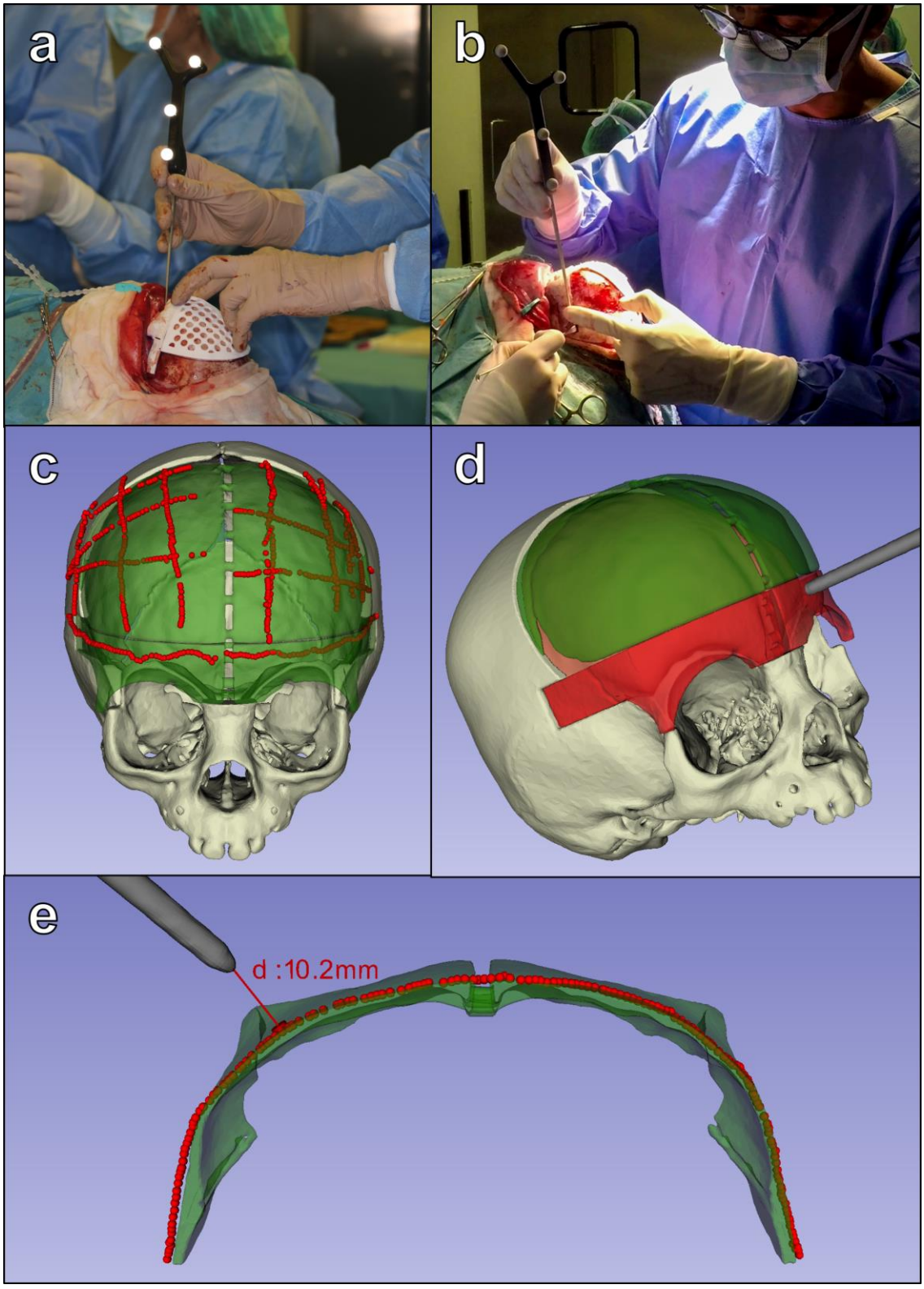

Figure 5.6. (a) Surgeon recording registration points on 3D printed osteotomy guides, (b) surgeon using the tracked pointer tool to compute bone fragment position; (c) Navigation points recorded on the remodeled bone surface (red) and VSP (green); (d-e) Navigation on the supraorbital bar using pointer tool.

5.3.6. Intraoperative 3D photography

Once remodeled bone fragments were positioned and fixed, intraoperative 3D photographs were acquired to document and evaluate the outcome of cranial vault reconstruction using Artec EVA® structured light scanner (Artec Group, Luxembourg) (**Figure 5.7**). Preoperative and postoperative scans were performed for each surgery. This hand-held scanning device illuminates the surgical area with striped-patterns of bright white light and computes a 3D surface mesh from the deformation of the patterns. In addition, a third camera is used to obtain color texture information. During the scanning process, this device was moved around the region of interest, and the acquired 3D images were automatically aligned and fused using geometric and textural information. The final 3D surface, texture, and mapping information were exported in Wavefront OBJ (.obj), Joint Photographic Experts Group (.jpg), and Material Template Library (.mtl) file formats, respectively.

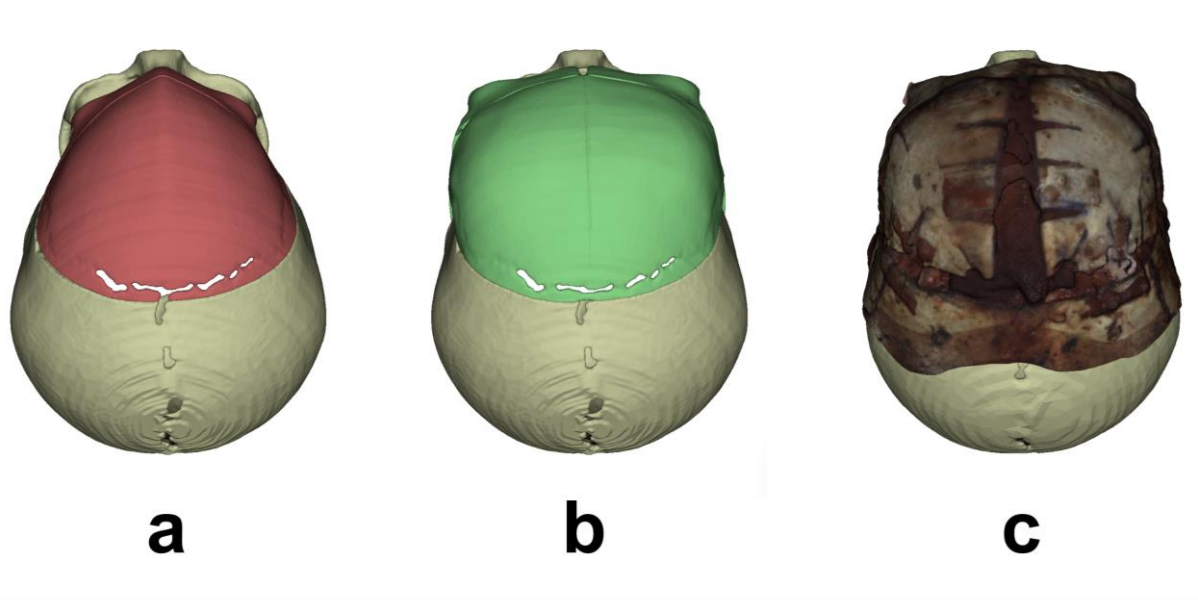

Figure 5.7. Superior view of (a) preoperative bone 3D model obtained from CT scan, (b) virtual surgical plan, and (c) postoperative bone 3D photograph.

5.3.7. Data analysis and evaluation

In order to evaluate the accuracy of intraoperative registration performed during the five navigated craniosynostosis reconstruction surgeries, the root-mean-square error (RMSE) was computed at the fiducials for all repetitions of primary and secondary registrations. The time spent on this task was also measured.

The accuracy of the navigation system was estimated by recording points along the surface of the remodeled bone. Intraoperative 3D photographs were used as the gold-standard to measure navigation error. The intraoperatively scanned bone surface was registered to the navigation data using the position of the resorbable pins used for secondary registration. These pins can be easily identified in the 3D photographs thanks to the texture information provided by the scanning device. Therefore, a fiducial-based registration can be performed to align the intraoperative 3D photograph with the navigation data. After registration, the navigation error was estimated as the average absolute Euclidean distance between the recorded navigation points and the intraoperative 3D photograph.

Finally, the surgical outcome of FOA was evaluated by measuring the IFA and TFW. These morphological metrics were computed using three landmarks, one located at the left frontal bone (LFL), one at the right frontal bone (RFL), and one along the metopic suture (MSL). These landmarks were manually selected for each subject. IFA is defined as the angle formed by the left frontal segment (LFL-MSL) and right frontal segment (RFL-MSL) and the TFW value is measured as the distance between the two most lateral landmarks (LFL and RFL). Both metrics were computed in the preoperative model, the VSP, and the intraoperative 3D photograph. Surgical outcome error was estimated as the difference between the virtual planned and the postoperative values.

5.4. Results

Primary registration, which was performed using six landmarks on the 3D printed surgical guides, yielded an average RMSE of 0.94 ± 0.27 mm for the five surgeries under study. The average time required to perform the registrations was 50 ± 10 seconds.

Secondary registration, which was performed using the position of six resorbable pins attached intraoperatively, yielded an average RMSE of 1.30 ± 0.47 mm. Of note, this secondary registration was performed 17, 9, 12, 9, and 9 times for surgeries 1, 2, 3, 4, and 5, respectively. This registration step must be repeated to avoid increased navigation errors caused by the patient's head movement. The average duration of secondary registrations was 40 ± 14 seconds. The results are summarized in **Table 5.1**.

Table 5.1. Root mean squared error and duration of primary and secondary registrations.

	Intraoperative Registration			
	Primary		Secondary	
Patient	RMSE (mm)	Duration (s)	RMSE (mm)	Duration (s)
1	0.65	42	1.87 ± 0.31	32.41 ± 9.17
2	1.07	65	1.16 ± 0.34	57.56 ± 5.31
3	1.25	55	0.96 ± 0.14	34.00 ± 8.13
4	0.58	54	1.19 ± 0.09	36.60 ± 5.00
5	1.18	36	0.90 ± 0.32	49.56 ± 14.84
Avg.	0.94 ± 0.27	50.40 ± 10.25	1.30 ± 0.47	40.50 ± 13.61

The results of the estimation of navigation accuracy using intraoperative 3D photography as a gold-standard are shown in **Figure 5.8**. An average error of 0.63 mm ± 0.42 mm was obtained. The error was 0.62 mm ± 0.39 mm in the remodeled frontal region and 0.64 mm ± 0.46 mm in the remodeled supraorbital bar. The statistical analysis of the error distribution data shows that 75% of the recorded points (third quartile) present an error below 0.97 mm.

IFA and TFW measurements are shown in **Table 5.2**. Preoperative values correlate with the bitemporal narrowing caused by metopic synostosis and unilateral supraorbital recession associated with unicoronal synostosis. The absolute difference between target and postoperative IFA was 6.31°, 0.48°, 1.05°, 5.38°, and 4.91° for surgery 1, 2, 3, 4, and 5, respectively. The average error was 3.63°. TFW absolute error was 3.27, 1.12, 1.68, 3.30 and 0.06 mm for surgery 1, 2, 3, 4 and 5, respectively. The average error was 1.89 mm.

This difference with respect to VSP is caused mainly by the flexibility of the remodeled bone, which is composed of several fragments fixed with resorbable plates and screws. In addition, surgeons usually make slight modifications to virtual planning based on their experience. As a general rule, increased overcorrection is applied in surgical planning, but the degree of overcorrection is usually reduced intraoperatively owing to practical limitations such as skin elasticity. This pattern can be observed in the IFA and TFW results since measured postoperative values were lower than target values in all five patients.

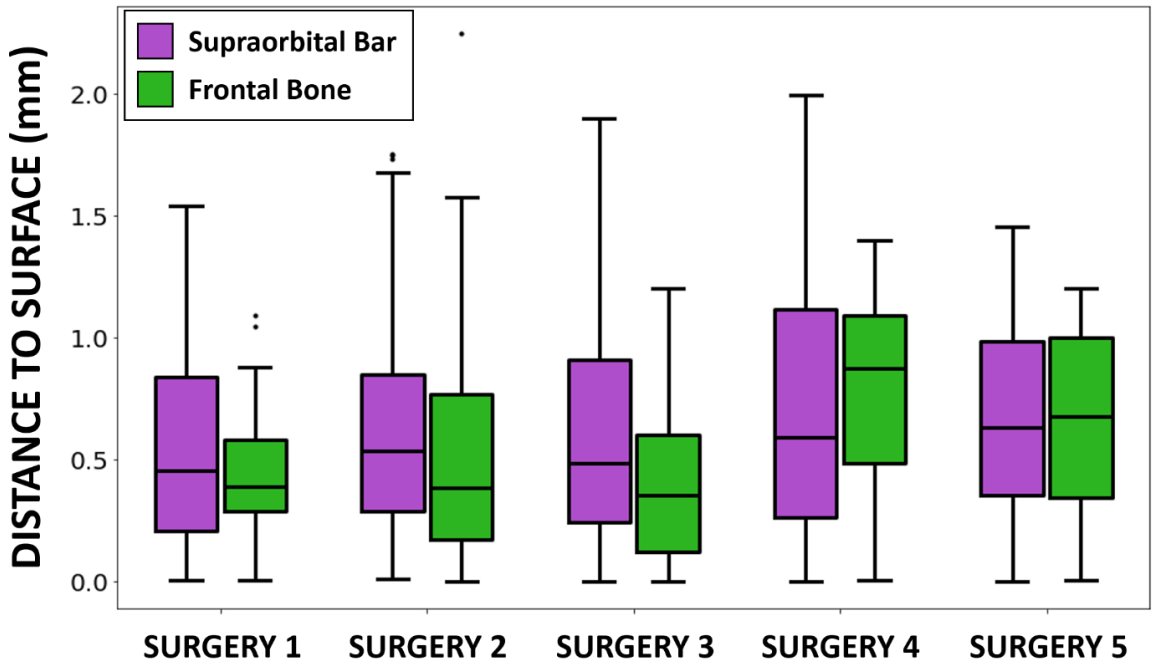

Figure 5.8. Estimated navigation error using the intraoperative 3D photograph as the gold-standard. Error is computed as the point-to-surface distance between the points recorded during the navigation and the cranial vault surface reconstructed intraoperatively using Artec Eva structured light scanner.

Table 5.2. Interfrontal angle and transverse forehead width measured in preoperative skull model (pre-op), virtual surgical plan (VSP), and postoperative 3D photograph (post-op).

		Interfrontal Angle (º)			Transverse Forehead Width (mm)		
ID	**Type**	**Pre-Op**	**VSP**	**Post-Op**	**Pre-Op**	**VSP**	**Post-Op**
1	Metopic	99.70	130.03	123.72	78.57	93.28	90.01
2	Metopic	99.41	135.14	134.66	73.78	88.41	87.29
3	Unicoronal	125.52	144.21	143.17	93.07	97.83	96.15
4	Metopic	112.24	130.38	125.00	88.51	95.46	92.16
5	Metopic	116.94	139.38	134.46	78.53	84.65	84.60

The surgical outcome for patients presenting trigonocephaly shows improved bitemporal width and correction of metopic ridging. Correction of plagiocephaly improved orbital symmetry and forehead projection. Symmetry, harmony, and balance between the face and cranial vault were achieved in all five patients (**Figure 5.9**).

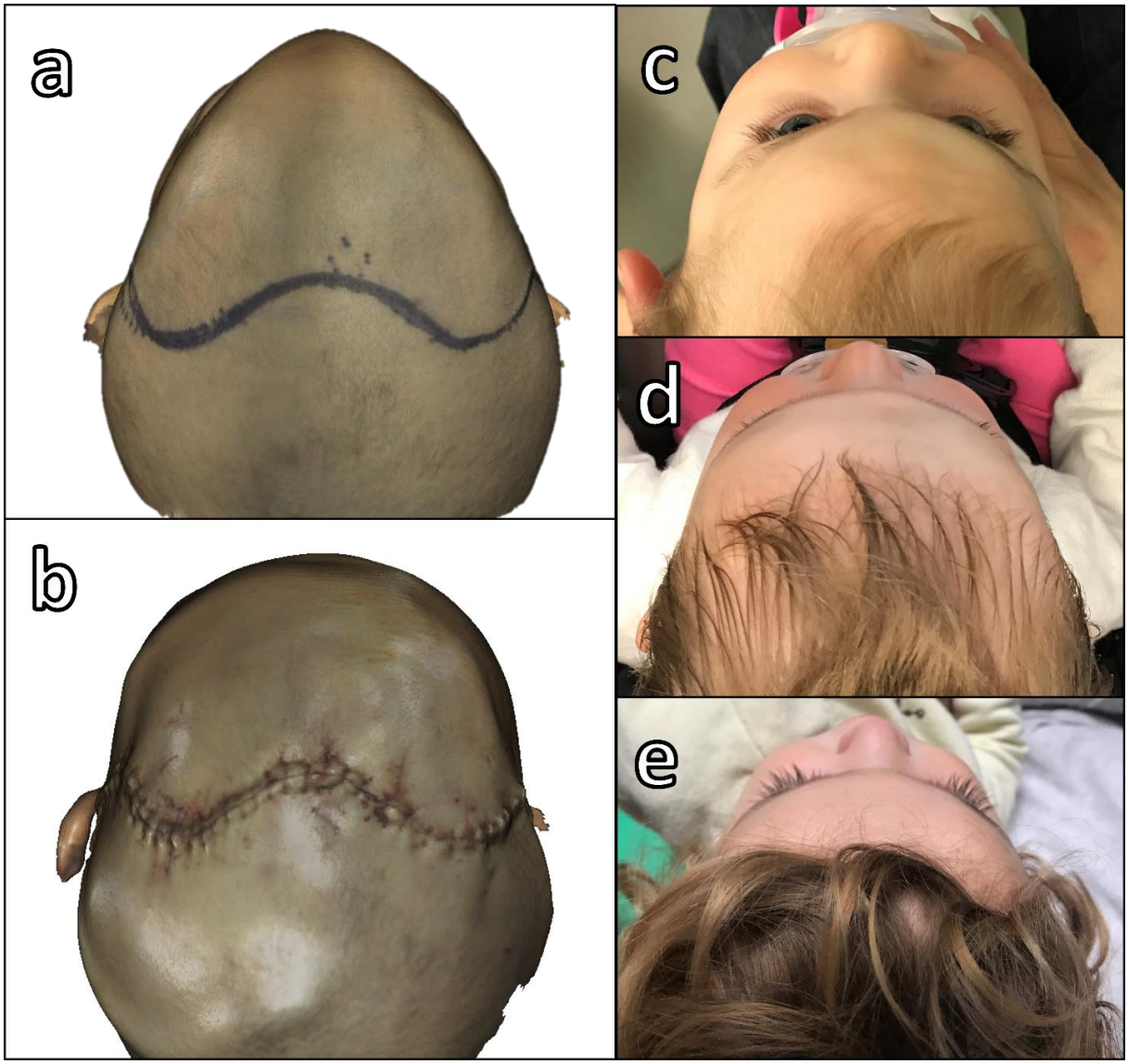

Figure 5.9. Surgical outcome of patient 1: (a) intraoperative 3D photograph before remodeling, (b) intraoperative 3D photograph after remodeling, (c) 2D photograph before surgery, (d) 2D photograph 4 months after surgery, and (e) 2D photograph 1 year after surgery.

5.5. Discussion and conclusion

In this study, we propose a novel methodology for the surgical correction of craniosynostosis. The workflow is based on the use of intraoperative navigation combined with patient-specific 3D printed guides and templates. The method was evaluated in the cranial vault reconstruction procedures of five patients with craniosynostosis and yielded optimal matching with preoperative virtual planning.

In comparison with the approach proposed by Hochfeld et al. [54] which requires the attachment of a stereotactic frame to the patient, our intraoperative navigation solution does not require the patient's head to be immobilized or external markers to be attached prior to surgery. The proposed two-step registration procedure uses 3D printed surgical guides and intraoperatively attached markers as landmarks. This methodology enables the user to repeat the registration multiple times during surgery to minimize navigation errors. The average time spent during the primary and secondary registration steps was 50 and 40 seconds, respectively. Therefore, intraoperative registration does not substantially increase surgical time and it is a good alternative to head immobilization in this kind of procedures.

While previous methodologies for surgical guidance in craniosynostosis do not provide real-time feedback to the surgeons [55], our intraoperative navigation system enables real-time control of the bone fragments position and comparison with respect to the VSP for accurate cranial vault remodeling. *CranioNav* displays real-time tool position with respect to 3D models and preoperative CT images. The position of remodeled bone tissue can be modified according to navigation data to ensure accurate matching with preoperative VSP. The available functionalities, such as real-time tool-to-surface distance or reconstructed bone outline recording, facilitate the surgeons' work. Navigation error was evaluated using intraoperative 3D photography as a reference. An average error of <0.7 mm was obtained, thus indicating the accuracy of real-time tool positioning and intraoperative registration achieved by the system. Surgeons were trained to use the navigation system by performing simulations on phantoms prior to surgeries. Our system presented a short learning curve, and surgeons were able to achieve good performance after several simulations.

The portable scanning device enables non-invasive, radiation-free, anesthetic-free and fast acquisition of 3D photographs of the reconstructed cranial vault. This technology could replace postoperative CT imaging studies for outcome and follow-up analysis, thus avoiding exposure to unnecessary radiation. Moreover, the portability of this device enables its use in the operating room for intraoperative reconstruction and outcome estimation. Intraoperative scans could be directly compared with the preoperative VSP to assess the quality of the surgical outcome.

Surgical outcome was evaluated by measuring the IFA and TFW in the preoperative skull model, VSP, and intraoperative 3D photograph. The average difference between the IFA and TFW defined during planning and the values achieved after surgical reconstruction was

3.63° and 1.89 mm, respectively. Moreover, the postoperative results show symmetry, harmony, and balance between the face and cranial vault in all five patients. The use of normative skull models as a reference during virtual planning could improve surgical outcomes and reduce inter-surgeon variability in the determination of the target cranial vault shape. Although normative age-matched skull models were not used in this study, their use would not require any modifications in our workflow.

This novel workflow for craniosynostosis reconstruction based on intraoperative navigation and 3D printing enables an accurate translation of preoperative surgical planning into the operating room, thus improving the reproducibility of craniosynostosis surgeries and reducing inter-surgeon variability. Therefore, interventional plans minimizing cranium malformations can be used in actual surgeries to ensure optimal outcomes without a substantial increase in surgical time.

The content of this chapter has been published in Scientific Reports journal:

D. García-Mato, S. Ochandiano, M. García-Sevilla, C. Navarro-Cuéllar, J.V. Darriba-Allés, R. García-Leal, J. A. Calvo-Haro, R. Pérez-Mañanes, J.I. Salmerón, J. Pascau. "Craniosynostosis surgery: workflow based on virtual surgical planning, intraoperative navigation and 3D printed patient-specific guides and templates". Sci. Rep., vol. 9, no. 1, p. 17691, 2019.

6

AUGMENTED REALITY

6.1. Introduction

Augmented reality (AR) technology is the process of overlaying computer-generated information on reality to enhance user experience or understanding [102]. While in virtual reality (VR) the users are completely immersed in a synthetic virtual world, AR technology blends the virtual information with the real world to improve the perception of reality. AR systems are based on two core components: a display device to combine the virtual data with the real-world scene, and a technique to continuously estimate the spatiotemporal relationship between the real and virtual worlds for optimal visualization [103].

The use of this AR technology in the medical field has exponentially increased in the past two decades. One common application of AR is the training of medical personnel. This technology has been used to create simulators for training and assessment of surgical skills in minimally invasive surgery [103], percutaneous needle insertion [104], neurosurgery [105], and other interventions. Several studies have demonstrated that AR-based simulation enhances the learning retention and performance of trainees by creating authentic simulated experiences [106].

In addition, AR has also been proposed for surgical planning and guidance. This technology enables the surgeons to focus on the surgical field while having access to external virtual information overlaid on the scene to improve the accuracy and safety of the procedures.

The use of AR for surgical guidance has been reported in a great variety of interventions, such as neurosurgery [107], cardiac surgery [108], or maxillofacial surgery [109]. AR is especially useful to improve the visual capabilities of surgeons during minimally invasive surgical procedures, where the intervention is performed through small incisions and the field of view of the surgeons is limited [110].

There are three main categories of display devices for AR visualization during surgery: video-based display, see-through display, and projection-based display [110]. Video-based displays overlay AR information on the video streams of cameras capturing the real environment. Video streams can be provided by hand-held devices (e.g. smartphones or tablets) [111], external cameras located around the patient [112], endoscopic cameras [113], or by head-mounted cameras [114]. Information can be displayed to users on hand-held devices, external screens, or in front of the surgeon's eyes. The main limitation of video-based systems is the display resolution, which does not enable users to perceive the real word naturally. Therefore, see-through displays have been developed to directly overlay the virtual information on the user's view using a semi-transparent mirror in front of the user's eyes. Nowadays, head-mounted devices with optical-see-through displays (e.g. Microsoft HoloLens or Magic Leap) are being reported for AR visualization in the operating room [115]. Finally, another alternative is to directly project the virtual information on the patient's anatomy using a video projector or other technologies [116]. This approach does not require users to wear or hold any device for visualization.

One of the main difficulties of AR visualization is the registration of the virtual data with the real environment [117]. An optimal alignment of the virtual and real worlds is essential and directly impacts the usability and performance of AR systems. Multiple approaches for AR visualization are based on manual registration, where the users manually translate and rotate the virtual models to find an appropriate matching [118], [119]. AR systems using manual registration usually rely on simultaneous localization and mapping (SLAM) to keep the rendered virtual images (holograms) in a fixed position in the scene, even if the user changes their viewpoint and position. However, multiple studies have demonstrated high tracking errors of approximately 6 mm caused by the uncertainty of the SLAM and, thus, the variability in the position of the holograms in the scene [120], [121].

In this context, AR systems have integrated the use of optical [107], [122], or electromagnetic [123] tracking systems to minimize tracking errors. Tracking systems can be

used to record the position of specific landmarks or surfaces in the scene to accurately align the virtual models (holograms) with the real environment for optimal visualization. Although tracking errors can be successfully minimized when using tracking systems, these approaches are limited by the extra hardware required, the complexity of the workflow, and the increased duration of the procedure.

Other techniques for AR visualization are based on visual pattern markers attached to the patient, which are tracked by an RGB camera [124]. Tracking of the marker enables the systems to update the position of the virtual data to ensure an accurate matching with the patient's anatomy. Several studies report the use of occlusal splints to attach AR markers to the teeth of the patient for intraoperative guidance during maxillofacial surgery [109], [124]. However, these occlusal splints are attached manually, and 3D laser scanning is required to calculate the spatial relationship between the marker and the patient's anatomy. Other studies have proposed 3D printed surgical guides that fit in a unique position of the bone and incorporate a marker for AR tracking [115], [125]. The use of 3D printed surgical guides enables the automatic registration with the intraoperative patient's anatomy and reduces the complexity of the surgical workflow and the operative time.

One previous study reports the use of AR technology for guidance during craniosynostosis reconstruction surgeries [126]. The reported system is based on an AR marker attached to the teeth of the patients with occlusal splints, and an external camera used to track the marker and project the virtual models in the video stream. Authors report the use of this system to guide osteotomy and remodeling during open cranial vault remodeling. However, the accuracy of the AR visualization was not evaluated, and only subjective metrics of the final surgical outcome were provided. In addition, the marker required for virtual-to-real registration is located in the lower face, while the region of interest during craniosynostosis surgical correction is the cranial vault. Therefore, a loss of accuracy should be expected in the cranial vault region when using occlusal splints for alignment [127], making this approach unsuitable for integration into the current surgical workflow of craniosynostosis.

6.2. Objective

In this work, we present and evaluate a novel workflow for AR guidance during craniosynostosis reconstruction surgeries. The proposed workflow combines smartphone-based AR display with 3D printed markers attached intraoperatively near the region of interest

to minimize the visualization error. Also, the workflow integrates intraoperative 3D photography for accurate registration of the virtual data with respect to the patient's anatomy. The aim of this work is the evaluation of the performance and the feasibility of this methodology to guide cranial osteotomies and remodeling in the operating room.

6.3. Materials and methods

We first describe the patients included in the study, the available data for each patient, and the design of patient-specific phantoms. Then, we describe the workflow for AR visualization and the components of the system. Finally, the performance evaluation and surgical deployment of the system are detailed.

6.3.1. Database

The proposed methodology was evaluated using the data of three patients presenting trigonocephaly malformation caused by premature fusion of the metopic suture. The average age of the patients was 10 ± 2 months old. All patients were treated with an open cranial vault remodeling with FOA in our center.

Available data for each patient includes a preoperative CT scan and a VSP. CT scans present an axial in-plane pixel size of 0.25 mm, a slice thickness ranged between 1 and 1.3 mm, and a spacing between slices ranged between 0.5 and 0.6 mm. VSP was defined by performing virtual surgery on a computer workstation in collaboration with biomedical engineers. A total of 8 different cutting planes were determined considering anatomical landmarks and using the Frankfurt plane as a reference (**Figure 6.1**). These planes were used to cut a virtual model of the skull generated from the preoperative CT scan using intensity-based segmentation. Six bone fragments were created in the fronto-orbital region and virtually transformed (translated, rotated, and deformed if necessary) to simulate the FOA procedure for the remodeling of the cranial vault. The target cranial shape was established considering the age and gender of the patient.

For each patient, two phantoms were designed and 3D printed to produce a realistic scenario for surgical simulation, training, and performance evaluation: one simulating the cranial surface before osteotomy, and another including the cranial surface and soft tissue after osteotomy (**Figure 6.2**). Reshaped bone fragments were also manufactured to reproduce the remodeling phase of the surgical intervention.

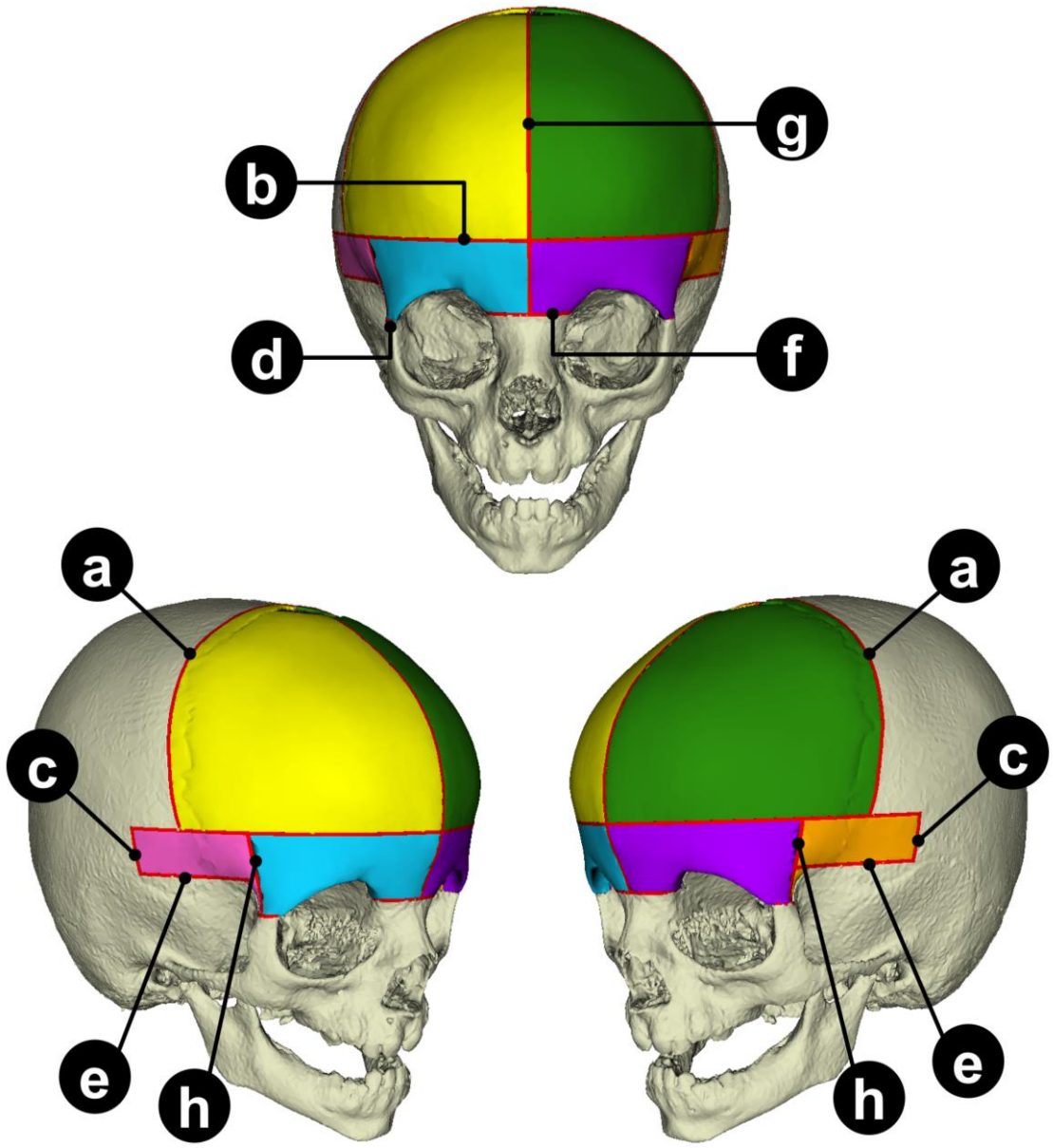

Figure 6.1. Fragments and osteotomies defined in the VSP of patient 1. Osteotomy cutting planes: (a) coronal plane, (b) supraorbital axial plane, (c) posterior temporal plane, (d) frontozygomatic plane, (e) inferior temporal plane, (f) frontonasal plane, (g) midsagittal plane, and (h) sphenofrontal plane. Planes (b), (d), (e), (f), and (h) are parallel to Frankfurt plane. Planes (a), (c), and (g) are perpendicular to the Frankfurt plane.

6.3.2. Augmented reality system

A smartphone application was developed on the Unity platform (version 2019.3) to visualize the VSP overlaid on the surgical field through an AR-based display (**Figure 6.3**). This application, compatible with Android and iOS devices, uses the smartphone internal camera to detect and track the position of two planar AR markers, containing a black-and-white

pattern, attached to the patient's anatomy. For each video frame, the Vuforia® development kit is used to identify the pattern of the markers, and the virtual image is overlaid on the surgical field in real-time.

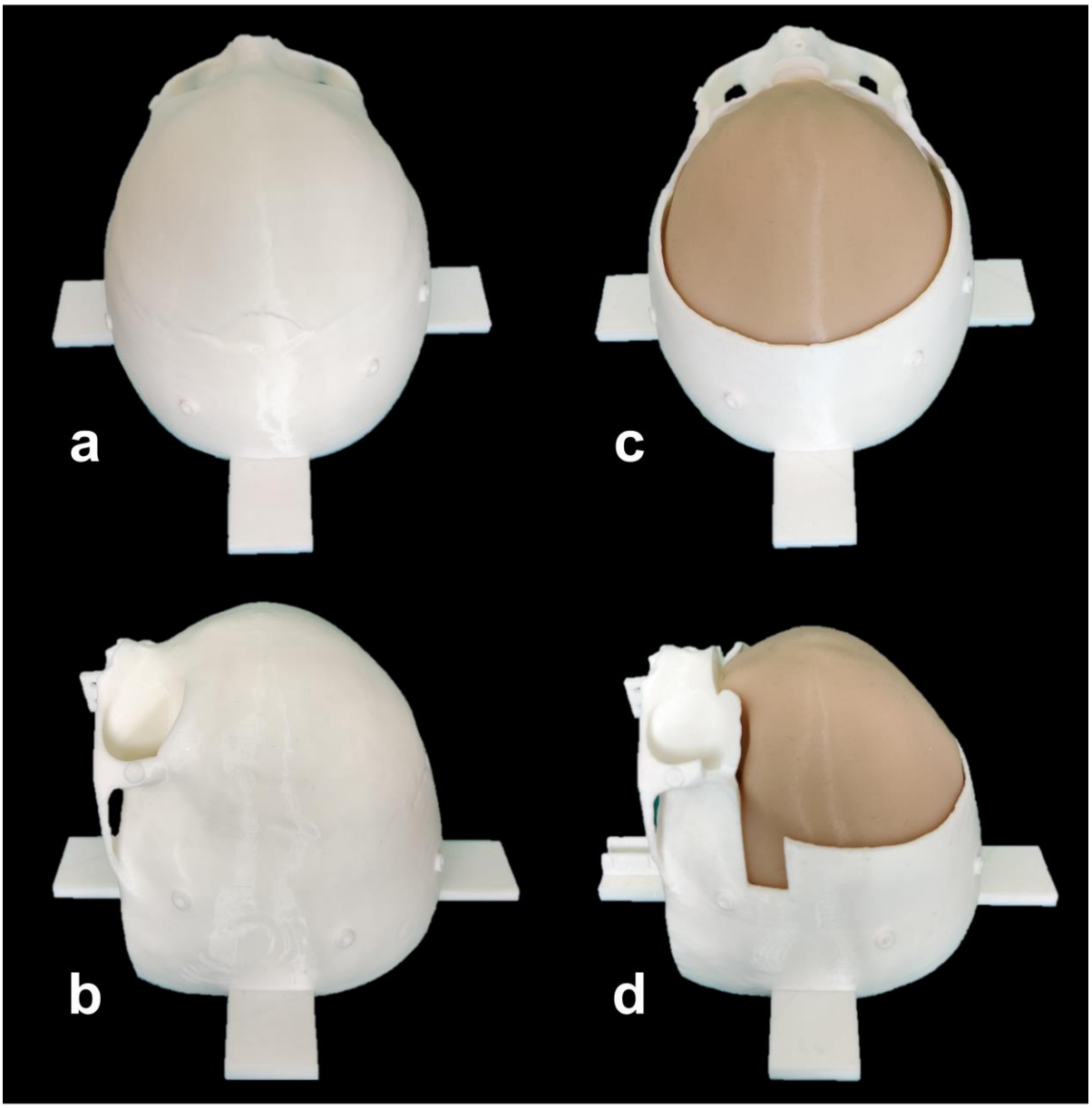

Figure 6.2. Superior and lateral views of a 3D printed patient-specific phantom (corresponding to patient 2): before osteotomy ((a) and (b)) and after osteotomy ((c) and (d)).

Two modes of visualization are available in the application: (1) osteotomy mode and (2) remodeling mode. In the osteotomy mode, virtual models of the osteotomy lines (1 mm wide) are overlaid on the surgical field guiding the surgeons to perform osteotomies along the lines defined during preoperative VSP (**Figure 6.3a**). In the remodeling mode, the target positions of the remodeled bone fragments (supraorbital bar and frontal bone) are virtually

projected on the surgical field guiding the surgeons during the positioning of the fragments to achieve the desired target shape (**Figure 6.3b**).

Figure 6.3. Smartphone application for AR guidance: (a) osteotomy visualization mode and (b) remodeling visualization mode.

The AR markers were designed to contain a unique black and white pattern. The dimensions of each marker were 30 mm x 35 mm x 1mm, and the approximate weight was 1 g. These markers were manufactured in PLA using a dual-extruder desktop 3D printer (Ultimaker B.V., Netherlands). These markers can be sterilized prior to surgery to maintain asepsis of the surgical field using a sterilization technique based on ethylene oxide at 37°C [115]. AR markers are attached to the parietal bone surface on the left and right sides of the cranium outside the area defined by the osteotomy lines of the VSP. The fixation of the markers

was performed using double-sided tape during simulations. During surgery, resorbable pins can be inserted in two holes included in the design to ensure rigid and stable fixation of the markers to the bone surface.

A mobile structured light scanner, Artec EVA® (Artec Group, Luxembourg), was used to acquire 3D photographs of the surgical field and to compute the exact position of the markers with respect to the patient's anatomy. After the attachment of the AR markers, 3D photographs of the surgical field were acquired including the geometric and textural information of the bone surface and the black and white patterns of the markers. Next, the acquired 3D textured surfaces were aligned with the preoperative CT scan using an iterative surface-to-surface registration algorithm, using the external fronto-orbital bone surface as a reference. Once aligned, the positions of the AR markers with respect to the patient's anatomy were estimated by manually identifying six landmarks on the outline of the AR marker patterns in the 3D textured surface and performing a fiducial-based registration. Finally, the virtual models of the VSP were transformed with respect to the estimated location of the AR markers, and their final positions were transferred to the smartphone application to ensure an accurate display of the virtual data in the surgical field.

6.3.3. Performance evaluation

The accuracy of the AR guidance using the developed smartphone application was evaluated by simulating the FOA surgical intervention on the 3D printed phantoms. Two users performed three simulations of the surgical intervention on the phantoms of each of the three patients. A total of eighteen complete simulations were performed. A navigation system, validated in a previous study [49], was used as a gold-standard for the performance evaluation. The simulation of the surgical intervention consisted of three different phases: registration, osteotomy, and remodeling.

In the registration phase, the mobile structured light scanner was used to reconstruct a 3D photograph of the simulation phantom with the AR markers already fixed to its surface. Then, the 3D scan was registered with the CT scan of the patient, and the position of the AR markers in the phantom was estimated as explained in the previous section. 3D photography registration error was recorded for each simulation.

In the osteotomy phase, the users were required to mark the osteotomy lines displayed on the smartphone AR display (**Figure 6.4a**). The smartphone was positioned around the

simulated surgical field to find the most appropriate viewpoint depending on the osteotomy line location on the cranial surface. The navigation system was used to record points along the osteotomy lines every 0.2 mm using a tracked surgical instrument for each of the cutting planes defined in VSP and on both sides of the cranium. The accuracy of the AR guidance was measured by two different metrics: linear and angular error. Linear osteotomy error was computed as the average distance of each recorded point and the corresponding VSP plane. The angular error was measured by computing the best-fitting plane of all points recorded in each osteotomy plane using singular value decomposition, and computing the angular deviation of that plane with respect to the VSP.

In the remodeling phase, the users were asked to fix the remodeled bone fragments on the target position defined in the VSP. The smartphone app overlaid the virtual models of the bone fragments in the final position with transparency, enabling the user to compare the location of the real fragments with the target position displayed with AR (**Figure 6.4b**). Two fragments, supraorbital bar and frontal bone, were fixed using modeling clay. The navigation system was used to compute the positioning error (translation and rotation) using five reference landmarks included in each fragment.

6.3.4. Surgical deployment

The proposed AR visualization system was tested during two real open cranial vault reconstruction surgeries of two patients with metopic synostosis. The objective was to assess the feasibility of integrating AR guidance into the current surgical workflow.

Two AR markers containing a unique pattern were 3D printed and sterilized prior to surgery using ethylene oxide at 37°C. Markers used for the real surgeries contained different patterns than those used during the surgical simulation on phantoms, but they were designed and manufactured following a similar methodology. These markers were attached to the parietal bone surface on the left and right sides of the cranium using two resorbable pins (SonicPins Rx, KLS Martin, Germany), which are inserted by drilling small holes (1.6 mm diameter) into the bone tissue. Due to the lack of a sterile mobile device cover at the time of surgery, an external camera (Intel® RealSense™ D415) was used for marker tracking and the AR information was displayed on an external screen adjacent to the surgical field.

An anonymous questionnaire survey was filled-in by 9 surgeons (6 from the Department of Oral and Maxillofacial Surgery and 3 from the Department of Neurosurgery),

involved in craniosynostosis correction surgeries, to determine the feasibility of this methodology and to identify potential improvements of this technology. All participants were familiar with the AR visualization system. Questions were scored on a 5-point Likert scale. The results are presented in the following section.

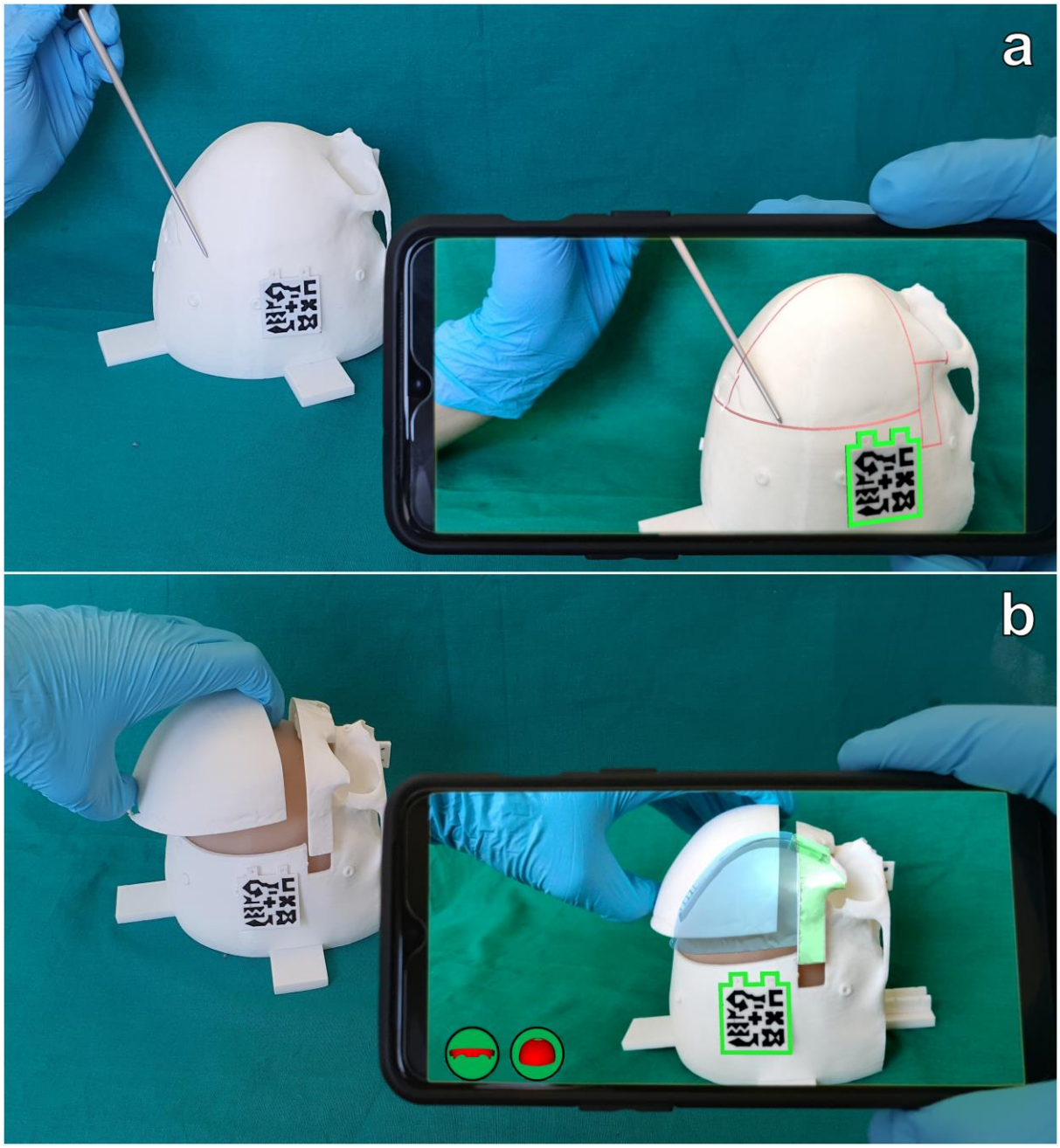

Figure 6.4. View of the simulation surgical field during osteotomy (a) and remodeling phases (b). A green frame around the AR marker indicates that the marker is being tracked by the app. During the osteotomy phase, cutting lines are displayed in red over the bone surface of the simulation phantom. During the remodeling phase, target bone fragment positions of the supraorbital bar (green) and frontal bone (blue) are virtually overlaid on the image.

6.4. Results

6.4.1. Performance evaluation

Registration errors for the alignment of 3D photographs with the preoperative CT scan and the identification of the position of the AR markers in the 3D photographs are presented in **Table 6.1**. The average surface-to-surface distance between preoperative CT and 3D photographs after registration was 0.15 ± 0.07 mm, while the average registration error to estimate AR marker positions was 0.31 ± 0.10 mm.

Table 6.1. Registration error values for the alignment of 3D photographs with preoperative CT scan and the estimation of the AR marker positions.

Phantom	Phase	Registration Error (mm)	
		3D Photograph Alignment	AR Marker Identification
1	Osteotomy	0.11	0.24
	Remodeling	0.11	0.43
2	Osteotomy	0.23	0.36
	Remodeling	0.16	0.16
3	Osteotomy	0.07	0.33
	Remodeling	0.23	0.32
Average		0.15 ± 0.07	0.31 ± 0.10

The average linear error during AR-guided osteotomy in all 18 surgery simulations on patient-specific phantoms was 0.62 ± 0.51 mm. The average angular deviation of the recorded osteotomy planes was 1.80 ± 1.88 degrees. Linear and angular errors for each osteotomy plane are shown in **Table 6.2**. Higher accuracy was found in those planes closer to the AR markers. Higher errors were detected on the frontozygomatic, inferior temporal, and frontonasal planes, which are the most distant planes to the reference AR markers.

Table 6.2. Linear and angular errors during AR-guided osteotomy for surgical simulations performed by 2 users on 3 different patient-based phantoms.

	Linear Error (mm)		Angular Error (°)	
Plane	**Mean**	**SD**	**Mean**	**SD**
Coronal	0.47	0.43	0.95	0.49
Supraorbital axial	0.48	0.42	0.71	0.47
Posterior temporal	0.48	0.37	1.07	0.84
Frontozygomatic	0.75	0.48	2.49	1.84
Inferior temporal	0.63	0.42	1.06	0.52
Frontonasal	0.70	0.55	4.16	3.40
Midsagittal	0.88	0.63	2.67	1.50
Lateral orbit projection	0.60	0.45	1.30	0.57
Overall	0.62	0.51	1.80	1.88

The average positioning error of the remodeled fragments using AR visualization for guidance is shown in **Figure 6.5**. The average translation error was 0.70 ± 0.24 mm and 0.67 ± 0.33 mm for the supraorbital bar and frontal bone fragments, respectively. The average rotation error was 0.43 ± 0.30 degrees for the supraorbital bar and 0.39 ± 0.33 degrees for the frontal bone.

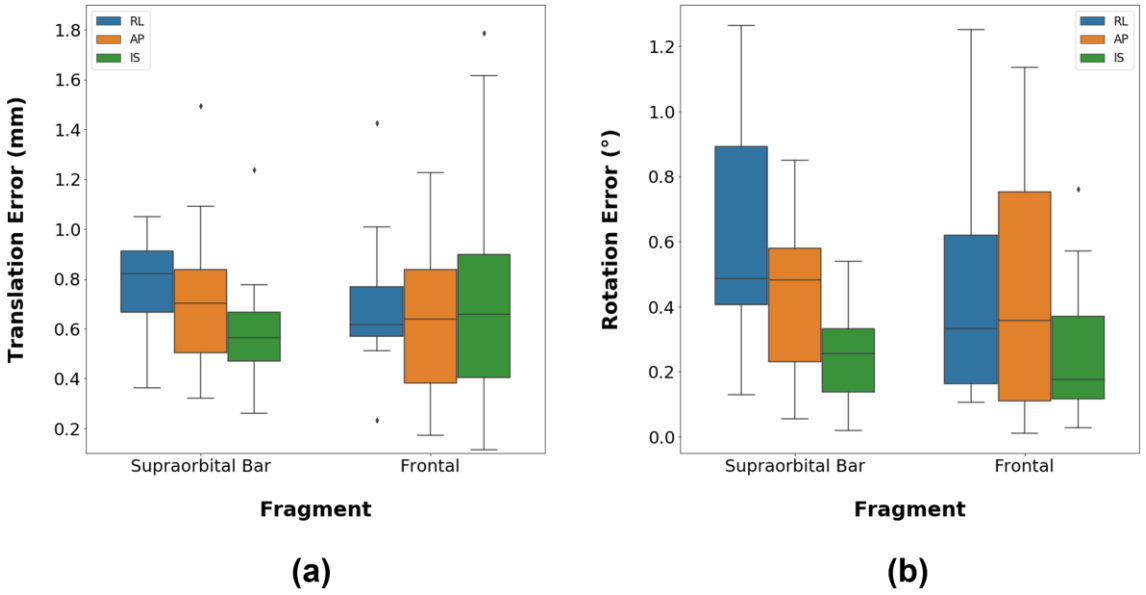

Figure 6.5. Fragment positioning error after AR-guided cranial vault remodeling. Translation (a) and rotation (b) errors were projected on the three anatomical axes: right-left, anterior-posterior, and superior-inferior.

6.4.2. Surgical deployment

The AR visualization was successfully tested in both surgeries (**Figure 6.6**). No deformations of the 3D printed markers occurred during sterilization, and accurate tracking was possible under the lighting conditions of the operating room.

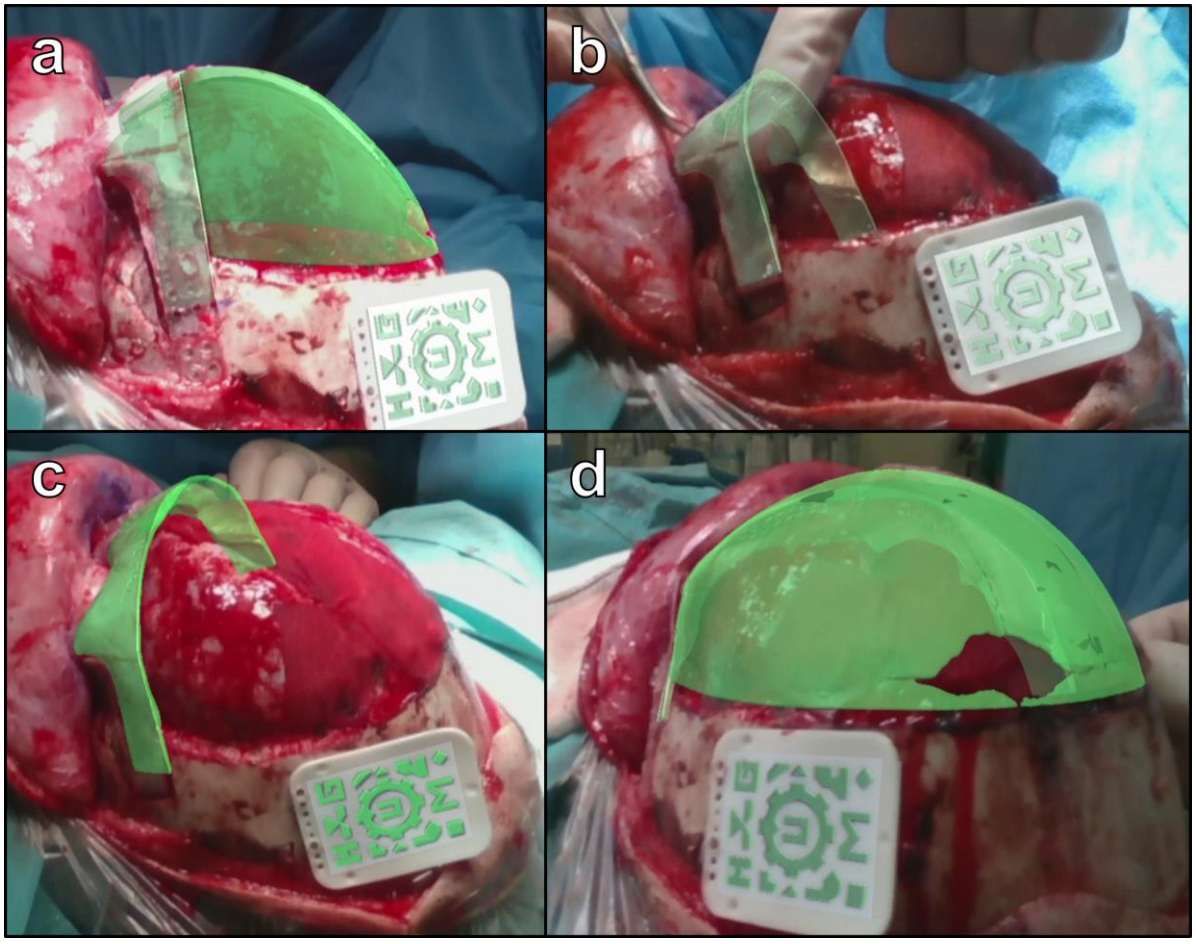

Figure 6.6. View of the surgical field with AR information overlaid on the image during open cranial vault remodeling. Virtual models of the target fragment positions are displayed in green with transparency. AR markers are attached to the parietal bone surface.

From the scores from the questionnaire (**Table 6.3**), it can be observed that surgeons support the integration of AR visualization for open cranial vault remodeling to correct craniosynostosis (avg. score = 4.6). In addition, surgeons believe that the virtual information displayed by the AR software is intuitive (avg. score = 4.3), but that preliminary training will be necessary prior to surgery to optimize the use of this technology in the operating room (avg. score = 4.8). Regarding the visualization of the AR information, surgeons would prefer to use

a head-mounted display (avg. score = 4.4) or a hand-held device (i.e. smartphone/tablet) (avg. score = 4.1) over using an external screen (avg. score = 3.6).

Surgeons agreed that AR technology will help to translate the preoperative virtual plan into the operating room and will increase the security and confidence of surgeons towards obtaining an optimal surgical outcome during craniosynostosis surgeries (avg. score = 4.6). According to the results of the questionnaire, surgeons like the use of stereolithographic cutting guides for assistance during osteotomy, but some of them will consider the use of AR for this purpose (avg. score = 3.1). However, most surgeons agreed that AR will be really useful during the positioning of the remodeled bone fragments in the target positions defined during VSP (avg. score = 4.4) and most of them consider that AR is more convenient than navigation for this purpose (avg. score = 3.6).

Table 6.3. Questionnaire scores given by the surgeons regarding the use of AR for guidance during craniosynostosis surgery.

Question	Individual scores (per surgeon)									Avg. score
	1	**2**	**3**	**4**	**5**	**6**	**7**	**8**	**9**	
AR for craniosynostosis	4	5	5	5	3	5	4	5	5	4.6
Increase security and confidence	4	5	5	5	3	5	4	5	5	4.6
Preliminary training required	5	4	5	5	4	5	5	5	5	4.8
Useful during fragment positioning	3	5	5	5	3	5	4	5	5	4.4
Can substitute cutting guides	3	4	3	4	2	3	3	3	3	3.1
Provides intuitive guidance	3	5	5	5	4	5	5	4	3	4.3
More convenient than navigation	5	4	3	4	2	4	3	4	3	3.6
AR visualization: external screen	3	5	1	5	4	5	3	3	3	3.6
AR visualization: hand-held device	4	5	5	4	4	4	3	4	4	4.1
AR visualization: head-mounted	4	5	4	5	3	5	4	5	5	4.4
Avg. score	3.8	4.7	4.1	4.7	3.2	4.6	3.8	4.3	4.1	

6.5. Discussion and conclusion

In this study, we propose and evaluate a workflow for AR visualization during open cranial vault remodeling of craniosynostosis patients. This system enables the visualization of the target virtual plan overlaid on the surgical field, guiding the surgeons to obtain an optimal surgical outcome matching the preoperative planning. In comparison with the methodology proposed by Hochfeld et al. (2014), which requires the invasive, complex, and time-consuming attachment of a stereotactic frame to the patient, our approach only requires the intraoperative attachment of two small 3D printed markers (weight < 1 g) using resorbable pins. In addition, while other approaches do not provide real-time guidance [55], our solution enables surgeons to perform multiple corrections of bone fragment position using the real-time feedback provided by AR visualization. Furthermore, the VSP virtual information can be displayed overlaid in the surgical field view. Thus, improved hand-eye coordination and reduced cognitive load are expected in comparison with intraoperative navigation [49].

One of the main difficulties for the introduction of AR in surgery is the alignment of the virtual data with patient anatomy [117]. Previous approaches, based on occlusal splints for registration [126], can present misalignments of the virtual models due to the distant position of the reference marker. Our solution includes the attachment of markers on the bone surface adjacent to the region of interest to minimize registration error and to enable multiple viewpoints for AR visualization and guidance. Our system relies on the smartphone camera to perform the AR marker pose estimation to control the virtual data position. Therefore, the main limitation will be that poor lighting conditions or marker occlusions might interrupt tracking and even cause inaccuracies in the AR visualization. However, the lighting conditions of the surgical room ensure a homogenous illumination of the markers during surgery, and the position of the markers is totally flexible and can be defined to avoid occlusions and maximize tracking capabilities.

In addition, we have introduced the use of 3D photography to perform an accurate registration between the virtual models and the patient's anatomy. Intraoperative 3D photographs can be performed and aligned with the preoperative CT scan to accurately estimate the position of the AR markers in the anatomy. Moreover, intraoperative 3D photography can be used, not only for alignment, but also as a tool for the intraoperative quantitative evaluation of the surgical outcome without exposure to ionizing radiation or anesthesia [128].

The proposed methodology for AR visualization in craniosynostosis was tested in surgical simulations performed on patient-specific phantoms. Our system was able to provide accurate guidance during both osteotomy and remodeling phases. During remodeling, a higher translation error was found in the RL axis, which may be due to the limited depth perception of the AR virtual image. However, this limited depth perception can be compensated by the visualization of the fragment target position from multiple viewpoints.

Finally, AR visualization using the proposed workflow was successfully tested during two craniosynostosis surgeries. Accurate tracking and AR visualization were possible during both surgeries. Surgeons' feedback indicates that physicians support the integration of AR visualization in the current workflow for open cranial vault remodeling, and agreed that AR technology will help them to translate the preoperative virtual plan into the operating room, increasing security and confidence during the procedure. Most of the participants found the AR visualization intuitive, but they all agree that preliminary training would be required to optimize the use of this technology. Although most of the surgeons believe that AR is more convenient than navigation, some of them disagree. AR visualization has demonstrated to be accurate and intuitive, but it lacks the real-time quantitative metrics provided by existing navigation systems [49]. Therefore, intraoperative guidance could benefit from the combination of both technologies to integrate real-time and accurate positioning feedback provided by navigation systems with valuable AR visualization within the surgical field.

In this work, we propose to visualize the AR information on a smartphone running the developed software application. The smartphone can be introduced into available sterile mobile device covers, maintaining full touchscreen interface functionality and clear optics, or inserted into a sterile ultrasound probe cover to maintain asepsis of the surgical field [129], [130]. To ensure optimal visualization, a mechanical arm can be used to hold the smartphone adjacent to the surgical field. In addition, our developed application is compatible with head-mounted displays, such as Microsoft HoloLens, which could be an alternative to directly overlay virtual 3D models on the surgeon’s field of view without requiring an external device (i.e. smartphone, external cameras, or screens).

To conclude, a novel workflow for AR visualization for guidance during craniosynostosis surgery has been evaluated on simulation phantoms and successfully tested in two craniosynostosis surgeries. The proposed AR system could be easily integrated into the current surgical workflow to ensure an accurate translation of the VSP into the operating room.

The use of this technology could lead to a reduction of inter-surgeon variability and an improvement in surgical outcomes.

The description and the evaluation of the augmented reality system described in this chapter was presented at the 23rd International Conference on Medical Image Computing & Computer Assisted Intervention (MICCAI) 2020, and published in the Journal of Computer Methods in Biomechanics and Biomedical Engineering: Imaging & Visualization:

D. García-Mato, R. Moreta-Martinez, M. García-Sevilla, S. Ochandiano, R. García-Leal, R. Pérez-Mañanes, J. A. Calvo-Haro, J.I. Salmerón, J. Pascau. "Augmented reality visualization for craniosynostosis surgery". Comput. Methods Biomech. Biomed. Eng. Imaging Vis., vol. 0, no. 0, pp. 1–8, 2020.

7

DISCUSSION

Although multiple technological advancements have arisen in the surgical management of craniosynostosis during the last decade, interventional planning and surgical correction are still highly dependent on the subjective assessment and artistic judgment of the surgeons. Surgical experience is crucial to achieve optimal clinical outcomes and, as a result, less experienced surgeons are more prone to errors [42]. The use of VSP and CAD/CAM technologies have demonstrated a positive impact in the clinical workflow, reducing operative time, and improving postoperative cranial morphology [68], [69]. However, despite these improvements, there is still a high variability in the surgeon's performance and, thus, in the outcomes.

In this context, we focused our research on reducing the subjectivity in all steps of the surgical workflow for the treatment of craniosynostosis, from the preoperative virtual planning phase to the intraoperative performance. We combined statistical shape models, intraoperative imaging, and image-guided techniques to ensure accurate planning and subsequent translation of the preoperative plan into the surgical intervention.

Computer-assisted surgical planning has demonstrated to increase the accuracy, efficiency, and reproducibility of craniosynostosis surgeries [17]. However, existing methods rely on the subjective definition of target cranial shapes based on mental constructions, and manual user interactions to define osteotomies and reconfiguration of fragments [44]–[46]. In addition, there are no planning techniques that incorporate the overcorrection of the cranial morphology, which is crucial to compensate for relapse or lack of growth following surgery and, thus, to ensure optimal long-term aesthetic and functional outcomes [63].

We developed an automatic method for interventional planning of fronto-orbital advancement. This method was integrated into a specific software platform, which enables surgeons to use automatic planning as a reference and to introduce any manual modifications in the plan according to the surgical needs and preferences. Our software enables the estimation of osteotomy locations in the fronto-orbital region, the automatic configuration of the bone fragments to minimize cranial malformations, and the integration of overcorrection to ensure optimal long-term surgical outcomes.

Our results demonstrated that this method can accurately estimate osteotomies in the fronto-orbital region, including tenon extensions, which are essential during FOA to facilitate advancement and subsequent stabilization of the remodeled fragments. Furthermore, automatic reconfiguration of fragments enabled a significant reduction of the cranial malformations and correct normalization of the morphology. Real-time quantification of morphological metrics and the incorporation of overcorrection enabled surgeons to evaluate multiple treatment strategies and to determine the best remodeling approach. Our planning software provides a valuable and objective tool for surgeons to generate repeatable and objective interventional plans while reducing planning duration. To our knowledge, this approach is the first to consider and apply overcorrection during the VSP of craniosynostosis surgeries.

Our automatic planning software enables surgeons to input the desire overcorrection degree into the interventional plan according to their clinical judgment. However, the software also provides automatic estimates of overcorrection, considering the results of long-term studies of cranial growth following craniosynostosis surgical correction [63]. Therefore, using this information, surgeons can determine the best approach for remodeling for each patient to ensure optimal long-term surgical outcomes.

Although preoperative planning is crucial to determine an optimal approach for surgical correction, the translation of the interventional plan into the operating room is the most critical step towards satisfactory surgical outcomes. CAD/CAM guides and templates are used in many hospitals to assist surgeons during osteotomy and reshaping of the bone fragments [44]. This way, bone tissue can be cut and reshaped as defined during preoperative VSP. However, there are no standard techniques to guide surgeons during placement and fixation of the remodeled bone fragments to the patient's anatomy. Some techniques for intraoperative guidance have been reported based on stereotactic frames [54] or intraoperative CT imaging [55]. Nevertheless, the integration of these approaches into clinical practice is limited by multiple

factors, such as invasiveness, increased surgical time, or exposure to harmful ionizing radiation.

In this thesis, we have evaluated 3D photography technology for the intraoperative quantification and analysis of cranial morphology. Our results have demonstrated that 3D photographs of the patient's anatomy can be acquired during craniosynostosis surgical interventions to quantify cranial morphology with similar accuracy to CT imaging [128]. These data can be used by surgeons to make any necessary corrections during cranial vault remodeling, ensuring accurate matching with preoperative VSP. After testing this solution in the operating room, the surgeon's feedback suggests that this technology can be easily integrated into the current surgical workflow for craniosynostosis correction without substantially increasing operative time. Furthermore, 3D photography could also be used for diagnosis [31] and patient follow-up [87].

The main advantages of 3D photography technology for surgical outcome evaluation include the scanning technology, which does not rely on ionizing radiation, and the simplicity of the acquisition process, which involves moving a hand-held scanning device around the area of interest. In contrast with the use of intraoperative CT imaging for surgical guidance [55], 3D photography enables the fast acquisition and reconstruction of images of the cranial vault using innocuous visible light. Therefore, our proposed methodology represents a valuable alternative to CT imaging.

The main limitation of intraoperative 3D photography is the lack of real-time feedback. Although multiple 3D photographs can be acquired during surgery for more accurate and continuous guidance, this methodology will be limited by the increased operative time. Therefore, we developed an intraoperative navigation system to provide real-time guidance during craniosynostosis surgeries [49]. Based on optical tracking, this system enables to record the positions of the remodeled bone fragments and compare them with the target VSP. Therefore, accurate and iterative quantitative feedback can be provided to surgeons on an external screen during open cranial vault remodeling. In comparison with navigation systems available for other medical applications [88], [96], our workflow does not rely on patient's head immobilization or the invasive attachment of dynamic reference frames. Our navigation system is based on CAD/CAM surgical guides, which fit into the patient's anatomy, to perform patient-to-image registration. Our results demonstrate a high navigation accuracy and optimal

surgical outcomes in all cases after testing our system in five craniosynostosis surgeries. In addition, the use of navigation does not substantially increase the operative time.

Also, we investigated the use of AR technology as an alternative to navigation for surgical guidance in craniosynostosis surgery. We developed an AR application that enables surgeons to visualize the VSP overlaid on the surgical field, indicating the predefined osteotomy locations and target bone fragment positions [131]. Our proposal presents important advantages over previous approaches [126], since reference markers can be located using structured light scanning, and positioned near the fronto-orbital region of the cranium to maximize visualization accuracy. Our results demonstrate that AR can provide sub-millimetric accuracy in guiding both osteotomy and remodeling phases of FOA. Surgeons' feedback indicated that this technology can be integrated into the current surgical workflow for the treatment of craniosynostosis.

In contrast with intraoperative navigation, AR technology enables the visualization of the virtual information directly on the surgical field and does not require external screens in the operating room. Therefore, surgeons do not need to look at two different information sources and can easily match the virtual data with the patient's anatomy. Besides, AR may lead to a reduction of the surgeons' cognitive load, and an improvement in hand-eye coordination during the surgical procedure. However, the main limitation of AR guidance is the lack of real-time quantitative metrics, which are accurately provided by intraoperative navigation.

While intraoperative navigation is a well-established technique for guidance in craniofacial surgery, AR visualization has recently emerged in the medical field and has not been yet integrated into the standard of care. Navigation systems are characterized by their accuracy and robustness during surgical instrument tracking with respect to patient anatomy [132]. On the other hand, AR technology is still under development and future research is yet required to achieve optimal performance and robustness. Thus, intraoperative guidance could benefit from the mixed integration of both technologies in the operating room combining real-time and accurate positioning feedback provided by navigation systems with valuable AR visualization within the surgical field.

In this thesis, we have presented and evaluated three different technologies to be used for surgical guidance during open cranial vault remodeling: 3D photography, intraoperative navigation, and AR. All three techniques can provide valuable intraoperative guidance to ensure optimal matching of the surgical outcomes with the preoperative VSP. However,

intraoperative navigation and AR approaches provide real-time guidance, while 3D photography does not. This functionality is valuable to enable multiple corrections of bone fragment positions and real-time comparison with the VSP.

Most of the technological developments presented in this thesis have been tested and validated in non-syndromic single-suture synostosis. However, these approaches could also be applied to syndromic multi-suture synostosis. In these complex cases, most anatomical references in the cranium are altered and optimal surgical correction is challenging. Therefore, these cases will highly benefit from computer-assisted diagnosis, planning, and intraoperative guidance to achieve optimal surgical outcomes. Furthermore, these techniques could also be applied to secondary surgical interventions performed to correct possible complications or relapses after initial treatment.

Although the contributions presented in this thesis can greatly benefit the management of craniosynostosis, there are some limitations to bear in mind. First of all, most of them are costly, and this factor may restrict their integration into clinical practice in some centers with limited budgets. However, many of the previously mentioned technological developments are based on free and open-source software platforms [99], which could reduce the technical complexity and the costs associated with the development and subsequent validation for clinical use. These systems could also be shared among different hospital departments, improving their impact at a lower cost.

Apart from the economic perspective, some indirect costs must also be considered. The addition of advanced cranial shape analysis, automatic planning algorithms, and design and manufacturing of CAD/CAM tools may increase the duration and complexity of the preoperative planning phase and will also require the collaboration of engineers. However, patient-specific planning of craniosynostosis surgeries is essential to improve surgical treatment. Advanced algorithms can provide valuable objective metrics to determine the best remodeling approach for each patient. Therefore, the benefits of these technological advancements may outweigh the increased duration and complexity.

In addition, most of the technologies developed for image-guided craniosynostosis surgeries require specialized training for craniofacial surgeons, and some of them present a steep learning curve. Nevertheless, surgeries can be simulated preoperatively using patient-specific phantoms to provide the trainees with realistic tactile feedback of the patient's anatomy. Simulation offers a safe environment where surgery can be replicated step-by-step,

leading to the acquisition of technical skills that can improve performance during the surgical task [133].

To conclude, multiple technological advancements have been evaluated in this thesis to improve the surgical management of craniosynostosis. The integration of these developments into the surgical workflow of craniosynostosis will have a positive impact on the surgical outcomes, increasing the efficiency of surgical interventions, and reducing the variability between surgeons and institutions.

8

CONCLUSIONS

The main contributions and conclusions of this thesis are as follows:

- An automatic planning software has been developed and evaluated to estimate osteotomy locations in the fronto-orbital region, the reconfiguration of bone fragments to minimize cranial malformations, and the required overcorrection to ensure optimal long-term surgical outcomes. This framework is based on statistical shape models generated from databases of normative subjects and, thus, it can determine a patient-specific optimal cranial shape to target during surgical intervention.

- We demonstrated that 3D photography is a valuable alternative to CT imaging for the intraoperative evaluation of surgical outcomes during craniosynostosis surgeries. This technology enables accurate 3D reconstruction and cranial shape quantification, which can be used to provide intraoperative feedback to surgeons.

- An intraoperative navigation system was developed to provide real-time guidance during open cranial vault remodeling. This system was specifically designed for craniosynostosis surgery, enabling accurate navigation while avoiding the invasive attachment of dynamic reference frames or infant's head immobilization. The evaluation of the system demonstrated an optimal accuracy for bone fragment positioning, and feasibility of integration into the surgical workflow without substantially increasing operative time.

- We proposed and evaluated a workflow for AR visualization to guide the osteotomy and remodeling phases of FOA by overlaying virtual information directly on the surgical field. Our results demonstrated the accuracy of AR technology for surgical

guidance in craniosynostosis, and its feasibility for integration into the surgical workflow. The developed software application can be used for visualization in smartphones, head-mounted displays, and external screens.

9

PUBLICATIONS

9.1. Related to this thesis

9.1.1. Articles in peer-reviewed journals

D. García-Mato, M. García-Sevilla, A.R. Porras, S. Ochandiano, J.V. Darriba-Allés, R. García-Leal, J.I. Salmerón, M.G. Linguraru, J. Pascau. Three-Dimensional Photography for Intraoperative Morphometric Analysis in Metopic Craniosynostosis Surgery. Int J CARS (2021) [*https://doi.org/10.1007/s11548-020-02301-0*] – Impact factor: 2.473 (Q2)

D. García-Mato, R. Moreta-Martinez, M. García-Sevilla, S. Ochandiano, R. García-Leal, R. Pérez-Mañanes, J. A. Calvo-Haro, J.I. Salmerón, J. Pascau. Augmented reality visualization for craniosynostosis surgery. Comput. Methods Biomech. Biomed. Eng. Imaging Vis., vol. 0, no. 0, pp. 1–8, 2020. [*https://doi.org/10.1080/21681163.2020.1834876*] – Impact factor: 1.502 (Q3)

D. García-Mato, S. Ochandiano, M. García-Sevilla, C. Navarro-Cuéllar, J. V. Darriba-Allés, R. García-Leal, J. A. Calvo-Haro, R. Pérez-Mañanes, J. I. Salmerón, J. Pascau. Craniosynostosis surgery: workflow based on virtual surgical planning, intraoperative navigation and 3D printed patient-specific guides and templates. Scientific Reports, vol. 9, 17691, 2019. [*https://doi.org/10.1038/s41598-019-54148-4*] – Impact factor: 3.998 (Q1)

D. García-Mato, A. R. Porras, S. Ochandiano, G. F. Rogers, J. Pascau, M. G. Linguraru. Automatic Planning of Fronto-Orbital Advancement for the Surgical Correction of

Metopic Craniosynostosis. Plast. Reconstr. Surg. (2021) [submitted] – Impact factor: 4.235 (Q1)

S. Ochandiano, **D. García-Mato**, C. Navarro Cuellar, J. V. Darriba-Allés, R. García-Leal, A. R. Porras, M. G. Linguraru, J. Pascau, J. I. Salmerón. Patient-specific virtual planning and image-guided surgical correction in craniosynostosis: a case report from a multi-institutional collaboration. Journal of Cranio-Maxillo-Facial Surgery [submitted] – Impact factor: 1.766 (Q3)

E. Marinetto, **D. García-Mato**, A. García, S. Martínez, M. Desco, J. Pascau. Multicamera Optical Tracker Assessment for Computer Aided Surgery Applications. IEEE Access, vol. 6, pp. 64359-64370, 2018. [*https://doi.org/10.1109/ACCESS.2018.2878323*] – Impact factor: 3.745 (Q1)

R Moreta-Martinez, **D. García-Mato**, M. García-Sevilla, R. Pérez-Mañanes, J. A. Calvo-Haro, J. Pascau. Combining Augmented Reality and 3D Printing to Display Patient Models on a Smartphone. J. Vis. Exp., 155, e60618, 2020. [*https://doi.org/10.3791/60618*] – Impact factor: 1.163 (Q3)

R. Moreta-Martinez, **D. García-Mato**, M. García-Sevilla, R. Pérez-Mañanes, J. A. Calvo, J. Pascau. Augmented reality in computer-assisted interventions based on patient-specific 3D printed reference. Healthcare Technology Letters, pp. 1–5, 2018 [*https://doi.org/10.1049/htl.2018.5072*]

9.1.2. Book chapters

D. García-Mato, J. Pascau, S. Ochandiano. New Technologies to Improve Surgical Outcome during Open-Cranial Vault Remodeling. In: Craniosynostosis - New Perspectives of Prevention and Treatment. IntechOpen, 2020. [*https://doi.org/10.5772/intechopen.94536*]

9.1.3. International conferences

D. García-Mato, R. Moreta-Martinez, M. García-Sevilla, S. Ochandiano, R. García-Leal, R. Pérez-Mañanes, J. A. Calvo-Haro, J. I. Salmerón, J. Pascau. Augmented Reality Visualization for Craniosynostosis Surgery. 23rd International Conference on Medical Image Computing & Computer Assisted Intervention (MICCAI), Lima, Peru (2020)

D. García-Mato, M. García-Sevilla, S. Ochandiano, R. Moreta-Martinez, J. V. Darriba-Allés, R. García-Leal, J. I. Salmerón, J. Pascau. Intraoperative Outcome Evaluation in Craniosynostosis Reconstruction Surgery using 3D Photography. In: CARS 2020 - Computer Assisted Radiology and Surgery Proceedings of the 34th International Congress and Exhibition, Munich, Germany, June 23–27, 2020. Int J CARS 15, 1–214 (2020)

D. García-Mato, M. García-Sevilla, S. Ochandiano, C. Navarro-Cuéllar, J. V. Darriba-Allés, R. García-Leal, J. Pascau. Morphometric Analysis in Craniosynostosis Reconstruction Surgery based on Structured Light Scanning. 18th meeting of the International Society of Craniofacial Surgery (ISCFS) 2019, Paris, France. Plastic and Reconstructive Surgery - Global Open: August 2019 - Volume 7 - Issue 8S-2 - p 196 (2019)

D. García-Mato, M. García-Sevilla, S. Ochandiano, C. Navarro-Cuéllar, J. V. Darriba-Allés, R. García-Leal, J. Pascau. Structured Light Scanning for Morphometric Analysis in Craniosynostosis Reconstruction Surgery. In: CARS 2019 - Computer Assisted Radiology and Surgery Proceedings of the 33rd International Congress and Exhibition, Rennes, France, June 18–21, 2019. Int J CARS 14, 1–194 (2019)

D. García-Mato, S. Ochandiano, S. Espías-Alonso, M. García-Sevilla, R. Moreta-Martinez, J. A. Calvo-Haro, R. Pérez-Mañanes, J. Pascau. Non-invasive computer-assisted dental implant surgery based on optical tracking and 3D printing. In: CARS 2019 - Computer Assisted Radiology and Surgery Proceedings of the 33rd International Congress and Exhibition, Rennes, France, June 18–21, 2019. Int J CARS 14, 1–194 (2019)

D. García-Mato, S. Ochandiano, M. Tousidonis, R. Moreta-Martínez, M. García-Sevilla, M. Desco, J. Pascau Orbital Floor Reconstruction Workflow based on 3D Printing and Surgical Navigation. In: CARS 2018 - Computer Assisted Radiology and Surgery Proceedings of the 32nd International Congress and Exhibition, Berlin, Germany, June 20–23, 2018. Int J CARS 13, 1–273 (2018)

R. Moreta-Martinez, **D. García-Mato**, M. García-Sevilla, S. Ochandiano, R. García-Leal, R. Pérez-Mañanes, J. A. Calvo-Haro, J. I. Salmerón, J. Pascau. Augmented reality for bone fragment positioning during craniosynostosis reconstruction surgery. In: CARS 2020 - Computer Assisted Radiology and Surgery Proceedings of the 34th International Congress and Exhibition, Munich, Germany, June 23–27, 2020. Int J CARS 15, 1–214 (2020)

S. Ochandiano, **D. García-Mato**, E. Bullejos, J. V. Darriba-Allés, R. García-Leal, J. Pascau, J. I. Salmerón. Intraoperative Navigation in Craniosynososis based on Virtual Surgical Planning and an "In-House" Technique. 18th meeting of the International Society of Craniofacial Surgery (ISCFS) 2019, Paris, France. Plastic and Reconstructive Surgery - Global Open: August - Volume 7 - Issue 8S-2 - p 176 (2019)

R. Moreta-Martinez, **D. García-Mato**, M. García-Sevilla, R. Pérez-Mañanes, J. A. Calvo, J. Pascau. AR in computer-assisted interventions based on patient-specific 3D printed reference. Augmented Environments for Computer-Assisted Interventions Workshop, 21st International Conference on Medical Image Computing & Computer Assisted Intervention (MICCAI), Granada, Spain (2018)

G. Arenas, **D. García-Mato**, M. Tousidonis, P. Montes, J. Pascau, S. Ochandiano. Open Source Navigation System and CAD-CAM Technology in Surgical Treatment of Craniosynostosis. European Association for Cranio-Maxillo-Facial Surgery, Munich, Germany (2018)

M. Tousidonis, **D. García-Mato**, G. Arenas, E. Bullejos, J. Pascau, S. Ochandiano. Orbital reconstruction workflow based on desktop 3D printing and open-source navigation system. European Association for Cranio-Maxillo-Facial Surgery, Munich, Germany (2018)

9.1.4. National conferences

D. García-Mato, E. Marinetto, L. Sanz-Díaz, M. Desco, J. Pascau. Calibration developments for multicamera optical tracking systems. Spanish Society of Biomedical Engineering Annual Conference 2015, Madrid, Spain (2015)

L. García-Duarte Sáenz, **D. García-Mato**, S. Ochandiano, J. Pascau. Real-Time Workflow Detection using Video Streams in Craniosynostosis Surgery. Spanish Society of Biomedical Engineering Annual Conference, virtual (2020)

R. Antúnez-Conde, E. Monteserín, S. Ochandiano, **D. García-Mato**, M. García-Sevilla, J. I. Salmerón. Uso de la Luz Estructurada para el Análisis Morfométrico en Cirugía Reconstructiva de Craneosinostosis. Sociedad Española de Cirugía Oral y Maxilofacial y de Cuello y Cabeza 2020, virtual (2020)

D. Gascón Alonso, E. Monteserín, E. Bullejos, **D. García-Mato**, J. Pascau, S. Ochandiano. Sistema de Navegación In-House, Tecnología CAD-CAM, Luz Estructurada y

Realidad Virtual Aplicada al Tratamiento de Craneosinostosis. Sociedad Española de Cirugía Oral y Maxilofacial y de Cuello y Cabeza, virtual (2020)

E. Bullejos, S. Ochandiano **D. García-Mato**, M. Tousidonis, G. Arenas, J. I. Salmerón. Planificación Virtual y Navegación Intraoperatoria en el Tratamiento de la Craneosinostosis. Congreso Nacional de Cirugía Oral y Maxilofacial 2019, Sevilla, Spain (2019)

S. Espías-Alonso, S. Ochandiano, **D. García-Mato**, J. Pascau, C. Navarro-Cuéllar, J. I. Salmerón. Empleo de Sistema de Realidad Aumentada en Craneosinostosis. Congreso Nacional de Cirugía Oral y Maxilofacial 2019, Sevilla, Spain (2019)

9.2. Other publications

9.2.1. Articles in peer-reviewed journals

E. León-Román, **D. García-Mato**, I. López-Torres, J. Vaquero-Martín, J.A. Calvo-Haro, J. Pascau, P. Sanz-Ruiz. The Knee Prosthesis Constraint Dilemma: Biomechanical Comparison Between Varus-Valgus Constrained Implants and Rotating Hinge Prosthesis. A Cadaver Study. Journal of Orthopaedic Research. 1-7 (2020)

M. García-Sevilla, J. De León-Luis, R. Moreta-Martínez, **D. García-Mato**, R. Pérez-Mañanes, J. A. Calvo-Haro, J. Pascau. Performance Evaluation to Improve Training in Forceps-Assisted Delivery. OR 2.0 Context-Aware Operating Theaters, Computer Assisted Robotic Endoscopy, Clinical Image-Based Procedures, and Skin Image Analysis, pp. 69-77 (2018)

9.2.2. International conferences

D. García-Mato, M. S. Holden, A. Lasso, A. Szulewski, J. Pascau, G. Fichtinger 3D Gaze Tracking for Skill Assessment in Ultrasound-Guided Needle Insertions. In: CARS 2018 - Computer Assisted Radiology and Surgery Proceedings of the 32nd International Congress and Exhibition, Berlin, Germany, June 20–23, 2018. Int J CARS 13, 1–273 (2018)

D. García-Mato, E. León-Román, M. García-Sevilla, P. Sanz-Ruiz, R. Pérez-Mañanes, J. A. Calvo, F. Forriol, M. Desco, J. Vaquero-Martín, J. Pascau Knee Joint Goniometry using MARG low-cost sensors. In: CARS 2018 - Computer Assisted Radiology and Surgery

Proceedings of the 32nd International Congress and Exhibition, Berlin, Germany, June 20–23, 2018. Int J CARS 13, 1–273 (2018)

D. García-Mato, A. Lasso, A. Szulewski, J. Pascau, G. Fichtinger. 3D Gaze Tracking based on Eye and Head Pose Tracking. 10th Hamlyn Symposium on Medical Robotics, London, United Kingdom (2017)

D. García-Mato, A. Lasso, A. Szulewski, J. Pascau, G. Fichtinger. 3D Gaze Tracking based on Eye and Head Pose Tracking. Queen's Graduate Computing Society Conference, Kingston, Canada (2017)

D. García-Mato, E. Marinetto, R. López, M. García-Sevilla, M. Desco, J. Pascau. Cervical Range of Motion Measurement using MARG Low-Cost Sensors. Interactive Medical Image Computing (IMIC) Workshop, 19th International Conference on Medical Image Computing & Computer Assisted Intervention (MICCAI), Athens, Greece (2016)

M. García-Sevilla, **D. García-Mato**, R. Moreta-Martinez, S. Ochandiano, M. Tousidonis, C. Navarro-Cuéllar, J. Pascau. Surgical navigation for palate carcinoma resection using a non-invasive 3D-printed reference frame. In: CARS 2020 - Computer Assisted Radiology and Surgery Proceedings of the 34th International Congress and Exhibition, Munich, Germany, June 23–27, 2020. Int J CARS 15, 1–214 (2020)

M. García-Sevilla, **D. García-Mato**, J. Calvo-Haro, R. Pérez-Mañanes, J. Pascau. Optimizing navigation with patient-specific 3D printed guides in pelvic tumor resection surgery. In: CARS 2019 - Computer Assisted Radiology and Surgery Proceedings of the 33rd International Congress and Exhibition, Rennes, France, June 18–21, 2019. Int J CARS 14, 1–194 (2019)

M. Concepción-Brito, R. Moreta-Martinez, J. Serrano, **D. García-Mato**, M. García-Sevilla, J. Pascau. Segmentation of Organs at Risk in Head and Neck Radiation Therapy with 3D Convolutional Networks. In: CARS 2019 - Computer Assisted Radiology and Surgery Proceedings of the 33rd International Congress and Exhibition, Rennes, France, June 18–21, 2019. Int J CARS 14, 1–194 (2019)

M. García-Sevilla, J. De León-Luis, R. Moreta-Martínez, **D. García-Mato**, R. Pérez-Mañanes, J. A. Calvo-Haro, J. Pascau. Performance Evaluation to Improve Training in Forceps-Assisted Delivery. OR 2.0 Context-Aware Operating Theaters Workshop, 21st

International Conference on Medical Image Computing & Computer Assisted Intervention (MICCAI), Granada, Spain (2018)

R. López-Velazco, **D. García-Mato**, G. Rodríguez-Lozano, M. García-Sevilla, E. Marinetto, D. García-Olmo, M. Desco, M. Ortega-López, J. Pascau. Image Guidance for Sacral Neuromodulation. In: CARS 2017 - Computer Assisted Radiology and Surgery Proceedings of the 31st International Congress and Exhibition Barcelona, Spain, June 20–24, 2017. Int J CARS 12, 1–286 (2017)

V. García-Vázquez, G. Rodríguez-Lozano, R. Pérez-Mañanes, J. A. Calvo, **D. García-Mato**, M. Cuervo-Dehesa, M. Desco, J. Pascau, J. Vaquero. Desktop 3D Printing in medicine to improve surgical navigation in acral tumors. In: CARS 2016—Computer Assisted Radiology and Surgery Proceedings of the 30th International Congress and Exhibition Heidelberg, Germany, June 21–25, 2016. Int J CARS 11, 1–286 (2016)

9.2.3. National conferences

R. López-Velazco, **D. García-Mato**, G. Rodríguez-Lozano, M. García-Sevilla, E. Marinetto, D. García-Olmo, M. Desco, M. Ortega-López, J. Pascau. Navegación quirúrgica de la Neuromodulación de las Raíces Sacras. Spanish Society of Biomedical Engineering Annual Conference, Valencia, Spain (2016)

E. León-Román, P. Sanz-Ruiz, **D. García-Mato**, I. López-Torres, J. Pascau , J. Vaquero-Martín Estudio comparativo experimental en rodillas de cadáveres entre la prótesis CCK y bisagra rotatoria. Congreso Nacional de la Sociedad Española de Cirugía Ortopédica y Traumatología, Valladolid, Spain (2018)

10

REFERENCES

[1] L. A. Opperman, “Cranial sutures as intramembranous bone growth sites.,” *Dev. Dyn.*, vol. 219, no. 4, pp. 472–485, Dec. 2000.

[2] B. J. Slater, K. A. Lenton, M. D. Kwan, D. M. Gupta, D. C. Wan, and M. T. Longaker, “Cranial sutures: A brief review,” *Plast. Reconstr. Surg.*, vol. 121, no. 4, pp. 170–178, 2008.

[3] R. Sharma, “Craniosynostosis,” *Indian J. Plast. Surg.*, vol. 46, no. 1, p. 18, 2013.

[4] J. Panchal and V. Uttchin, “Management of Craniosynostosis,” *Facial Plastic Surgery*, vol. 32, no. 2. pp. 123–132, 2016.

[5] E. Lajeunie, M. Le Merrer, C. Bonaiti-Pellie, D. Marchac, and D. Renier, “Genetic study of nonsyndromic coronal craniosynostosis,” *Am. J. Med. Genet.*, vol. 55, no. 4, pp. 500–504, 1995.

[6] C. F. Kweldam, J. J. Van Der Vlugt, and J. J. N. M. Van Der Meulen, “The incidence of craniosynostosis in the Netherlands, 1997-2007,” *J. Plast. Reconstr. Aesthetic Surg.*, vol. 64, no. 5, pp. 583–588, 2011.

[7] O. Kirmi, S. J. Lo, D. Johnson, and P. Anslow, “Craniosynostosis: A Radiological and Surgical Perspective,” *Semin. Ultrasound, CT MRI*, vol. 30, no. 6, pp. 492–512, 2009.

[8] S. R. Cohen, R. C. Frank, H. S. Meltzer, and M. L. Levy, “Craniosynostosis,” *Handb. Craniomaxillofacial Surg.*, pp. 343–368, 2014.

[9] R. Virchow, “Uber den cretinismus, namentilich in franken, und uber pathologische schadelformen,” *Verh Phys Med Ges Wurzbg.*, vol. 2, pp. 230–256, 1851.

[10] J. Van Der Meulen, “Metopic synostosis,” *Child’s Nerv. Syst.*, vol. 28, no. 9, pp. 1359–1367, 2012.

[11] H. Matushita, N. Alonso, D. D. Cardeal, and F. De Andrade, “Frontal-orbital advancement for the management of anterior plagiocephaly,” *Child’s Nerv. Syst.*, vol. 28, no. 9, pp. 1423–1427, 2012.

[12] M. H. Huang *et al.*, “The differential diagnosis of posterior plagiocephaly: true lambdoid synostosis versus positional molding,” *Plast. Reconstr. Surg.*, vol. 98, no. 5, pp. 765—74; discussion 775—6, Oct. 1996.

[13] G. Tamburrini, M. Caldarelli, L. Massimi, P. Santini, and C. Di Rocco, “Intracranial pressure monitoring in children with single suture and complex craniosynostosis: a review,” *Child’s Nerv. Syst.*, vol. 21, no. 10, pp. 913–921, 2005.

[14] G. Baranello, G. Vasco, D. Ricci, and E. Mercuri, “Visual function in nonsyndromic craniosynostosis: past, present, and future,” *Child’s Nerv. Syst.*, vol. 23, no. 12, pp. 1461–1465, 2007.

[15] A. R. Porras, D. Zukic, A. Equobahrie, G. F. Rogers, and M. G. Linguraru, “Personalized Optimal Planning for the Surgical Correction of Metopic Craniosynostosis.,” *Clin. image-based Proced. from Plan. to Interv. Int. Work. CLIP ..., held conjunction with MICCAI ... Revis. Sel. Pap. CLIP*, vol. 2016, pp. 60–67, 2016.

[16] H. M. Branson and M. M. Shroff, “Craniosynostosis and 3-Dimensional Computed Tomography,” *Semin. Ultrasound, CT MRI*, vol. 32, no. 6, pp. 569–577, 2011.

[17] D. M. Steinbacher, “Three-Dimensional Analysis and Surgical Planning in Craniomaxillofacial Surgery,” *J. Oral Maxillofac. Surg.*, vol. 73, no. 12, pp. S40–S56, 2015.

[18] N. R. Saber *et al.*, “Generation of normative pediatric skull models for use in cranial vault remodeling procedures,” *Child’s Nerv. Syst.*, vol. 28, no. 3, pp. 405–410, 2012.

[19] C. S. Mendoza, N. Safdar, K. Okada, E. Myers, G. F. Rogers, and M. G. Linguraru, “Personalized assessment of craniosynostosis via statistical shape modeling,” *Med. Image Anal.*, vol. 18, no. 4, pp. 635–646, 2014.

[20] B. Kotrikova, R. Krempien, K. Freier, and J. Mühling, “Diagnostic imaging in the management of craniosynostoses,” *Eur. Radiol.*, vol. 17, no. 8, pp. 1968–1978, 2007.

[21] J. R. Marcus *et al.*, “Use of a three-dimensional, normative database of pediatric craniofacial morphology for modern anthropometric analysis,” *Plast. Reconstr. Surg.*, vol. 124, no. 6, pp. 2076–2084, 2009.

[22] D. Dean *et al.*, “Average African American three-dimensional computed tomography skull images: The potential clinical importance of ethnicity and sex,” *Journal of Craniofacial Surgery*, vol. 9, no. 4. pp. 348–359, 1998.

[23] C. S. Mendoza, N. Safdar, E. Myers, T. Kittisarapong, G. F. Rogers, and M. G. Linguraru, “An optimal set of landmarks for metopic craniosynostosis diagnosis from shape analysis of pediatric CT scans of the head,” *Med. Imaging 2013 Comput. Diagnosis*, vol. 8670, p. 86702T, 2013.

[24] B. C. Wood *et al.*, “What’s in a Name? Accurately Diagnosing Metopic Craniosynostosis Using a Computational Approach,” *Plast. Reconstr. Surg.*, vol. 137, no. 1, pp. 205–213, 2015.

[25] E. Robertson, P. Kwan, G. Louie, P. Boulanger, and D. Aalto, “Test-retest validation of a cranial deformity index in unilateral coronal craniosynostosis,” *Comput. Methods Biomech. Biomed. Engin.*, vol. 0, no. 0, pp. 1–13, 2020.

[26] M. Tenhagen *et al.*, “Three-Dimensional Handheld Scanning to Quantify Head-Shape Changes in Spring-Assisted Surgery for Sagittal Craniosynostosis,” *J. Craniofac. Surg.*, vol. 27, no. 8, pp. 2117–2123, 2016.

[27] T. Schweitzer, H. Böhm, P. Meyer-Marcotty, H. Collmann, R. I. Ernestus, and J. Krauß, “Avoiding CT scans in children with single-suture craniosynostosis,” *Child’s Nerv. Syst.*, vol. 28, no. 7, pp. 1077–1082, 2012.

[28] J. Y. Wong *et al.*, “Validity and reliability of craniofacial anthropometric measurement of 3D digital photogrammetric images,” *Cleft Palate-Craniofacial J.*, vol. 45, no. 3, pp. 232–239, 2008.

[29] J. W. Meulstee *et al.*, “A new method for three-dimensional evaluation of the cranial shape and the automatic identification of craniosynostosis using 3D stereophotogrammetry,” *Int. J. Oral Maxillofac. Surg.*, vol. 46, no. 7, pp. 819–826, 2017.

[30] J. F. Wilbrand *et al.*, “Objectification of cranial vault correction for craniosynostosis by three-dimensional photography,” *J. Cranio-Maxillofacial Surg.*, vol. 40, no. 8, pp. 726–

730, 2012.

[31] A. R. Porras *et al.*, “Quantification of head shape from three-dimensional photography for pre- and post-surgical evaluation of craniosynostosis,” *Plast. Reconstr. Surg.*, Aug. 2019.

[32] C. Freudlsperger, S. Steinmacher, H. Bächli, E. Somlo, J. Hoffmann, and M. Engel, “Metopic synostosis: Measuring intracranial volume change following fronto-orbital advancement using three-dimensional photogrammetry,” *J. Cranio-Maxillofacial Surg.*, vol. 43, no. 5, pp. 593–598, 2015.

[33] N. Rodriguez-Florez *et al.*, “Quantifying the effect of corrective surgery for trigonocephaly: A non-invasive, non-ionizing method using three-dimensional handheld scanning and statistical shape modelling,” *J. Cranio-Maxillofacial Surg.*, vol. 45, no. 3, pp. 387–394, 2017.

[34] D. F. Jimenez and C. M. Barone, “Early treatment of anterior calvarial craniosynostosis using endoscopic-assisted minimally invasive techniques,” pp. 1411–1419, 2007.

[35] S. R. Cohen, R. E. Holmes, B. M. Ozgur, H. S. Meltzer, and M. L. Levy, “Fronto-orbital and cranial osteotomies with resorbable fixation using an endoscopic approach.,” *Clin. Plast. Surg.*, vol. 31, no. 3, pp. 429–42, vi, Jul. 2004.

[36] S. Hirabayashi, Y. Sugawara, A. Sakurai, and K. Harii, “Frontoorbital advancement by gradual distraction,” *J. Neurosurg.*, vol. 89, no. 6, pp. 1058–1061, 1998.

[37] A. Gomi, A. Sunaga, H. Kamochi, H. Oguma, and Y. Sugawara, “Distraction osteogenesis update: Introduction of multidirectional cranial distraction osteogenesis,” *J. Korean Neurosurg. Soc.*, vol. 59, no. 3, pp. 233–241, 2016.

[38] J. A. Persing, “MOC-PS(SM) CME Article: Management Considerations in the Treatment of Craniosynostosis,” *Plast. Reconstr. Surg.*, vol. 121, no. Supplement, pp. 1–11, 2008.

[39] S. Mardini, S. Alsubaie, C. Cayci, H. Chim, and N. Wetjen, “Three-dimensional preoperative virtual planning and template use for surgical correction of craniosynostosis,” *J. Plast. Reconstr. Aesthetic Surg.*, vol. 67, no. 3, pp. 336–343, 2014.

[40] J. Selber *et al.*, “Evolution of Operative Techniques for the Treatment of Single-Suture Metopic Synostosis,” *Ann. Plast. Surg.*, vol. 59, no. 1, 2007.

[41] R. J. Havlik, D. J. Azurin, S. P. Bartlett, and L. A. Whitaker, “Analysis and treatment of severe trigonocephaly.,” *Plast. Reconstr. Surg.*, vol. 103, no. 2, pp. 381–390, Feb. 1999.

[42] J. Burge *et al.*, “Application of CAD/CAM Prefabricated Age-Matched Templates in Cranio-Orbital Remodeling in Craniosynostosis,” *J. Craniofac. Surg.*, vol. 22, no. 5, pp. 1810–1813, 2011.

[43] J. Soleman, F. Thieringer, J. Beinemann, C. Kunz, and R. Guzman, “Computer-assisted virtual planning and surgical template fabrication for frontoorbital advancement,” vol. 38, no. May, pp. 1–8, 2015.

[44] M. Seruya, D. E. Borsuk, S. Khalifian, B. S. Carson, N. M. Dalesio, and A. H. Dorafshar, “Computer-Aided Design and Manufacturing in Craniosynostosis Surgery,” *J. Craniofac. Surg.*, vol. 24, no. 4, pp. 1100–1105, 2013.

[45] T. Rodt, A. Schlesinger, A. Schramm, M. Diensthuber, M. Rittierodt, and J. K. Krauss, “3D visualization and simulation of frontoorbital advancement in metopic synostosis,” *Child’s Nerv. Syst.*, vol. 23, no. 11, pp. 1313–1317, 2007.

[46] S. Horvath, B. Paniagua, J. Andruejol, A. R. Porras, M. G. Linguraru, and A. Enquobahrie, “Osteotomy planner: an open-source tool for osteotomy simulation,” in *Medical Imaging 2018: Image-Guided Procedures, Robotic Interventions, and Modeling*, 2018, vol. 10576, pp. 654–659.

[47] A. R. Porras, D. Zukic, A. Equobahrie, G. F. Rogers, and M. G. Linguraru, “Personalized Optimal Planning for the Surgical Correction of Metopic Craniosynostosis.,” *Clin. image-based Proced. from Plan. to Interv. Int. Work. CLIP ..., held conjunction with MICCAI ... Revis. Sel. Pap. CLIP*, vol. 2016, pp. 60–67, 2016.

[48] A. R. Porras *et al.*, “Locally Affine Diffeomorphic Surface Registration and Its Application to Surgical Planning of Fronto-Orbital Advancement,” *IEEE Trans. Med. Imaging*, vol. 37, no. 7, pp. 1690–1700, 2018.

[49] D. García-Mato *et al.*, “Craniosynostosis surgery: workflow based on virtual surgical planning, intraoperative navigation and 3D printed patient-specific guides and templates,” *Sci. Rep.*, vol. 9, no. 1, p. 17691, 2019.

[50] B. Lethaus *et al.*, “‘Black bone’: the new backbone in CAD/CAM-assisted craniosynostosis surgery?,” *Acta Neurochir. (Wien).*, 2020.

[51] D. Y. Khechoyan *et al.*, “Surgical outcomes in craniosynostosis reconstruction: The use of prefabricated templates in cranial vault remodelling,” *J. Plast. Reconstr. Aesthetic Surg.*, vol. 67, no. 1, pp. 9–16, 2014.

[52] C. Queiros *et al.*, “Use of cutting guides during craniosynostosis sequelae surgery: A comparative study between computer-assisted planning and post-operative results,” *J. Cranio-Maxillofacial Surg.*, vol. 45, no. 7, pp. 1062–1068, 2017.

[53] R. R. Iyer *et al.*, “Use of computer-assisted design and manufacturing to localize dural venous sinuses during reconstructive surgery for craniosynostosis.,” *Childs. Nerv. Syst.*, vol. 34, no. 1, pp. 137–142, Jan. 2018.

[54] M. Hochfeld, H. Lamecker, U.-W. Thomale, M. Schulz, S. Zachow, and H. Haberl, “Frame-based cranial reconstruction,” *J. Neurosurg. Pediatr.*, vol. 13, no. 3, pp. 319–323, 2014.

[55] A. J. Kobets *et al.*, “Virtual modeling, stereolithography, and intraoperative CT guidance for the optimization of sagittal synostosis reconstruction: a technical note,” *Child’s Nerv. Syst.*, vol. 34, no. 5, pp. 965–970, 2018.

[56] L. A. Whitaker, S. P. Bartlett, L. Schut, and D. Bruce, “Craniosynostosis: an analysis of the timing, treatment, and complications in 164 consecutive patients.,” *Plast. Reconstr. Surg.*, vol. 80, no. 2, pp. 195–212, Aug. 1987.

[57] J. G. . McCarthy *et al.*, “Twenty-year experience with early surgery for craniosynostosis: I. Isolated craniofacial synostosis--results and unsolved problems,” *Plast. Reconstr. Surg.*, vol. 96, no. 2, pp. 272–283, 1995.

[58] B. M. Greenberg and S. J. Schneider, “Trigonocephaly: surgical considerations and long term evaluation.,” *J. Craniofac. Surg.*, vol. 17, no. 3, pp. 528–535, May 2006.

[59] J. C. Selber, C. Brooks, J. E. Kurichi, T. Temmen, S. S. Sonnad, and L. A. Whitaker, “Long-term results following fronto-orbital reconstruction in nonsyndromic unicoronal synostosis,” *Plast. Reconstr. Surg.*, vol. 121, no. 5, pp. 251–260, 2008.

[60] G. D. Pearson, R. J. Havlik, B. Eppley, M. Nykiel, and A. M. Sadove, “Craniosynostosis: a single institution’s outcome assessment from surgical reconstruction.,” *J. Craniofac. Surg.*, vol. 19, no. 1, pp. 65–71, Jan. 2008.

[61] M. Seruya *et al.*, “Long-term outcomes of primary craniofacial reconstruction for

craniosynostosis: A 12-year experience," *Plast. Reconstr. Surg.*, vol. 127, no. 6, pp. 2397–2406, 2011.

[62] M. Engel, G. Castrillon-Oberndorfer, J. Hoffmann, J. Mühling, R. Seeberger, and C. Freudlsperger, "Long-term results in nonsyndromatic unilateral coronal synostosis treated with fronto-orbital advancement.," *J. Craniomaxillofac. Surg.*, vol. 41, no. 8, pp. 747–754, Dec. 2013.

[63] J. A. Fearon, K. Ditthakasem, W. N. J. Chan, and M. Herbert, "Long-Term Growth following Trigonocephaly Repairs: Are Overcorrections Necessary?," *Plast. Reconstr. Surg.*, vol. 145, no. 3, 2020.

[64] J. A. Fearon, R. A. Ruotolo, and J. C. Kolar, "Single sutural craniosynostoses: surgical outcomes and long-term growth.," *Plast. Reconstr. Surg.*, vol. 123, no. 2, pp. 635–642, Feb. 2009.

[65] J. A. Taylor *et al.*, "A critical evaluation of long-term aesthetic outcomes of fronto-orbital advancement and cranial vault remodeling in nonsyndromic unicoronal craniosynostosis," *Plast. Reconstr. Surg.*, vol. 135, no. 1, pp. 220–231, 2015.

[66] A. Dean, F. Alamillos, S. Heredero, and J. Solivera, "A Novel Technique to Secure the Skull Post in a Thin Skull Allowing for Surgical Navigation in Infants," *J. Oral Maxillofac. Surg.*, vol. 78, no. 2, pp. 284.e1-284.e4, 2020.

[67] C. Berry, D. I. Sandberg, D. J. Hoh, M. D. Krieger, and J. G. McComb, "USE OF CRANIAL FIXATION PINS IN PEDIATRIC NEUROSURGERY," *Neurosurgery*, vol. 62, no. 4, pp. 913–919, Apr. 2008.

[68] M. LoPresti, B. Daniels, E. P. Buchanan, L. Monson, and S. Lam, "Virtual surgical planning and 3D printing in repeat calvarial vault reconstruction for craniosynostosis: technical note," *J. Neurosurg. Pediatr. PED*, vol. 19, no. 4, pp. 490–494, 2017.

[69] M. Y. Mommaerts, G. Jans, J. Vander Sloten, P. F. J. Staels, G. Van Der Perre, and R. Gobin, "On the assets of CAD planning for craniosynostosis surgery," *J. Craniofac. Surg.*, vol. 12, no. 6, pp. 547–554, 2001.

[70] D. García-Mato, J. Pascau, and S. Ochandiano, "New Technologies to Improve Surgical Outcome during Open-Cranial Vault Remodeling," IntechOpen, Nov. 2020.

[71] S. Pieper, M. Halle, and R. Kikinis, "3D Slicer," *2004 2nd IEEE Int. Symp. Biomed.*

Imaging Macro to Nano, vol. 1, pp. 632–635, 2004.

[72] R. Adams and L. Bischof, "Seeded region growing," *IEEE Trans. Pattern Anal. Mach. Intell.*, vol. 16, no. 6, pp. 641–647, Jun. 1994.

[73] R. Kellogg, A. C. Allori, G. F. Rogers, and J. R. Marcus, "Interfrontal angle for characterization of trigonocephaly: Part 1: Development and validation of a tool for diagnosis of metopic synostosis," *J. Craniofac. Surg.*, vol. 23, no. 3, pp. 799–804, 2012.

[74] S. Ruiz-Correa *et al.*, "New Severity Indices for Quantifying Single-Suture Metopic Craniosynostosis," *Neurosurgery*, vol. 63, no. 2, p. 325, 2008.

[75] L. Farkas, *Anthropometry of the head and face*, 2nd ed. New York: Raven Press, 1994.

[76] S. E. Bishara, G. J. Jorgensen, and J. R. Jakobsen, "Changes in facial dimensions assessed from lateral and frontal photographs. Part I--Methodology.," *Am. J. Orthod. Dentofacial Orthop.*, vol. 108, no. 4, pp. 389–393, Oct. 1995.

[77] T. K. Dixon, B. P. Caughlin, N. Munaretto, and D. M. Toriumi, "Three-dimensional evaluation of unilateral cleft rhinoplasty results.," *Facial Plast. Surg.*, vol. 29, no. 2, pp. 106–115, Apr. 2013.

[78] C. Lane and W. Harrell, "Completing the 3-dimensional picture," *Am. J. Orthod. Dentofac. Orthop.*, vol. 133, no. 4, pp. 612–620, Apr. 2008.

[79] M. Mikolajek, Z. Machacek, and J. Koziorek, "Modern Sensor Technology for Alphanumeric Recognition in Metallurgy Industry," *Elektron. ir Elektrotechnika*, vol. 20, no. 5, May 2014.

[80] D. Allegra *et al.*, "Low cost handheld 3D scanning for architectural elements acquisition," *Smart Tools Apps Comput. Graph. STAG 2016*, pp. 127–131, 2016.

[81] A. Modabber *et al.*, "Evaluation of the accuracy of a mobile and a stationary system for three-dimensional facial scanning," *J. Cranio-Maxillofacial Surg.*, vol. 44, no. 10, pp. 1719–1724, 2016.

[82] K. C. Koban and R. E. Giunta, "Using Mobile 3D Scanning Systems for Objective Evaluation of Form, Volume, and Symmetry in Plastic Surgery: Intraoperative Scanning and Lymphedema Assessment," 2016.

[83] V. García-Vázquez, B. Sesé-Lucio, F. A. Calvo, J. J. Vaquero, M. Desco, and J. Pascau,

"Surface scanning for 3D dose calculation in intraoperative electron radiation therapy.," *Radiat. Oncol.*, vol. 13, no. 1, p. 243, Dec. 2018.

[84] A. Fedorov *et al.*, "3D Slicer as an image computing platform for the Quantitative Imaging Network," *Magn. Reson. Imaging*, vol. 30, no. 9, pp. 1323–1341, Nov. 2012.

[85] N. Phillips, *Berry & Kohn's operating room technique*, 13th ed. St. Louis: Elsevier Inc., 2016.

[86] P. J. Besl and N. D. McKay, "A method for registration of 3-D shapes," *IEEE Trans. Pattern Anal. Mach. Intell.*, vol. 14, no. 2, pp. 239–256, 1992.

[87] M. Martini, M. Schulz, A. Röhrig, J. Nadal, and M. Messing-Jünger, "A 3D morphometric follow-up analysis after frontoorbital advancement in non-syndromic craniosynostosis," *J. Cranio-Maxillofacial Surg.*, vol. 43, no. 8, pp. 1428–1437, 2015.

[88] S. L. Bobek, "Applications of navigation for orthognathic surgery," *Oral and Maxillofacial Surgery Clinics of North America*, vol. 26, no. 4. W.B. Saunders, pp. 587–598, 01-Nov-2014.

[89] K. Cleary and T. M. Peters, *Image-guided interventions: technology review and clinical applications*, vol. 12, no. 1. Annual Reviews, 2010.

[90] N. D. Glossop, "Advantages of Optical Compared with Electromagnetic Tracking," *JBJS*, vol. 91, no. Supplement_1, 2009.

[91] A. I. Omara, M. Wang, Y. Fan, and Z. Song, "Anatomical landmarks for point-matching registration in image-guided neurosurgery," *Int. J. Med. Robot. Comput. Assist. Surg.*, vol. 10, no. 1, pp. 55–64, Mar. 2014.

[92] J. Schlaier, J. Warnat, and A. Brawanski, "Registration accuracy and practicability of laser-directed surface matching.," *Comput. Aided Surg.*, vol. 7, no. 5, pp. 284–290, 2002.

[93] C. R. Maurer and J. M. Fitzpatrick, "A Review of Medical Image Registration," 1993.

[94] W. Manning and S. Zhijian, "Distribution Templates of the Fiducial Points in Image-Guided Neurosurgery," *Oper. Neurosurg.*, vol. 66, no. suppl_1, p. ons-143-ons-151, Mar. 2010.

[95] M. Ammirati, J. D. Gross, G. Ammirati, and S. Dugan, "Comparison of registration accuracy of skin- and bone-implanted fiducials for frameless stereotaxis of the brain: a

prospective study.," *Skull Base*, vol. 12, no. 3, pp. 125–130, Aug. 2002.

[96] H. Yu, G. Shen, X. Wang, and S. Zhang, "Navigation-Guided Reduction and Orbital Floor Reconstruction in the Treatment of Zygomatic-Orbital-Maxillary," *J. Oral Maxillofac. Surg.*, vol. 68, no. 1, pp. 28–34, 2010.

[97] S. Pieper, M. Halle, and R. Kikinis, "3D Slicer," in *2004 2nd IEEE International Symposium on Biomedical Imaging: Macro to Nano (IEEE Cat No. 04EX821)*, 2004, vol. 1, pp. 632–635.

[98] F. M. Anderson, "Treatment of Coronal and Metopic Synostosis," *Neurosurgery*, vol. 8, no. 2, pp. 143–149, Feb. 1981.

[99] T. Ungi, A. Lasso, and G. Fichtinger, "Open-source platforms for navigated image-guided interventions," *Med. Image Anal.*, vol. 33, pp. 181–186, 2016.

[100] A. Lasso, T. Heffter, A. Rankin, C. Pinter, T. Ungi, and G. Fichtinger, "PLUS: Open-source toolkit for ultrasound-guided intervention systems," *IEEE Trans. Biomed. Eng.*, vol. 61, no. 10, pp. 2527–2537, 2014.

[101] J. Tokuda *et al.*, "OpenIGTLink: an open network protocol for image-guided therapy environment," *Int. J. Med. Robot. Comput. Assist. Surg.*, vol. 5, no. 4, pp. 423–434, Dec. 2009.

[102] D. R. Berryman, "Augmented Reality: A Review," *Med. Ref. Serv. Q.*, vol. 31, no. 2, pp. 212–218, 2012.

[103] V. Lahanas, C. Loukas, N. Smailis, and E. Georgiou, "A novel augmented reality simulator for skills assessment in minimal invasive surgery.," *Surg. Endosc.*, vol. 29, no. 8, pp. 2224–2234, Aug. 2015.

[104] C. T. Yeo, T. Ungi, P. U-Thainual, A. Lasso, R. C. McGraw, and G. Fichtinger, "The effect of augmented reality training on percutaneous needle placement in spinal facet joint injections.," *IEEE Trans. Biomed. Eng.*, vol. 58, no. 7, pp. 2031–2037, Jul. 2011.

[105] C. J. Luciano *et al.*, "Learning retention of thoracic pedicle screw placement using a high-resolution augmented reality simulator with haptic feedback.," *Neurosurgery*, vol. 69, no. 1 Suppl Operative, pp. ons14-9; discussion ons19, Sep. 2011.

[106] E. Z. Barsom, M. Graafland, and M. P. Schijven, "Systematic review on the

effectiveness of augmented reality applications in medical training," *Surg. Endosc.*, vol. 30, no. 10, pp. 4174–4183, 2016.

[107] D. Inoue *et al.*, "Preliminary study on the clinical application of augmented reality neuronavigation.," *J. Neurol. Surg. A. Cent. Eur. Neurosurg.*, vol. 74, no. 2, pp. 71–76, Mar. 2013.

[108] M. E. Currie *et al.*, "Augmented Reality System for Ultrasound Guidance of Transcatheter Aortic Valve Implantation," *Innovations*, vol. 11, no. 1, pp. 31–39, Jan. 2016.

[109] M. Zhu *et al.*, "A novel augmented reality system for displaying inferior alveolar nerve bundles in maxillofacial surgery," *Sci. Rep.*, vol. 7, no. July 2016, pp. 1–11, 2017.

[110] S. Nicolau, L. Soler, D. Mutter, and J. Marescaux, "Augmented reality in laparoscopic surgical oncology," *Surg. Oncol.*, vol. 20, no. 3, pp. 189–201, 2011.

[111] A. Marien *et al.*, "Three-dimensional navigation system integrating position-tracking technology with a movable tablet display for percutaneous targeting," *BJU Int.*, vol. 115, no. 4, pp. 659–665, 2015.

[112] S. Nicolau, A. Garcia, X. Pennec, L. Soler, and N. Ayache, "An augmented reality system to guide radio-frequency tumour ablation," *Comput. Animat. Virtual Worlds*, vol. 16, no. 1, pp. 1–10, Feb. 2005.

[113] M. Feuerstein, T. Mussack, S. M. Heining, and N. Navab, "Intraoperative laparoscope augmentation for port placement and resection planning in minimally invasive liver resection.," *IEEE Trans. Med. Imaging*, vol. 27, no. 3, pp. 355–369, Mar. 2008.

[114] F. Sauer, A. Khamene, and S. Vogt, "An Augmented Reality Navigation System with a Single-Camera Tracker: System Design and Needle Biopsy Phantom Trial," in *Medical Image Computing and Computer-Assisted Intervention --- MICCAI 2002*, 2002, pp. 116–124.

[115] R. Moreta-Martinez, D. García-Mato, M. García-Sevilla, R. Pérez-Mañanes, J. Calvo-Haro, and J. Pascau, "Augmented reality in computer-assisted interventions based on patient-specific 3D printed reference," *Healthc. Technol. Lett.*, vol. 5, no. 5, pp. 162–166, 2018.

[116] R. Krempien *et al.*, "Projector-Based Augmented Reality for Intuitive Intraoperative

Guidance in Image-Guided 3D Interstitial Brachytherapy," *Int. J. Radiat. Oncol.*, vol. 70, no. 3, pp. 944–952, 2008.

[117] L. Chen, T. W. Day, W. Tang, and N. W. John, "Recent developments and future challenges in medical mixed reality," *Proc. 2017 IEEE Int. Symp. Mix. Augment. Reality, ISMAR 2017*, pp. 123–135, 2017.

[118] E. Rae, A. Lasso, M. S. Holden, E. Morin, R. Levy, and G. Fichtinger, "Neurosurgical burr hole placement using the Microsoft HoloLens," in *Medical Imaging 2018: Image-Guided Procedures, Robotic Interventions, and Modeling*, 2018, vol. 10576, pp. 190–197.

[119] P. Pratt *et al.*, "Through the HoloLens™ looking glass: augmented reality for extremity reconstruction surgery using 3D vascular models with perforating vessels," *Eur. Radiol. Exp.*, vol. 2, no. 1, pp. 0–6, 2018.

[120] R. Vassallo, A. Rankin, E. C. S. Chen, and T. M. Peters, "Hologram stability evaluation for Microsoft HoloLens," *Med. Imaging 2017 Image Perception, Obs. Performance, Technol. Assess.*, vol. 10136, p. 1013614, 2017.

[121] E. Auvinet, B. Galna, A. Aframian, and J. Cobb, "Validation of the precision of the Microsoft HoloLens augmented reality headset head and hand motion measurement," *Gait Posture*, vol. 57, no. July, pp. 175–176, 2017.

[122] R. Tang *et al.*, "Augmented reality navigation in open surgery for hilar cholangiocarcinoma resection with hemihepatectomy using video-based in situ three-dimensional anatomical modeling: A case report.," *Medicine (Baltimore).*, vol. 96, no. 37, p. e8083, Sep. 2017.

[123] I. Kuhlemann, M. Kleemann, P. Jauer, A. Schweikard, and F. Ernst, "Towards X-ray free endovascular interventions - using HoloLens for on-line holographic visualisation.," *Healthc. Technol. Lett.*, vol. 4, no. 5, pp. 184–187, Oct. 2017.

[124] T. Jiang, M. Zhu, G. Chai, and Q. Li, "Precision of a Novel Craniofacial Surgical Navigation System Based on Augmented Reality Using an Occlusal Splint as a Registration Strategy," *Sci. Rep.*, vol. 9, no. 1, p. 501, 2019.

[125] R. Moreta-Martinez, D. García-Mato, M. García-Sevilla, R. Pérez-Mañanes, J. A. Calvo-Haro, and J. Pascau, "Combining Augmented Reality and 3D Printing to Display

Patient Models on a Smartphone," *J. Vis. Exp.*, no. 155, p. e60618, 2020.

[126] W. Han *et al.*, "A new method for cranial vault reconstruction: Augmented reality in synostotic plagiocephaly surgery," *J. Cranio-Maxillofacial Surg.*, vol. 47, no. 8, pp. 1280–1284, 2019.

[127] M. Zhu, G. Chai, Y. Zhang, X. Ma, and J. Gan, "Registration strategy using occlusal splint based on augmented reality for mandibular angle oblique split osteotomy," *J. Craniofac. Surg.*, vol. 22, no. 5, pp. 1806–1809, 2011.

[128] D. García-Mato *et al.*, "Three-dimensional photography for intraoperative morphometric analysis in metopic craniosynostosis surgery," *Int. J. Comput. Assist. Radiol. Surg.*, 2021.

[129] B. Eftekhar, "Smartphone as a Remote Touchpad to Facilitate Visualization of 3D Cerebral Angiograms during Aneurysm Surgery," *J. Neurol. Surgery, Part A Cent. Eur. Neurosurg.*, vol. 78, no. 5, pp. 502–506, 2017.

[130] C. Carusi and C. Bernardi, "An easy, efficient, and safe method for intraoperative digital photography by smartphone," *Aesthetic Surg. J.*, vol. 36, no. 9, pp. NP284–NP286, 2016.

[131] D. García-Mato *et al.*, "Augmented reality visualization for craniosynostosis surgery," *Comput. Methods Biomech. Biomed. Eng. Imaging Vis.*, vol. 0, no. 0, pp. 1–8, 2020.

[132] T. Peters and K. Cleary, *Image-guided interventions: Technology and applications*. 2008.

[133] V. N. Palter and T. P. Grantcharov, "Simulation in surgical education," *Can. Med. Assoc. J.*, vol. 182, no. 11, pp. 1191 LP – 1196, Aug. 2010.